Diss. ETH Nr. 16179

A hybrid unsteady flamelet model for large eddy simulation of turbulent diffusion flames

A dissertation submitted to the
EIDGENÖSSISCHE TECHNISCHE HOCHSCHULE ZÜRICH
for the degree of
Doctor of Technical Sciences

Presented by
ŞEVKET A. BAYKAL
M.Sc., METU
born October 7th, 1972
Citizen of Turkey

Accepted on the recommendation of
Prof. Dr. D. Poulikakos, examiner
Prof. Dr. K. Boulouchos, co-examiner
Dr. J. Gass, co-examiner

Zurich, 2005

To my Parents

Nebahat and Osman

Acknowledgement

This thesis is the result of a research project, which was initiated at the Laboratory Thermodynamics in Emerging Technologies of the Institute of Energy Technology at ETH Zurich and which was funded by Dr. Alphons Hintermann from the Swiss Federal Office of Energy.

I would like to express my sincere thanks to Prof. Dimos Poulikakos for offering me the possibility to continue my research in his group. I would like to thank my reading committee member, Prof. Konstantinos Boulouchos, for his helpful comments on a draft of this dissertation. I thank Dr. Jürg Gass for managing the project, his constant support and advice. I am thankful to all my teachers especially Prof. Yurdanur Tulunay and Prof. Ayşe H. Bilge to share their knowledge with me.

I am grateful to Drs. Lale Demiraydın, Andreas Chaniotis, and Christian Del Taglia for adapting me to the research environment at LTNT. I am also grateful to Mathias Dietzel, Gloria Romera, Salvatore Arcidiacono and the other present and former members of LTNT for their friendship and contributions. It would not have been possible to accomplish this work without all the other employees of the laboratory. Thanks to the help of Marianne Ulrich with administrative work, and Martin Meuli for his technical support.

I had the luck of sharing my office Dr. Lale Demiraydın, Evangelos Boutsianis, and Stefano Piffaretti. I would like to thank them for sharing their knowledge, their thought, their successes and their worries with me and allowing me to share mine with them. I would like to thank our system administatrators Tonko Racic, Dr. Tilo Steiger, Stefan Benz, and Georges Bammatter for their efforts to keep the systems running.

I wish to mention my big brothers, İbrahim Uslu and Engin Candan. They spent a lot of time supporting me throughout the project. Bu tez Engin olmadan kesinlikle bitemezdi. Hem babalık, hem annelik, hem de ağabeylik yapabilmek bir tek ona özgüdür. Except these two, was sie gemacht haben, hätte niemand machen können. I found another good friend in Zurich to share a laugh, thank you Merthan.

My special thank goes to my lovely friends, Özcan Yüksek, Alper Özcan, Mete Bıyık, Erdal Arıöz, Erdem Yoldaş, Taylan Ercan, Nil Ercan, and Bülent Gümüş. We have shared everything that we had since we met in 202. Turker Tezal have initiated, encouraged, and supported me during our long and constant friendship. Special thanks are also addressed to the lady who touched my heart once.

My greatest appreciation is reserved for my parents, Nebahat and Osman Fevzi Baykal whose support and encouragement during all the years make this dissertation possible. Last but actually first, Dr. Ülkü Baykal, my sister and my other side. If I were a chance to select my sister, I would select you.

Abstract

Premixed and nonpremixed flames can be characterized according to their reactant injection. Partially premixed combustion is a hybrid form of these two combustion regimes. Nonpremixed turbulent flames may not exactly feature diffusion flame properties when the flame develops further downstream because fuel and oxidizer can be mixed at the molecular level before they react. This situation can be described with the time dependent solutions of the flamelet equations. Therefore, the parameters characterized only by nonpremixed combustion may not be adequate to model a turbulent diffusion flame. Recently, Large Eddy Simulation (LES) has become a new and popular approach in simulation of the turbulent jet flames. In this approach, the large-scale structures are solved and the small-scale structures are modelled. Therefore, the mixing process controlled by large scale structures is resolved and the small scale effects such as leading edge flames involved in the flame base dynamics are modelled by the subgrid scale models in LES. Three Sandia flames D, E and F have been simulated by combining these two new approaches. Results showed that the introduced coupling model could be a candidate for lifted turbulent jet flames.

The transient laminar flamelet model with the new coupling strategy has been formulated as a combustion model for Large Eddy Simulations of turbulent diffusion flames especially when local extinction and reignition phenomena are dominant. The coupling study of interface routines and the flow solver is one of the critical tasks in the flamelet modelling studies. In this study, the new and more efficient coupling strategy was developed and implemented. In contrast to the classical flamelet models coupling method, the presented coupling strategy makes the library interpolations and then calculates the pdf integrals that are stored as a part of the libraries. This improvement is very crucial in terms of computational costs since it increases the speed of the simulation up to 30 times compared to the classical models. In this method, there is almost no limitation for the number of the simulated species and types of the integrals in PDF calculations. Another flexibility is also offered for the number of the nodes in the computational domain due to the drastic decreases in the computational costs.

The time averaged results are compared with experimental data for velocity, mixture fraction, temperature and mass fractions of the species at the centreline and various radial profiles. The

radial profiles of main and minor species are consistent with the experimental data. This modelling approach leads to the prediction of local extinction and reignition phenomena by well-predicted temperature fields in the fuel rich area of the flame. The hybrid flamelet model overcomes the limitations of the fast chemistry and steady flamelet models by using a dynamic chemical variable, progress variable, in addition to the kinematic variable, dissipation rate, in order to parameterize the flamelet evolution.

The comprehensive comparisons of basic dynamic characteristics of the Sandia flames between measurements and calculations are performed by using scalar statistics conditional on mixture fraction and bimodality analysis. These analyses together with time averaged comparisons may validate that the presented model can account for local extinction and reignition phenomena in the unsteady reacting turbulent flow fields.

Zusammenfassung

Vorgemischte und nicht vorgemischte Verbrennung werden unterschieden nach der Art und Weise, wie die Reaktionspartner dem Prozess zugeführt werden. Es existiert auch eine Hybridform dieser zwei Fälle, nämlich die teilvorgemischte Verbrennung. Auch in abgehobenen turbulenten nicht vorgemischten Flammen kann vor der Zündung eine Teilvormischung auftreten. Dieser Vorgang kann mit zeitabhängigen Lösungen der Flamelet-Gleichung beschrieben werden. Deshalb sind die Parameter, welche für die Beschreibung einer reinen Diffusionsflamme benützt werden nicht immer genügend. In letzter Zeit wurde die LES Methode zum bevorzugten Ansatz für die Simulation von turbulenten Jet-Flammen. Bei diesem Ansatz werden die groben Strukturen exakt gelöst und nur die feineren modelliert. Deshalb wird bei der Verwendung von LES der Mischungsprozess in den groben Strukturen aufgelöst und Modelle werden nur für die Prozesse innerhalb der Zellen des Rechengitters benützt. Mit Hilfe dieser Kombination von LES und instationärem Flamelet wurden die sog. Sandia Flammen D, E und F simuliert und die Resultate zeigen, dass diese Methode abgehobene Flammen sehr gut beschreiben kann.

Das transiente Flameletmodell gekoppelt mit LES wurde speziell als Verbrennungsmodell formuliert für Fälle, wo lokales Erlöschen und Wiederzünden dominante Vorgänge sind. Die „Interface-Routinen“ für die Kopplung des Flamelet-Modells mit dem Strömungslöser stellen einen kritischen Schritt dar in Bezgug auf Rechenzeit. Eine neue effizientere Strategie wurde entwickelt und implementiert. Als wesentliche Neuerung wurde die Integration über die PDF vorgängig der Strömungsimulation durchgeführt und in die Flamelet-Libraries integriert. Diese Neuerung verküzt die Rechenzeit um einen Faktor 30, was die Möglichkeit ergibt eine grössere Anzahl von Spezies einzubeziehen. Auch gibt diese Neuerung erst die Möglichkeit mit einer für LES genügend feinen Gitterauflösung zu arbeiten.

Die zeitlich gemittelten Resultate für Geschwindigkeit, Mischungsbruch, Temperatur und verschiedene Spezieskonzentrationen werden mit experimentellen Daten verglichen, dies für das axiale Profil und verschiedene radiale Profile. Die Profile der Haupt- und Nebenspezies zeigen gute Übereinstimmung mit den experimentellen Werten. Speziell erwähnenswert ist die gute Übereinstimmung des Temperaturprofils im fetten Bereich, was zeigt dass durch

dieses Modell die Effekte des Löschens und Wiederzündens gut vorhergesamt werden können. Das hybride Flamelet-Modell kann die Grenze des stationären Flamelet-Modells mit unendlich schneller Chemie überwinden, indem zu den bisherigen Kopplungsparametern Mischungsbruch und skalare Dissipation die Reaktionsfortschrittsvariable für die Beschreibung der chemischen Dynamik hinzugefügt wird.

Umfangreiche Vergleiche wurden durchgeführt zwischen Experiment und Rechung der dynamischen Charakteristik der Sandia-Flammen, indem auf den Mischungsbruch kondizionierte Mittelwerte der Temperatur und Spezieskonzentrationen untersucht wurden. Auch diese Resultate zeigen eindrücklich, wie gut dieses Modell die Vorgänge des Löschens und Wiederzündens und die zeitabhängige Entwicklung der Reaktion wiedergeben kann.

Contents

List of Figures viii

List of Tables xi

Nomenclature xii

1 General Background 1

1.1 Introduction 1
1.2 The Objective of the Thesis 4

2 Literature Survey on Computational Methods 7

2.1 Computational Methods in Turbulent Flows 7
2.1.1 Reynolds Averaged Navier Stokes (RANS) Equations 7
2.1.2 Eddy Viscosity Models 10
2.1.3 Reynolds Stress Turbulence Models 12
2.1.4 Large Eddy Simulation 12
2.2 Combustion Modes 20
2.2.1 Non-Premixed Flames 21
2.3 Modeling Strategies on Non-premixed Turbulent Flames 25
2.3.1 Eddy Dissipation Concept (EDC) 25
2.3.2 Conditional Moment Closure (CMC) 26
2.3.3 Probability Density Function Transport Equation Model (PDF) 26
2.3.4 Flamelet Model 27
2.3.5 The Conventional Coupling Strategy between Laminar Flamelet and Turbulent Flow Field 30

3 The Model Study 35

3.1. The Governing Equations 35
3.2. The Transient Laminar Flamelet Model (TFLM) 37
3.3. Discussions on the Flamelet Assumption 38
3.4. Unsteadiness Nature of Scalar Dissipation Rate and Its Interaction with Strain Rate 40
3.5. The Additional Variable 43
3.6. The Initial Conditions for Flamelet Equations 44
3.7. Different Library Approaches for Flamelet Equations 44
3.8. The Coupling Strategy 49
3.8.1. Mixture Fraction Variable and Its variance 50
3.8.2. Scalar Dissipation Rate 51
3.8.3. The Residence Time 53
3.8.4. Progress Variable 53
3.8.5. The Presumed Pdf Method 54
3.9. The Alternative Coupling Strategy 55

4 Analysis of the Sandia Flames (D, E, F) 59

4.1. Burner Types 59
4.1.2. Experimental Details 60
4.2. Computational Domain 63
4.2.1. Initial and Boundary Condition Setup 63
4.3. Results and Discussions 66
4.4. Flame D 68
4.4.1. Centerline Axial Profiles 68
4.4.2. Radial Profiles 73
4.5. Flame E 76
4.5.1. Centerline Axial Profiles 76
4.6. Flame F 80
4.6.1. Centerline Axial Profiles 80
4.6.2. Radial Profiles 82

5 Dynamic Analysis of the Flames **87**

5.1. Extinction and Reignition 87
5.2. Bimodality 92
5.3. Reactedness Parameter 100

6 Summary and Conclusions **107**

A Interpolation Scheme **111**

Bibliography **115**

List of Figures

1 General Background

1.1: World energy production by fuel [2] 2

1.2: The share of total primary energy supply for Switzerland in 2002 [1]. 3

2 Literature Survey on Computational Methods

2.1: The flamelet concept for the turbulent diffusion flames 31

3 The Model Study

3.1: Sheet-like dissipation layer (or reaction zone) resulting from principal strain rates that are compressive in one direction (x, defined as being normal to the layer) and extensive in the two orthogonal directions (y and z). 42

3.2: The orientation of the highest-dissipation layer with respect to the 2-D principal compressive strain rate axis. 43

3.3: Time evolution of temperature in transient flamelet libraries for the given scalar dissipation rate and progress variable both for non-premixed and partially premixed mixtures. 45

3.4: Time evolution of species in transient flamelet libraries for the given scalar dissipation rate and progress variable, both for non-premixed and partially premixed mixtures. 46

3.5: Effects of scalar dissipation rate changes on the scalar field in the transient flamelet libraries both non-premixed and partially premixed mixtures for the given progress variable. 47

3.6: Effects of the progress variable changes on the scalar field in the transient flamelet libraries both non-premixed and partially premixed mixtures for the given scalar dissipation rate. 48

3.7: Flow chart of coupled TFLM/LES model 52

3.8: The new flow chart of coupled TFLM/LES model using pre-calculated solution fields. 58

4 Analysis of the Sandia Flames (D, E, F)

4.1: Schematic configuration of piloted jet flames 62
4.2: The picture of Sandia piloted jet flames 62
4.3: The front and bottom views of the computational domain. 64
4.4: Normalized inlet velocity profiles 65
4. 5: Mean values of scalars along the centreline (lines:simulation; symbols:experiments). 71
4. 6: Radial distribution of mean values of scalars at x/d=15d (lines:simulation; symbols:experiments). 74
4. 7: Radial distribution of mean values of scalars at x/d=30d (lines:simulation; symbols:experiments). 75
4. 8: Radial distribution of mean values of scalars at x/d=45d (lines:simulation; symbols:experiments). 77
4. 9: Mean values of scalars along the centreline (lines:simulation; symbols:experiments). 79
4. 10: Mean values of scalars along the centreline (lines:simulation; symbols:experiments). 81
4. 11: Radial distribution of mean values of scalars at x/d=15d (lines:simulation; symbols:experiments). 83
4. 12: Radial distribution of mean values of scalars at x/d=35d (lines:simulation; symbols:experiments). 85
4. 13: Radial distribution of mean values of scalars at x/d=45d (lines:simulation; symbols:experiments). 86

5 Dynamic Analysis of the Flames

5.1: The instantaneous variations of the scalars on the stoichiometric mixture fraction isosurface 89

5.2(a): Scatter plots of Sandia flames (D-F) for temperature at x/d=15d 90

5.2(b): Scatter plots of Sandia flames (D-F) for temperature at x/d=30d 91

5.2(c): Scatter plots of Sandia flames (D-F) for temperature at x/d=45d 91

5.3: Conditional probability density function of the reactedness calculated from temperature for the flame E at x/d=15d 94

5.4: Conditional probability density function of the reactedness calculated from temperature for the flame F at x/d=15d 95

5.5: Conditional probability density function of the reactedness calculated from temperature for the flame F at x/d=30d 96

5.6: Conditional probability density function of the reactedness calculated from temperature for the flame F at x/d=45d 97

5.7: Conditional probability density function of the reactedness calculated from CO2 for the flame F at x/d=15d 98

5.8: Conditional probability density function of the reactedness calculated from CO2 for the flame F at x/d=30d 99

5.9: Conditional probability density function of the reactedness calculated from CO2 for the flame F at x/d=45d 100

5.10: Conditional probability density function of the reactedness calculated from Eqn.4 for the flame E at x/d=15d 102

5.11: Conditional probability density function of the reactedness calculated from Eqn.4 for the flame F at x/d=15d 103

5.12: Conditional probability density function of the reactedness calculated from Eqn.4 for the flame F at x/d=30d 104

5.13: Conditional probability density function of the reactedness calculated from Eqn.4 for the flame F at x/d=45d 105

List of Tables

1 General Background

2 Literature Survey on Computational Methods

2.1: Turbulent Combustion Models in terms of chemistry and mixing [16] 23

3 The Model Study

3.1: The combination of the variable in the artificial solution field. 57

4 Analysis of the Sandia Flames (D, E, F)

4.1: Sandia flames flow parameters. 63

4.2: Specification of inlet boundary conditions for D, E and F flames. 66

5 Dynamic Analysis of the Flames

5.1: The classified mixture fraction intervals for bimodality analysis 92

Nomenclature

Latin symbols

Symbol	Units	Description
c	-	Reaction progress variable
c_{fl}	-	Local reaction progress variable
c_p	J/kgK	Specific heat capacity at constant pressure
D	m^2/s	Molecular diffusivity
d	m	Diameter
G	-	Filter function of LES
H	J	Enthalpy
i	-	Number of species
k	m^2/s^2	Turbulent kinetic energy
k	-	Iteration number
k	-	Number of species
m	kg	Mass
n_i	mole	number of moles of species i
n_{tot}	mole	total number of moles
O_2	-	Oxidizer
P	-	Probability density function
R	J/molK	Reactedness
$\Re$	J/molK	Reactedness
S	*	Chemical source term
T	K	Temperature
t	s	Time
u	m/s	Velocity
W_i	kg/mole	Molecular weight of species i.
X	-	Mole fraction of species
x_i	m	Cartesian coordinate component

Y	-	Mass fraction of species
Z	-	Mixture fraction

Greek symbols

Symbol	Units	Description
α	W/m^2K	Thermal diffusivity
α,β,γ	-	Coefficients of beta function
Γ	-	Gamma function
Δ	m	Computational mesh size
δ_{ij}	-	Kronecker symbol
ε	m^2/s^2	Dissipation rate of kinetic energy
λ	W/Km	Thermal diffusivity
μ	kg/ms	$=\rho\nu$ Dynamic viscosity
μ_{eff}	kg/ms	Efficient viscosity
μ_l	kg/ms	Laminar viscosity
μ_t	kg/ms	Turbulent viscosity
ν	-	stoichiometric mass ratio
ρ	kg/m^3	Density
τ_{ij}	N/m^2	Stress tensor
τ_t	s	Turbulent time scale
ϕ	-	Any flow variable
χ	1/s	Scalar dissipation rate
ω	*	Reaction rate

(*) Depending on the chosen scalar

Subscripts

Symbol	Description
1	fuel inlet
2	oxidizer inlet
b	burned
f	fuel inlet
fl	flamelet
i,j,k	space direction
n	n^{th} chemical species
o	oxidizer
p	product
st	stoichiometric
t	turbulent
tot	total
unb	unburnt
μ	model constant

Superscripts

Symbol	Description
-	time averaged
~	Favre averaged
*	starting condition in mixture fraction space
$\overline{\psi}$	Reynolds averaged value
$\widetilde{\psi}$	Favre averaged value

Abbrevations

Symbol	Description
CFD	Computational Fluid Dynamics
CMC	Conditional Moment Closure
CPDF	Conditional Probability Density Function
DNS	Direct Numerical Simulation
EDM	Eddy Dissipation Model
ILDM	Intrinsic Low Dimensional Manifold
LES	Large Eddy Simulation
PDF	Probability Density Function
RANS	Reynolds Averaged Navier Stokes
TLFM	Transient Laminar Flamelet Model

Chapter I

General Background

1.1 Introduction

Fuel may be defined as any substance, which can be burned as a source of heat or power. The provision of energy as heat or power in either mechanical or electrical form is the major reason for burning fuels. Economic activities would be limited and restrained without heat and electricity from the fuel combustion. Modern society uses more and more energy for industry, services, homes and transport.

The generation of electricity from fuels requires the combustion of the fuels and some of the energy in the heat (steam) produced is converted into electricity. Most fuels are mixtures of hydrocarbons and these are the main heating agents. Both carbon and hydrogen combine with oxygen during the combustion and the reactions provide heat. Carbon and hydrogen present in the original fuels are emitted into the atmosphere as carbon dioxide (CO_2) and water. What will limit the usage of fossil fuels is the potential climatic and ecosystem changes as a result of rising CO_2 levels in the atmosphere. In Switzerland, heating systems and industrial combustion produce 91% of sulphur dioxide (SO_2), while motor vehicles produce 8%. Motor vehicles produce 56% of nitrogen oxides (NO_x), another 30% is produced by combustion equipment and 85% of carbon monoxide (CO) is produced from a combination of motor vehicles, heating and industrial combustion. [1].

Combustion systems have been a crucial tool for industrial development throughout the world. Manufacturing sector continues to rely on these systems for heat and steam generation. Combustion systems include turbines, process heaters, boilers, combined heat and power technologies. In current technology, it is not easy to replace fossil fuel usage by wind, solar cell power, or some other renewable methods. We are faced with a serious energy problem

related with the diminishing reserves of fossil fuels as the population of the planet increases. Nevertheless, world energy demand is forecast to increase by 54% from 2001 to 2025 and to require about $16 trillion in new investments by 2030 to meet demands [2]. All the renewable energy sources together may make useful contributions, but they are completely incapable of coming anywhere near to tackling the scale of the energy problem. Demand for energy in the developing Asia countries are projected to double between 2001 and 2025, accounting for 40% of the world's increase.

Despite the growth in renewable energy production and engineering improvements, the global share of renewable energy will be less than 10% in 2025 and oil will still account for nearly 40% of world energy consumption. The world could consume more than twice the amount of fossil fuels over the next 60 years as during the last 60 years (see Fig. 1.1). The impact of greenhouse gases on global warming is cumulative [2].

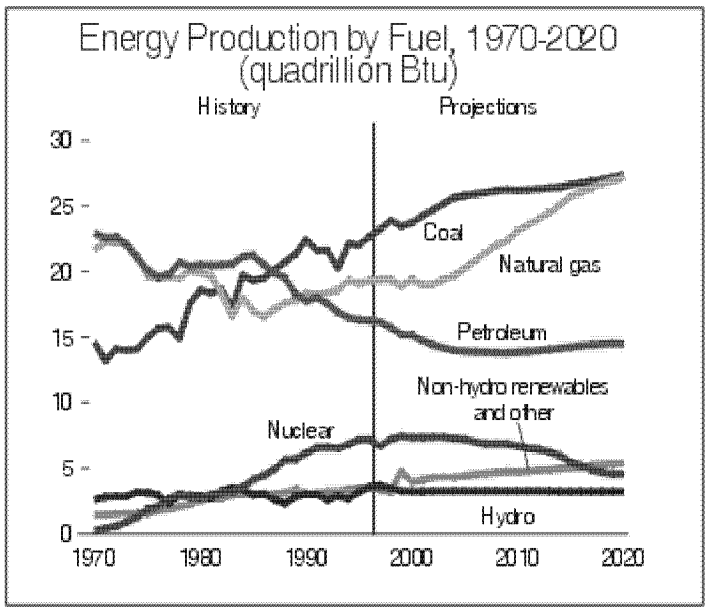

Figure 1.1: World energy production by fuel [2].

In 2003, Iceland opened the world's first filling station for hydrogen-fueled vehicles and it plans to use geothermal-produced electricity within 30-40 years, becoming the first non-fossil-fuel country. Renewable energy accounts for 6% of the EU's energy use, which the EU

hopes to increase to 12% by 2010.

VEL2 Programme in Canton Ticino is supported by Swiss Energy and promotes alternative, low or zero emitting vehicles (hybrid and internal combustion engine vehicles) through subsidised pricing. Internal combustion engines can be combined with some other cycles, for example with steam or gas turbines, and have a variety of applications. They are popular as reserve capacity in hospitals, nuclear power stations, etc., and are also used in regular power production. Gaseous and traditional liquid fuels can be used in internal combustion engines [1].

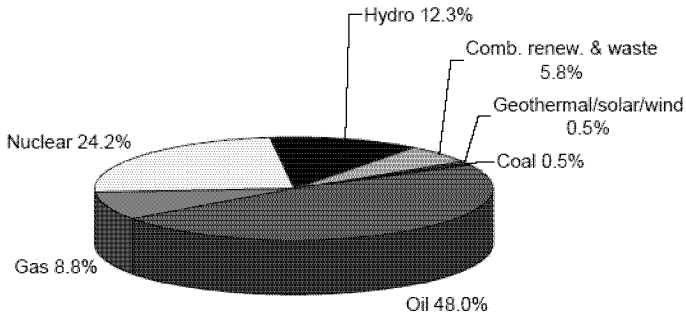

Figure 1.2: The share of total primary energy supply for Switzerland in 2002 [1].

The share of combustion based energy production from the renewable energy sources and the waste was 6% in Switzerland's total energy production for 2002 (see Fig. 1.2). Combustion systems are used to generate steam and heat for manufacturing processes. Environmental concerns such as global warming and ozone transport, emission requirements and cost of fuels have had a major influence on the studies on efficient energy generation by minimizing the pollutant emissions. This increases research and development (R&D) needs for fundamental combustion science. Combustion engines processes are being developed in close co-operation with industry. The key research activities are laser optical measures, numerical simulation of combustion processes, formation of pollutants in combustion (particularly reduction of nitrogen) and low-pollution combustion technologies (e.g. catalytic combustion) and retention procedures (e.g. for diesel soot in heavy duty vehicles). R&D studies in combustion systems lead developments in energy-efficient and environmentally friendly industrial technologies. Improvements in industrial combustion systems can reduce energy consumption through more

efficient heat transfer to reduce NO_x, SO_2, CO, and particulate emissions; and improve product quality. The challenge is to develop clean systems without compromising their efficiency.

1.2 The Objective of the Thesis

The historical approach for the design of combustion systems and tuning is trial and error. It is imperative to attain higher levels of sophistication in computational science and systems engineering. Combustion is one of the known most complex chemical processes, and effective computational modeling and simulation of combustion comprise a great part of the challenge. The aid of advanced modeling and improved systems engineering capabilities can bring more predictability to combustion design.

The computational fluid dynamics (CFD) is a numerical tool to simulate the fluid flow, heat transfer, chemical reactions and their interactions. Popularity of CFD has been drastically increased in the last decade due to the tremendous progress in computational powers. The graphical user interface tools can be used easily to set up complicated geometries in today's world. Furthermore, the results can be easily post- processed and visualized by the end users. The increased computational power creates some new opportunities such as making numerical experiments (DNS) in order to compare and validate the outputs of laboratory experiments. This method has also been used to create databases in the absence of availability of laboratory data. The numerical simulation methods are being validated with the reliable sets of the experimental data at selected basic conditions before attempting to simulate the complex geometry flows and reactions. Once a stable and reliable simulation model is developed for complex geometries and the combustion systems, the application of the model to new design geometries and reactions would be relatively easy. Therefore the new geometries may be tested much more economically with numerical methods compared to building and testing an entire combustion system.

The formation and the removal of pollutant species such as nitrogen oxides and carbon monoxide are of particular interest for advanced combustion systems. In most of the practical combustion systems chemical reaction and turbulence are coupled with each other strongly.

While turbulence increases the mixing rates and enhances combustion, combustion causes instabilities in the flow field in terms of expansion due to exothermicity and buoyancy by releasing heat.

The understanding and the prediction of the behaviour of turbulent reacting flows are generally much more difficult than non-reacting flows. First of all the flow is usually compressible, so that, in addition to the conservation of mass and momentum and constitutive relationships, also the conservation of energy as well as gas laws must be considered. Furthermore, conservation equations for chemical species must be included, often for many chemical species and numerous chemical reactions. The reactions can result in large heat release, resulting, for example, in large temperature and density variations.

The turbulent combustion systems can be investigated under three categories in terms of mixing: premixed, non-premixed and partially premixed combustion. In premixed combustion, like a homogeneous internal combustion engine, the premixed fuel and oxidant are ignited locally by a spark. Then the flame propagates through the mixture, leaving hot products in its wake. In non-premixed combustion, such as fuel jet issuing into air, the fuel and air are introduced in two separate streams. The chemical reaction can occur as fuel and air mix locally at the molecular level. Therefore the flame can exist where fuel and air mixed locally, so that the chemical reaction is controlled by the mixing rate at least up to some extent. Finally, some reactions occur with partially premixed species. For example, in the problem of a fuel jet into air, it is possible for fuel and air to mix somewhat before ignition.

Reduction in the pollutant emissions is one of the most important challenges for the next generation of gas turbine and internal combustion engines. The knowledge of the temporal and spatial distribution of fuel in gas turbine combustors is significant in terms of pollution, combustion efficiency and combustor dynamics. The time dependent fluctuations in a combustor often lead to poorer performance. Inefficient temporal fuel-air mixing increases NO_x emissions. The statistical turbulence models (RANS) are time independent models so that the resolved scales do not reflect any temporal information. Even though at some additional expenses of the method, LES produces time dependent predictions. LES is a new and popular approach for simulation of turbulent jet flames in the last decade. The large-scale structures are solved and the small-scale structures are modelled in this method.

Flamelet models allow the chemistry and turbulent flow to be treated separately. The transient laminar flamelet model (TFLM) is developed in our group (LTNT) for the applications of non-premixed flames subjected to high strain rates in unsteady turbulent flow field. The objective of the thesis is to introduce an easy implementation of transient laminar flamelet model coupled with LES in order to capture unsteady thermochemical dynamics of highly turbulent flow fields at low Damköhler numbers. The model validation study is designed to investigate local extinction and re-ignition effects especially for the lift-off non-premixed flames.

Chapter II

Literature Survey on Computational Methods

2.1 Computational Methods in Turbulent Flows

Combustion problems involve strong coupling among chemical reactions, molecular transport and fluid dynamics. The mechanisms by which turbulence, chemical reactions, and heat release interactions are still under investigation. Different methods have been suggested to model turbulent combustion flows. In recent years, interest has grown in applying Large Eddy Simulation (LES) to reactive flows. The motivation behind this trend is the inaccessibility of real turbulent flames to direct numerical simulation due to their prohibitively fine resolution requirements. The majority of current methods for calculating the properties of turbulent flames and practical combustion systems are based on Reynolds or Favre averaging of the Navier Stokes equations (RANS).

Simulation of the RANS equations reduces the computational effort compared to DNS and LES. So it is generally adopted for practical engineering calculations. However, averaging procedure introduces additional unknown terms containing products of the fluctuating quantities, which act like additional stresses in the fluid. These terms, called 'turbulent' or 'Reynolds' stresses, are difficult to determine directly and so become further unknowns. The Reynolds stresses need to be modelled by additional equations of known quantities in order to achieve "closure" of the conservation equation.

2.1.1 Reynolds Averaged Navier Stokes (RANS) Equations

In the conventional averaging procedure a time averaged quantity, such as velocity, can be defined as;

$$\bar{u} = \frac{1}{\Delta t}\int_{t_0}^{t_0+\Delta t} u\, dt \tag{1}$$

where Δt is a time scale that is large compared to the period of random fluctuations, but small with respect to the time scale to which the equations are solved.

In the Reynolds decomposition, the randomly changing flow variables are replaced by time averages plus fluctuations about the average. For example we may write the velocity u in terms of an average component $\bar{u}$, and a time varying component u'

$$u = \bar{u} + u' \tag{2}$$

By definition, the time average of a fluctuating quantity is zero:

$$\overline{u'} = \frac{1}{\Delta t}\int_{t_0}^{t_0+\Delta t} u'dt = 0 \tag{3}$$

Substituting the time averaged quantities into the original transport equations results in the Reynolds-averaged equations. The Reynolds form of the conservation of mass can be written

$$\frac{\partial \bar{\rho}}{\partial t} + \frac{\partial}{\partial x_j}\left(\overline{\rho u_j}\right) = 0 \tag{4}$$

For incompressible flows the momentum equation in Reynolds-averaged form can be written as

$$\frac{\partial}{\partial t}\left(\rho\overline{u_i}\right) + \frac{\partial}{\partial x_j}\left(\rho\overline{u_i}\,\overline{u_j}\right) = -\frac{\partial \bar{p}}{\partial x_i} + \frac{\partial}{\partial x_j}\left(\overline{\tau_{ij}} - \overline{\rho u_i' u_j'}\right) \tag{5}$$

where the Reynold stress $\overline{\tau_{ij}}$ takes on the reduced form

$$\overline{\tau_{ij}} = \mu\left(\frac{\partial \overline{u_i}}{\partial x_j} + \frac{\partial \overline{u_j}}{\partial x_i}\right) \tag{6}$$

The transport equation of a scalar ϕ can also be written in this form

$$\frac{\partial}{\partial t}\left(\rho\overline{\phi_i}\right) + \frac{\partial}{\partial x_j}\left(\rho\overline{u_i}\,\overline{\phi_j}\right) = -\frac{\partial \overline{p}}{\partial x_i} + \frac{\partial}{\partial x_j}\left(\overline{\tau_{ij}} - \rho\overline{u_i'\phi_j'}\right) \tag{7}$$

The Reynolds-averaged form of the energy equation is given below

$$\frac{\partial}{\partial t}\left(\rho\overline{h_{tot}}\right) + \frac{\partial}{\partial x_j}\left(\rho\overline{u_i}\,\overline{h_{tot}}\right) = -\frac{\partial \overline{p}}{\partial x_i} + \frac{\partial}{\partial x_j}\left(\overline{\tau_{ij}} - \rho\overline{u_i'\phi_j'}\right) \tag{8}$$

where the mean total enthalpy is composed by the contributions of the static enthalpy , mean flow kinetic energy and the turbulent kinetic energy

$$\overline{h_{tot}} = \bar{h} + \frac{1}{2}\bar{u}^2 + k \tag{9}$$

The turbulent kinetic energy reads;

$$k = \frac{1}{2}\overline{u'^2} \tag{10}$$

The continuity equation has not been altered, but the momentum and scalar transport equations contain turbulent flux and the molecular diffusive flux terms respectively. These are the Reynolds stress, $\rho\overline{u_i'u_j'}$, and the Reynolds flux, $\rho\overline{u_i'\phi_j'}$. These terms arise from the nonlinear convective term in the un-averaged equations. They reflect the fact that convective transport due to turbulent velocity fluctuations will act to enhance mixing over and above that caused by thermal fluctuations at the molecular level. At high Reynolds numbers, turbulent velocity fluctuations occur over a length scale much larger than the mean free path of thermal fluctuations, because of this, the turbulent fluxes are much larger than the molecular fluxes. Turbulence models close the Reynolds-averaged equations provide with models for the

computation of the Reynolds stresses and Reynolds fluxes. These models can be divided into two classes: Eddy Viscosity Models and Reynolds Stress Models. Eddy Viscosity Models use the Boussinesq assumption and models that close the Reynolds equations without this assumption are grouped under Reynolds Stress Models.

2.1.2 Eddy Viscosity Models

This model is based on the idea that turbulence consists of small eddies which are continuously forming and dissipating, and in which the Reynolds stresses are assumed to be proportional to mean velocity gradients. By using the gradient diffusion hypothesis, the turbulent eddy viscosity can be written

$$\overline{\rho u_i' u_j'} = 2\mu_t S_{ij} - \frac{2}{3}\delta_{ij}\left(\mu_t \frac{\partial u_k}{\partial x_k} + \rho\bar{k}\right) \tag{11}$$

where S_{ij} and k are the strain rate tensor and turbulent kinetic energy respectively.

Boussinesq suggested this approach more than 100 years ago. This method assumes the apparent turbulent shearing stress might be related to the rate of mean strain through an apparent scalar turbulent (eddy) viscosity.

The Eddy Diffusivity Hypothesis is analogous to the Eddy Viscosity Hypothesis, which states that the Reynolds fluxes of a scalar are linearly related to the mean scalar gradient:

$$\overline{\rho u_i' \phi_j'} = \Gamma_t \nabla \phi_j \tag{12}$$

Here Γ_t is the eddy diffusivity and prescribed as

$$\Gamma_t = \frac{\mu_t}{\mathrm{Pr}_t} \tag{13}$$

where $\mathbf{Pr}_t$ is the turbulent Prandtl number.

In order to close the above equations the turbulent viscosity, μ_t, should be known. The Eddy Viscosity Turbulence Models are different from each other in terms of the way they define the turbulent viscosity. Zero Equation Models compute a global value for μ_t from the mean velocity and a geometric length scale using an empirical formula. There are no additional transport equations to be solved. Prandtl has suggested:

$$\mu_t = \rho \ell^2 \left| \frac{\partial u}{\partial y} \right| \tag{14}$$

where ℓ is a mixing length and the product of $\ell \left| \frac{\partial u}{\partial y} \right|$ can be interpreted as the characteristic velocity of turbulence.

Two Equation Models compute the turbulence velocity scale from the turbulent kinetic energy, which is provided from the solution of its transport equation. The turbulent length scale is estimated from two properties of the turbulence field, usually the turbulent kinetic energy and its dissipation rate. The dissipation rate of the turbulent kinetic energy is obtained from the solution of its transport equation. $k-\varepsilon$ and $k-\omega$ models are classified under Two Equation Models. The $k-\varepsilon$ model assumes that the turbulence viscosity is linked to the turbulence kinetic energy and dissipation via the relation

$$\mu_t = C_\mu \rho \frac{k^2}{\varepsilon} \tag{15}$$

where C_μ is a constant. The $k-\omega$ models assumes that the turbulence viscosity is linked to the turbulence kinetic energy and turbulent frequency as

$$\mu_t = \rho \frac{k}{\omega} \tag{16}$$

There are also several modified and hybrid models derived from the original $k-\varepsilon$ and $k-\omega$ models.

2.1.3 Reynolds Stress Turbulence Models

Reynolds Stress Models do not assume that the turbulent shearing stress is proportional to the rate of mean strain. These models are based on transport equations for all components of the Reynolds Stress tensor and the dissipation rate. Reynolds Stress Models are more general than those based on the Boussinesq assumption (Eddy Viscosity Models) and can be expected to provide better predictions for the flows with sudden changes in the mean strain. The exact production term and the inherent modeling of stress anisotropies theoretically make Reynolds Stress Models more suited to complex flows, however in practice they are often not superior to Two Equation Models. There are many forms of Reynolds Stress Turbulence Models, and the detailed discussions can be followed from [4].

2.1.4 Large Eddy Simulation

Development in computer technologies and improvements in numerical methods make possible to avoid some of modelling restrictions required for the treatment of the Reynolds Averaged Navier Stokes equations. Two closely related approaches have been developed for this purpose; Direct Numerical Simulation (DNS) and Large Eddy Simulation (LES).

DNS involves solving the three-dimensional, time dependent Navier Stokes equations and species conservation equations. No Reynolds or Favre averaging is employed. All of the relevant length and time scales are resolved numerically. The size of the computational domain must be at least in the order of the integral scale of the turbulence, l_t, the flow must be resolved down to at least the Kolmogorov scale, η, and the simulations must be three-dimensional, the number of computational grid points, N_g, must be

$$N_g \approx \left(\frac{l_t}{\eta}\right)^3 \approx \mathbf{Re}^{9/4} . \qquad (17)$$

Furthermore, due to numerical stability and accuracy considerations, the time step size must decrease proportional to the grid spacing, so that the number of the time steps, N_t, must scale like

$$N_t \approx \mathbf{Re}^{3/4} \quad . \qquad (18)$$

In order to calculate the evolution of the solution in a volume for a duration equal to the characteristic time of the most energetic scale, we have to solve the Navier Stokes equations numerically order of Re^3 times. These conditions are very restrictive, and limit the range of Reynolds numbers that can be simulated by DNS.

There are some differences between DNS and RANS simulations. The instantaneous, unsteady, three-dimensional flow structures are directly computed in DNS. In a RANS computation, however, only the averaged fields are computed, so that no direct information is obtained regarding the turbulent flow structures.

The approach of DNS has the advantage of avoiding the closure problem, when compared to the RANS approach. All dependent variables are known at each point in space and time compare to the experimental results. This situation allows the statistical studies and the analysis of flow structures in detail. At present time DNS is mainly useful as a research tool.

Because of the computational limitations in DNS approach for high Reynolds numbers, the technique of LES has been developed. LES lies between Reynolds Stress Models and DNS, and it is motivated by the limitations of each of these approaches. LES can be expected to be more accurate and reliable than Reynolds Stress Models for flows in which large scale unsteadiness is significant such as the flow over bluff bodies, which involves unsteady separation and vortex shedding. Although the energy and anisotropy are contained predominantly in the larger scales of motion, DNS computations are expended on smallest, dissipative motions. In LES, the dynamics of the larger scale motions, which are affected by the flow geometry and are not universal, are computed explicitly, the influence of the smaller scales, which have a universal character, being represented by the models.

DNS may not be applicable to turbulent flow problems at high Reynolds numbers because of its limitations such as requirement of very fine meshes to map the computational domain. The computational advantage of LES is to use larger mesh sizes in its model. So we no longer solve the dynamics of all the scales of the exact solution directly. Instead of this, we introduce a new and coarser level of description of the flow system. This comes down to picking out

certain scales, more exactly: there is a clear separation (filter) which is represented directly in the simulation that the others are not. The non-linearity of the Navier Stokes equations reflects the dynamic coupling that exists among all the scales of the solution, which implies that the scales cannot be calculated independently from each other. So, if we want a quality representation of the scales that are solved, their interactions with the scales that are not have to be considered in the simulation. In order to model these interactions, an additional term is introduced to the equations governing the evolution of the resolved scales, since these terms represent the action of a large number of other scales with those that are solved. They reflect only the global or average action of these scales. They are therefore only statistical models; an individual deterministic representation of the inter-scale interactions would be equivalent to a direct numerical simulation. Such modelling offers a gain only to the extent that is universal, i.e. if it can be used in cases other than the one for which it is established or has been validated.

The non-filtered Navier Stokes equations for momentum are:

$$\frac{\partial}{\partial t}\left(\rho u_i\right)+\frac{\partial}{\partial x_j}\left(\rho u_i u_j\right)=-\frac{\partial p}{\partial x_i}+\mu\frac{\partial^2 u_i}{\partial x_j \partial x_j} \tag{19}$$

The filter function decomposes the flow variables into a large scale (resolved) and a small scale (unresolved) parts. Any flow variable can be written as:

$$f=\overline{f}+f' \tag{20}$$

where $\overline{f}$, the large scale part, is defined through volume averaging as:

$$\overline{f}(x_i,t)=\int_V G(x_i-x_i')f(x_i',t)dx_i' \tag{21}$$

where the filter $G(x_i-x_i')$, usually a top-hat or a Gaussian function, is chosen with the following properties:

$$\begin{aligned} G(x) &= G(-x) \\ G(x) &\geq 0 \\ \int G(x)dx &= 1 \end{aligned} \tag{22}$$

After performing the volume averaging and neglecting density fluctuations, the filtered Navier Stokes equations become:

$$\frac{\partial}{\partial t}\left(\rho\overline{u_i}\right)+\frac{\partial}{\partial x_j}\left(\rho\overline{u_i u_j}\right)=-\frac{\partial p}{\partial x_i}+\mu\frac{\partial^2\overline{u_i}}{\partial x_j\partial x_j} \tag{23}$$

However we cannot solve the system for both $\overline{u_i}$ and $\overline{u_i u_j}$, the convective flux has to be represented in terms of decomposed variables

$$\overline{u_i u_j}=\overline{u_i}\,\overline{u_i}+\tau_{ij} \tag{24}$$

the previous filter equation now is formed in

$$\frac{\partial}{\partial t}\left(\rho\overline{u_i}\right)+\frac{\partial}{\partial x_j}\left(\rho\overline{u_i u_j}\right)=-\frac{\partial p}{\partial x_i}+\mu\frac{\partial^2\overline{u_i}}{\partial x_j\partial x_j}-\frac{\partial\tau_{ij}}{\partial x_j} \tag{25}$$

where τ_{ij} is the subgrid scale stress (SGS) tensor,

$$\tau_{ij}=\left(\overline{\overline{u_i}\,\overline{u_j}}-\overline{u_i}\,\overline{u_j}\right)+\left(\overline{\overline{u_i}u_j'}+\overline{u_i\overline{u_j'}}\right)+\left(\overline{u_i'u_j'}\right) \tag{26}$$

The first term in the parentheses is known as the Leonard stress, the second term is, the cross-term stress, and the third term is, the Reynolds stress. If the time averaging were being employed instead of filtering, the first two terms would be zero, leaving only the Reynolds stress.

In LES the effect of the subgrid scale stresses must be modelled. The small scale motion tends to be fairly isotropic and universal. Using this fact the earliest model was proposed by

Smagorinsky [5]. It is a modified form of mixing-length or gradient diffusion model with the length, $\ell = C_s\Delta$, being proportional to the filter width, Δ. Thus the SGS stress tensor can be represented by

$$\tau_{ij} = 2\mu_t S_{ij} \tag{27}$$

where S_{ij} is the strain rate tensor,

$$S_{ij} = \frac{1}{2}\left(\frac{\partial \overline{u_i}}{\partial x_j} + \frac{\partial \overline{u_j}}{\partial x_i}\right) \tag{28}$$

This yields the SGS viscosity as

$$\mu_t = \rho\left(C_s\Delta\right)^2\sqrt{2S_{ij}S_{ij}} \tag{29}$$

The Smagorinsky constant, C_s, is changed depending on the type of flow and mesh resolution. Values ranging from 0.1 to 0.24 have been reported [79-81]. Van Driest type exponential damping function is multiplied with the mixing length in order to force the length scale to approach zero at the wall for wall shear flows.

There are ongoing studies on LES for complex flows. This simulation method has been started to use predominantly in the fluid mechanics research areas since 1990's. The universal coefficient viscosity models, classical Smagorinsky models, are consistent with the idea of an energy cascade (i.e. the net energy flow is from larger scales to smaller scales). Locally, energy can flow in either direction; from the sub-grid scales to the resolved scales, which is called backscattering, or vice versa. But viscosity models are purely dissipative and cannot represent this process properly. On the other hand viscosity models improve the numerical stability of the simulation [82].

It is not easy to determine a single appropriate universal coefficient for the complex engineering flows. Akselvoll has reported a wide range of model coefficients [6]. The Smagorinsky type viscosity models are also called Zero Equation Eddy Viscosity Model.

Menon[7] and Ghosal [8] have proposed a transport equation for the sub-grid kinetic energy to improve the original model. One of the advantages of this method is to allow coarser grids. This model is also required to specify a universal coefficient.

As it was discussed above it is difficult to set a universal model coefficient for the complex flows. For this reason a model coefficient dynamically determined from resolved field, as a function of both time and space would be more reliable. Germano has proposed his dynamic SGS model in 1991 [9]. This approach is based on an assumed scaling between resolved and sub-grid scales, and a mathematical identity that arises. The dynamic Smagorinsky model calculates the model coefficient by relating the subgrid scale Reynolds stress to two different sizes of filters. An explicit test filter with a filter width of $\widehat{\Delta}$, where $\widehat{\Delta} > \Delta$, to determine the turbulent stress on the filter.

$$T_{ij} = \widehat{\overline{u_i u_j}} - \widehat{\overline{u}_i}\,\widehat{\overline{u}_j} \tag{30}$$

The Germano identity introduces a relationship between calculated stress tensors using Δ and $\widehat{\Delta}$ [19].

$$L_{ij} = T_{ij} - \widehat{\tau_{ij}} \tag{31}$$

where the Leonard stress term, L_{ij}, is defined by

$$L_{ij} = \widehat{\overline{u_i u_j}} - \widehat{\overline{u}_i}\,\widehat{\overline{u}_j} \tag{32}$$

The Leonard stress term can be calculated explicitly from the resolved velocity field in the simulation. So, Eqn. (32) is very useful because it relates the unknown stress tensors at the two scales, T_{ij} and τ_{ij}, to a known tensor, L_{ij}. With the definition of the Smagorinsky model, the stresses of the test filter, T_{ij}, and that of the grid filter, τ_{ij}, are:

$$\tau_{ij} = -2C_\tau \Delta^2 \left|\overline{S}\right| \overline{S_{ij}} + \frac{1}{3}\delta_{ij}\tau_{kk} = -C_\tau \beta_{ij} \tag{33}$$

$$T_{ij} = -2C_T\widehat{\Delta}^2\left|\widehat{\bar{S}}\right|\widehat{\bar{S}}_{ij} + \frac{1}{3}\delta_{ij}T_{kk} = -C_T\alpha_{ij} \tag{34}$$

Substitution of these modeled stress tensor terms into the Germano identity gives the dynamic model.

$$L_{ij} - \frac{1}{3}\delta_{ij}L_{kk} = C_T\alpha_{ij} - \widehat{C_\tau\beta_{ij}} \tag{35}$$

where

$\alpha_{ij} = -2\widehat{\Delta}^2\left|\widehat{\bar{S}}\right|\widehat{\bar{S}}_{ij}$ and $\beta_{ij} = -2\Delta^2\left|\bar{S}\right|\bar{S}_{ij}$.

The C_τ in Eqn. (35) cannot be solved explicitly because it is in the test filtering operation. Germano extracted the C_s from the filtering operation, and assumed:

$$C_s \approx C_\tau \approx C_T \tag{36}$$

$$\widehat{C_\tau\beta_{ij}} = C_\tau\widehat{\beta_{ij}} \tag{37}$$

With these assumptions Eqn. (35) becomes:

$$L_{ij} - \frac{1}{3}\delta_{ij}L_{kk} = C_sM_{ij} \tag{38}$$

where $M_{ij} = \alpha_{ij} - \widehat{\beta_{ij}}$.

Now this problem has reduced to a set of nine algebraic equations. Using the least-square approach suggested by Lilly, the C_s can be obtained [83].

$$C_s = \frac{\langle L_{ij}M_{ij}\rangle}{\langle M_{kl}M_{kl}\rangle} \tag{39}$$

where the angle brackets denote an averaging operation [8].

The dynamic coefficient can either be positive or negative. The positive coefficient implies that energy flows from resolved to the sub-grid scales while the negative one implies energy flows from sub-grid scales to resolved scales. This back-scattering phenomenon can lead to numerical instability in the simulations [10]. The dynamic type models have been widely used in different modeling approaches. Moin has extended the application of dynamic model to compressible flows [11]. Akselvoll has applied the same approach to flows with heat transfer and reported the accuracy and reliability of dynamic LES [12].

Test filtering is costly to perform in LES of complex geometry flows, especially on unstructured grids. Chester has proposed a method based on Taylor series expansions of the resolved velocity fields [13]. Accuracy is governed by the derivative schemes used in the calculation and the number of terms considered in the approximation to the test filtering operator.

In the last decade, many studies have tested applicability of LES in combustion [14]. Despite the many advantages of LES compared to RANS model reported in the literature, because of the computational cost of the method, so far LES has been used mostly for research studies rather than industrial applications. LES has the capability of resolving the major part of the turbulent kinetic energy spectrum. By modeling only the small turbulent scales a reliable accuracy in predictions of turbulent flow field is possible. While LES may provide a more reliable turbulence model than RANS especially for the large-scale unsteady motions, it is not recommended for wall bounded flows, due to the high resolution requirements and computing times as reported by Chapman [15].

The chemical reactions in non-premixed combustion occur only by molecular mixing of oxidizer and fuel. This mixing process occurs mostly on the dissipative turbulent scales. LES may resolve the major part of the energy containing turbulent scales. The combustion process on the other hand occurs essentially at smallest scales of the sub-filter level. For this reason the accuracy of the models for the sub-filter level turbulent scales is crucial for reliability of the simulation. Most of LES approaches use the scale similarity technique while modelling the sub-filter scales [84-91]. The scale similarity assumption implies that the smallest

resolved scales are statistically similar to the largest unresolved scales. Most of the models for simulation of combustion turbulence interactions by LES have been applied by RANS based models before. In the following section the combustion types and their modelling approaches are discussed especially for non-premixed combustion.

2.2 Combustion Modes

Combustion modes can be classified in various ways. Based upon how the fuel and oxidizer reach the reaction front, there are non-premixed (diffusion), premixed and partially premixed combustion. The fuel and oxidizer are present on either side of the reaction zone in non-premixed combustion. The fuel and oxidizer are brought to the reaction zone in an unmixed state primarily due to diffusion of reactants into, and products out of the reaction zone. This type of combustion is also called diffusion combustion because of the controlled mixing by diffusion of reactants. The non-premixed combustion appears in the diesel engines, steam boilers and furnaces. The reaction ideally takes place at stoichiometric conditions so it involves very high peak temperature and this phenomenon leads to high NO_x emissions.

In premixed combustion, the fuel and the oxidizer are thoroughly mixed prior to reaching the reaction zone, also known as the flame front. Spark ignition engines, jet engine afterburners and gas-fuelled gas turbines are example of premixed combustion. In contrast to non-premixed combustion the position of the reaction zone is not defined by the diffusion of reactants, but by balancing the local convective velocity of the reactants with the rate of consumption of the reactants, which corresponds flame speed. The main concern of this type of combustion is the propagation of the flame front due to the local imbalance between diffusion of heat and chemical composition of the mixture. Premixed combustion can take place at equivalence ratios other than one. The excess amount of air in the mixture helps in the reduction of the maximum temperature in the reaction zone. So, the production of thermal NO_x in combustion systems can be controlled.

The partially premixed combustion is neither purely non-premixed, nor fully premixed, hence it is termed as partially premixed. Examples of this type of combustion are gas-fired furnaces, some spray burning devices, automotive engines and aircraft engines. In partially premixed

combustion, the fuel is injected into the oxidized flow just upstream of the flame. So there is not enough time for the fully mixing thoroughly and thus, concentration gradients across the flow are generated in the reactant stream, which enters the flame front. This type of combustion mode is characterized by its degree of unmixedness, which is a measure of how much the radial concentration profiles of the flow deviate from a fully premixed case. Partially premixed flames could be a remedy for the disadvantageous of premixed and non-premixed flames. Partially premixed combustion helps to achieve a reduction in the maximum flame temperature while keeping the flame stable. Therefore, the emission problem for non-premixed flames and the flame propagation and stability problems for premixed flames could be handled by this "hybrid" flame.

2.2.1 Non-Premixed Flames

The process of turbulent diffusion flames controls the majority of practical combustion applications. These flames are encountered in a large number of industrial systems for two main reasons. First, compared to premixed flames, burners are simpler to design and to build because a perfect reactant mixing, in given proportions, is not required. Non-premixed flames are also safer to operate as they do not exhibit propagation speeds and cannot flashback. Some specific processes make nonpremixed flames probably more difficult to understand and to describe than turbulent premixed flames. The reacting species have to reach, by molecular diffusion, the flame front before reaction. During this travel, they are exposed to turbulence and their diffusion speeds may be strongly modified by turbulent motions. The overall reaction rate is often limited by species molecular diffusion towards the flame front. Then, in many models, the chemical reaction is assumed to be fast, or infinitely fast, compared to transport processes.

The development of new combustion technologies especially for gas turbines operating in the non-premixed regime implies the accurate determination of the position in the flow where combustion starts and the control of pollutant emission. The trend in the industry is to make shorter design cycles by increasing the computational efforts. Even in burners operating in the premixed regime, the premixing of the reactants is not always complete at the molecular level and some partial premixing may be observed. Sometimes, partial premixing is even desirable to limit pollutant emissions.

The modelling studies on turbulent non-premixed flames can be grouped in terms of the assumption used in chemistry and transport phenomenon modelling. There are two major assumptions in the chemistry model studies: Infinitely fast chemistry assumption and finite rate chemistry assumption. The chemistry models using finite chemistry assumptions can also be divided into three main subgroups: Flamelet models, PDF transport and Conditional Moment Closure (CMC) models.

There are varieties of combustion models that are being used by different groups in the combustion community. Here, we will not discuss all these models, the comprehensive details can be obtained in Peters [16] and Poinsot&Vervisch [17,18]. The models are represented schematically in table 2.1 with respect to their capacity to treat premixed or nonpremixed combustion, or both, and with respect to assumptions about the chemistry. In this section we mainly focus on the flamelet models. Before going into further detail, to describe the combustion process, some fundamental definitions are introduced.

Species are characterized through their mass fractions Y_i for i=1 to N where N is the number of species in the reacting mixture. The mass fractions Y_i are defined by

$$Y_i = \frac{m_i}{m} \tag{40}$$

where m_i is the mass of species i present in a given volume and m is total mass of gas in this volume. Many studies of diffusion flames assume idealized situations using the passive scalar (mixture fraction). Considering that a single step chemical reaction involves only fuel (F), oxidizer (O) and products (P):

$$\nu_F F + \nu_o O \leftrightarrow \nu_P P \tag{41}$$

where ν_F, ν_O and ν_P are molar stoichiometric coefficients of fuel, oxidizer and products respectively.

The mass fraction Y_i of each species (F, O, and P) follows a balance equation; these equations will not be derived here but refer to Williams [19]:

$$\frac{\partial}{\partial t}(\rho Y_i) + \frac{\partial}{\partial x_i}(\rho u_i Y_i) = \frac{\partial}{\partial x_i}\left(\rho D \frac{\partial Y_i}{\partial x_i}\right) + \dot{\omega}_i \tag{42}$$

Species reaction rates $\dot{\omega}_i$ are all related to the single step reaction rate Θ

$$\dot{\omega}_i = W_i \nu_i \Theta \tag{43}$$

where W_i is the molecular weight of the specie i.

	Premixed Combustion	**Nonpremixed Combustion**
Infinitely fast chemistry	Bray-Moss-Libby Model Coherent Flame Model	Conserved Scalar Equilibrium Model
Finite Rate Chemistry	Pdf Transport Equation Model	
	Flamelet Model Based on the G-Equation	Flamelet Model Based on Mixture Fraction
		Conditional Moment Closure
	Linear Eddy Model	

Table 2.1: Turbulent Combustion Models in terms of chemistry and mixing [16].

Therefore, the oxidizer reaction rate is linked to the fuel reaction rate

$$\dot{\omega}_O = s\dot{\omega}_F \text{ with } s = \frac{\nu_O W_O}{\nu_F W_F} \tag{44}$$

where s is the mass stoichiometric ratio.The source term for temperature is also linked to the fuel reaction rate

$$\dot{\omega}_T = -\Theta\dot{\omega}_F \tag{45}$$

Using these relations, the conservation equations for fuel, oxidizer and temperature become:

$$\frac{\partial}{\partial t}(\rho Y_F) + \frac{\partial}{\partial x_i}(\rho u_i Y_F) = \frac{\partial}{\partial x_i}\left(\rho D \frac{\partial Y_F}{\partial x_i}\right) + \dot{\omega}_F \tag{46}$$

$$\frac{\partial}{\partial t}(\rho Y_O) + \frac{\partial}{\partial x_i}(\rho u_i Y_O) = \frac{\partial}{\partial x_i}\left(\rho D \frac{\partial Y_O}{\partial x_i}\right) + s\dot{\omega}_F \tag{47}$$

$$\frac{\partial}{\partial t}(\rho T) + \frac{\partial}{\partial x_i}(\rho u_i T) = \frac{\partial}{\partial x_i}\left(\frac{\lambda}{C_p}\frac{\partial T}{\partial x_i}\right) - \frac{\Theta}{C_p}\dot{\omega}_F \tag{48}$$

Combining the equations (46) and (47) one can find the following balance equation for the passive scalar, without source term:

$$\frac{\partial}{\partial t}(\rho Z) + \frac{\partial}{\partial x_i}(\rho u_i Z) = \frac{\partial}{\partial x_i}\left(\rho D \frac{\partial Z}{\partial x_i}\right) \tag{49}$$

where Z is a passive (conserved) scalar and it is called mixture fraction. Mixture fraction is changed because of diffusion and convection but not reaction. Reaction still plays an indirect role in mixture fraction controlling temperature and, therefore, density and velocity fields. Basically mixture fraction measures the local fuel oxidizer ratio and it is expressed as:

$$Z = \frac{sY_F - Y_O + Y_O^o}{sY_F^o + Y_O^o} \tag{50}$$

Y_F^o and Y_O^o are fuel and oxidizer mass fractions in pure fuel and oxidizer streams respectively. Therefore, Z is equal to one in the fuel stream and zero in the oxidizer stream. Using the equations (46) and (48) one can also describe mixture fraction in terms of temperature and mass fractions as another scalar invariant based on enthalpy.

$$\mathbb{Z} = \frac{\frac{C_p}{\Theta}\left(T - T_O^o\right) - Y_F}{\frac{C_p}{\Theta}\left(T_F^o - T_O^o\right) - Y_F^o} \tag{51}$$

Equations (50) and (51) show that all species mass fractions are function of the mixture fraction Z and temperature T.

$$Y_i = f(Z,T) \text{ for i=1,N} \tag{52}$$

It is assumed that the diffusion flame depends on the mixture fraction Z and the time t only, temperature and species mass fractions can be written as

$$T = T(Z,t) \text{ and } Y_i = Y_i(Z,t) \tag{53}$$

The functions $T(Z,t)$ and $Y_i(Z,t)$ can define the flame structure.

2.3 Modeling Strategies on Non-premixed Turbulent Flames

2.3.1 Eddy Dissipation Concept (EDC)

This model is a manipulated and extended form of the Eddy Break Up (EBU) model for the diffusion flames. It has been introduced by Magnussen [20]. The Eddy Dissipation Model is based on the concept that chemical reaction is fast relative to the transport processes in the flow. When reactants mix at the molecular level, they instantaneously form products. The model assumes that the reaction rate may be related directly to the time required to mix reactants at the molecular level. The fuel mean burning rate is calculated according to:

$$\bar{\rho}\bar{\dot{\omega}}_F = C\bar{\rho}\frac{\varepsilon}{k}\min\left(\tilde{Y}_F, \frac{\tilde{Y}_O}{s}, \beta\frac{\tilde{Y}_P}{(1+s)}\right) \tag{54}$$

where C and β are model constants. $\tilde{Y}_F$, $\tilde{Y}_O$, and $\tilde{Y}_P$ are the mass fractions of fuel, oxidizer and products respectively. This model is based on one step chemistry. It is computationally inexpensive and able to simulate certain type of industrial problems. Because of the nature of the model, it is not capable to predict minor species. The result of the simulation would be used for more advance models as an initial guess.

2.3.2 Conditional Moment Closure (CMC)

The CMC approach has been introduced by Klimenko and Bilger [21, 22] independently. The method proposes a more refined description of turbulent combustion. The idea was to solve transport equations for reactive species mass fractions which were conditionally averaged on a conserved scalar. The main advantage is that detailed chemistry can be accounted for at rather low computational cost.

The first-order CMC model assumes that the conditional fluctuations are negligible and that the conditional chemical source term is only a function of the first-order moments, like, the conditional species concentrations and temperature. This closure assumption may be inaccurate for flame stabilization problems. One possible improvement is to close the conditional chemical source term using a second-order approximation [23]. Similar to the flamelet approach the assumption of a thin reaction zone is not particularly good for CMC since CMC is not expected to be valid for very thin reaction zones [24]. The links between finite chemistry models and the assumptions used in these models were discussed in detail in literature [25]. CMC method is applicable arbitrarily complex chemistry with reasonable computational cost.

2.3.3 Probability Density Function Transport Equation Model (PDF)

PDF transport methods have been applied to the simulation of turbulent flows for almost 30 years [26]. In this class of models, a transport equation is solved for the evolution of the single-point, single-time joint scalar, or joint velocity-scalar, PDF. Probability density function methods have been applied to various types of flows such as reacting flows [27], inhomogeneous flows [28], compressible flows [29], and multiphase flows [30].

The primary advantage of PDF methods for combustion modeling lies in the fact that chemical reaction source terms appear in closed form and therefore do not require modelling [28]. Binary mixing in incompressible isotropic turbulence has been widely used as a model flow for studying unclosed mixing terms and closure models. Since the PDF is high dimensional, the transport equation is solved by a stochastic method such as Monte-Carlo algorithm. This method approximates the probability density function by many discrete values

referred to stochastic particles each representing a single state of the reacting flows [31]. Mass and Pope have proposed a method that reduces the number of independent variables to a minimum while still maintaining a high accuracy. This is the method of Intrinsic Low Dimensional Manifolds (ILDM). In this method the ILDM provides a way to reduce detailed kinetics schemes systematically. The method requires two inputs: the detailed kinetics mechanism and the desired number of degrees of freedom in the reduced mechanism [92,93].

2.3.4 Flamelet Model

Flamelet models allow the chemistry and turbulent flow to be treated seperately. This model assumes a turbulent flame as an ensemble of thin, locally one-dimensional laminar flamelets. The turbulent eddies, acoustic perturbations, and radii of flame curvature have larger scales than the flamelets thickness. These flamelets are strained and stretched by the turbulent flow field, but maintain their inner structure. If turbulence is too intense, Kolmogorov length scale eddies become smaller than the inner layer and can penetrate into it. They are able to destroy its structure. If the local flame thickness is smaller than the Kolmogorov length scale, the flamelet approach is applicable. Since the Kolmogorov length scale varies approximately as $\mathbf{Re}^{-0.75}$ and non-premixed combustion occurs at high Reynolds number in industrial combustors, the flamelet model is applicable to those systems.

In this method, the species concentrations can be determined from the solution of laminar flamelet equations. Finite rate kinetics can be readily included into the flamelet model to capture detailed kinetics. In this way the chemical reaction is effectively decoupled from the turbulent flow field computation. In classical flamelet approach the species and temperature in the flame can be completely described by two parameters, namely the mixture fraction, $\boldsymbol{Z}$ and the scalar dissipation rate, χ. The scalar dissipation rate is a measure of the strain on the flame such as in Eqn. (55) [35]. The governing equations for species and temperature are transformed by relating them to a conserved scalar, the mixture fraction, denoted $\boldsymbol{Z}$.

$$\chi_{st} = \frac{a}{\pi}\exp\left\{-2\left[erfc^{-1}(2Z_{st})\right]^2\right\} \approx 4aZ_{st}^{\,2}\left[erfc^{-1}(2Z_{st})\right]^2 \qquad (55)$$

The mixture fraction can be derived by summing all species conservation equations, and then the chemical source terms are cancelled (Eqns. (46-48)). The mixture fraction is a scalar invariant which defines mixing and is not changed in reaction. The iso-surface of stoichiometric mixture fraction, denoted Z_{st}, defines the location of the flame surface. Scalar profiles, given as functions of the mixture fraction, are assumed to be attached to the flame surface. In order to extract the scalar profiles from the turbulent flow field, the location of the flamelets anywhere in the flow field must be known. To be able to describe the location of the flamelets a new coordinate system has been introduced by Peters [32] and Kuznetsov [33]. For premixed and diffusion flames the flamelet concept has been reviewed by Peters [34] and Bray & Peters [35]. After applying the following transformation rules:

$$\frac{\partial}{\partial t} = \frac{\partial}{\partial \tau} + \frac{\partial Z}{\partial t}\frac{\partial}{\partial Z}$$

$$\frac{\partial}{\partial x_i} = \frac{\partial}{\partial Z_i} + \frac{\partial Z}{\partial x_i}\frac{\partial}{\partial Z}\left(i = 2,3\right) \tag{56}$$

$$\frac{\partial}{\partial x_1} = \frac{\partial Z}{\partial x_1}\frac{\partial}{\partial Z}$$

One can assume that the species diffusivities are equal (i.e., $\mathbf{D}_i = D$), Z is a conserved quantity (called a Schvab-Zeldovich variable) governed by the convection/diffusion equation:

$$\frac{\partial}{\partial t}(\rho Z) + \frac{\partial}{\partial x_i}(\rho u_i Z) = \frac{\partial}{\partial x_i}\left(\rho \mathbf{D}\frac{\partial Z}{\partial x_i}\right) \tag{57}$$

The balance equation for temperature is given:

$$\rho\frac{\partial T}{\partial t} + \rho u_i\frac{\partial T}{\partial x_i} - \frac{\partial}{\partial x_i}\left(\rho \mathbf{D}\frac{\partial T}{\partial x_i}\right) = -\frac{1}{\mathbf{c}_p}\sum_{i=1}^{n}\mathbf{h}_i\dot{m}_i \tag{58}$$

By using the assumption of a constant Lewis number, preferential diffusion effects are neglected, and above transformations the flamelet equations for temperature and species can be derived by following "Peters technique".

$$\rho\left(\frac{\partial T}{\partial \tau}+u_2\frac{\partial T}{\partial Z_2}+u_3\frac{\partial T}{\partial Z_3}\right)-\frac{\partial(\rho D)}{\partial x_2}\frac{\partial T}{\partial Z_2}-\frac{\partial(\rho D)}{\partial x_3}\frac{\partial T}{\partial Z_3}$$
$$-(\rho D)\left[\left(\frac{\partial Z}{\partial x_\alpha}\right)^2\frac{\partial^2 T}{\partial Z^2}+2\frac{\partial Z}{\partial x_2}\frac{\partial^2 T}{\partial Z\partial Z_2}+2\frac{\partial Z}{\partial x_3}\frac{\partial^2 T}{\partial Z\partial Z_3}+\frac{\partial^2 T}{\partial Z_2{}^2}+\frac{\partial^2 T}{\partial Z_3{}^2}\right] \qquad (59)$$
$$=-\frac{1}{\rho c_p}\sum_{i=1}^{n}h_i\dot{m}_i+\frac{q_R}{c_p}+\frac{1}{c_p}\frac{\partial P}{\partial t}$$

Since the flamelet is assumed to be thin, only gradients normal to the surface of stoichiometric mixture are large, and all terms without a second derivative in respect to the mixture fraction Z can be neglected. The term containing the time derivative is important only if very rapid changes such as extinction or reignition, occur [34]. So the flamelet structure is to leading order described by the one-dimensional time-dependent temperature equation:

$$\rho\frac{\partial T}{\partial t}+\rho\frac{\partial \chi}{2}\frac{\partial^2 T}{\partial Z^2}=-\frac{1}{c_p}\sum_{i=1}^{n}h_i\dot{m}_i \qquad (60)$$

By using the same approach and transformed variable Z one can derive the flamelet equation for the species:

$$\rho\frac{\partial Y_i}{\partial t}+\rho\frac{\partial \chi}{2}\frac{\partial^2 Y_i}{\partial Z^2}-\dot{m}_i=0 \qquad (61)$$

Here h_i are the specific heats and $\dot{m}_i$ are the chemical production rates of reacting species. T and Y_i are the temperature and the mass fractions of species i, respectively. The specific heat capacities are assumed constant and equal to each other. χ denotes the scalar dissipation rate at stoichiometric mixture and defines the influence of the outer flow field on the inner reaction zone. In other words, it describes the impact of the turbulent flow field on the laminar flamelet. Scalar dissipation rate decreases due to diffusion, and increases due to strain of the flow field [34]. It has the dimension of $[1/s]$ and may be interpreted as the inverse of a characteristic turbulent time. This quantity requires knowledge of the instantaneous value of

mixture fraction. Except LES and DNS methods in turbulent flow field, statistical average models need to model scalar dissipation rate. We will discuss this in the next section.

As mentioned in the previous paragraphs, the flamelet concept assumes the turbulent flame as an ensemble of thin, laminar and locally one-dimensional flamelet structures embedded within the turbulent flow field. In order to justify this idea some parameters must be conserved to represent correctly turbulent flamelets using laminar diffusion flames such as the chemical scheme should be the same for turbulent flamelets and for laminar diffusion flames. The counterflow geometry, which consists of opposed, axisymmetric fuel and oxidizer jets, of diffusion flames is widely used in experimental and numerical studies because it leads to one dimensional diffusion flame structure. The distance between the two concentric counter flow jets is variable and laminar flame is stabilized near the stagnation plane. The counterflow diffusion flame is a common laminar flame used to represent a flamelet in the reacting turbulent flow field. Figure 2.1 shows how the flamelet concept is carried out in practice interacting with the laminar counterflow flame structures.

2.3.5 The Conventional Coupling Strategy Between Laminar Flamelet and Turbulent Flow Field

In this section the conventional coupling strategy between laminar flamelet and turbulent flow is discussed for the statistical averaged models. The method used in this thesis for the LES formulation of the flow will be introduced. As mentioned before, the flame structure can be determined by solving the flamelet equations. These solutions for steady or transient flamelets may be stored in the flamelet libraries. By using the mixture fraction and scalar dissipation rate the laminar flamelet solutions for species mass fractions may be attached to the turbulent flow field. Models in diffusion turbulent combustion are often based on the presumed shape probability density function PDF approach. Typically, turbulent fluctuations are not resolved and the equations governing turbulent reacting flows are averaged. Accordingly, averaged variables are determined rather than instantaneous quantities. In order to compensate the information lost during averaging, a PDF can be generated for fluctuating quantities. With the known PDF, the probability of the finding an instantaneous value is known and averaging

techniques can be used to determine mean quantities. This requires knowledge of the Favre mean mixture fraction $\widetilde{Z}$ and its variance $\widetilde{Z''^2}$.

In the turbulent flow field the Favre averaged mixture fraction equation is expressed:

$$\frac{\partial(\bar{\rho}\widetilde{Z})}{\partial t} + (\bar{\rho}\widetilde{u_i}.\nabla\widetilde{Z}) = -\nabla.\left(\overline{\rho u_i'' Z''}\right) \tag{62}$$

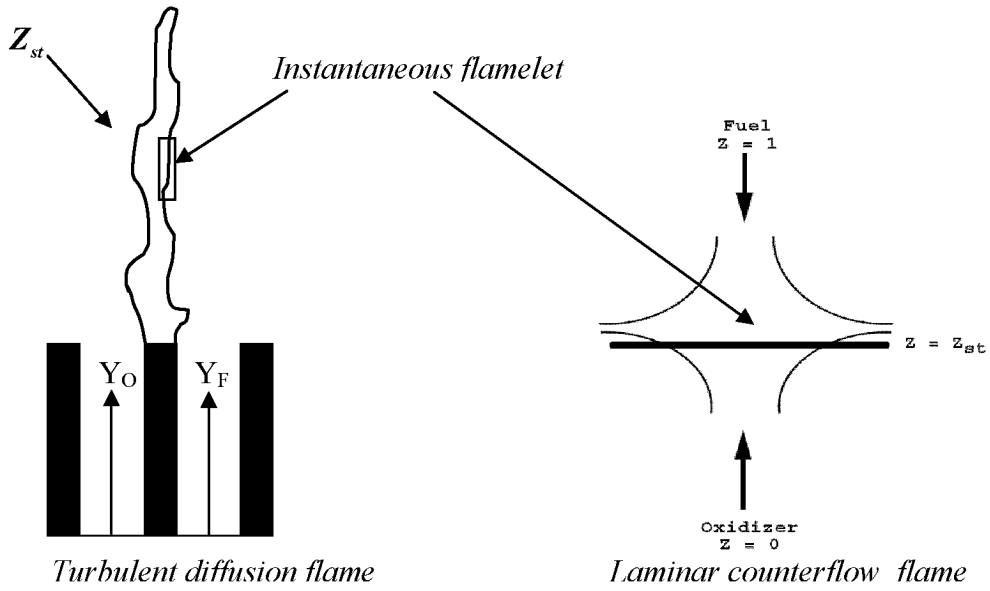

Figure 2.1: The flamelet concept for the turbulent diffusion flames.

with the gradient transport assumption $\widetilde{u_i'' Z''} = -D_t \nabla\widetilde{Z}$ and assuming that the molecular diffusivity's contribution into the total diffusivity can be neglected. The Favre averaged mixture fraction equation reads:

$$\frac{\partial(\bar{\rho}\widetilde{Z})}{\partial t} + \frac{\partial}{\partial x_i}(\bar{\rho}\widetilde{u_i}\widetilde{Z}) = \frac{\partial}{\partial x_i}(D_t\widetilde{Z}) \tag{63}$$

The $\widetilde{Z''^2}$ term can be extracted from its own transport equation:

$$\frac{\partial(\bar{\rho}\widetilde{Z''^2})}{\partial t}+(\bar{\rho}\tilde{u}_i.\nabla\widetilde{Z''^2})=-\nabla.\left(\overline{\rho u_i''Z''^2}\right)+2\bar{\rho}D_t\left(\nabla\tilde{Z}\right)^2-\bar{\rho}\tilde{\chi} \tag{64}$$

The scalar dissipation rate is defined as

$$\chi=-2D\left|\nabla Z\right|^2 \tag{65}$$

The scalar dissipation rate is modeled in turbulent flow field using the empirical relation $\tilde{\chi}=C_\chi\frac{\tilde{\varepsilon}}{\tilde{k}}\widetilde{Z''^2}$ where $\tilde{k}$ and $\tilde{\varepsilon}$ are mean turbulent kinetic energy and its dissipation rate respectively. C_χ is the model constant and usually it is selected as $C_\chi=2.0$.

One of the easiest ways to obtain mean values of the reactive scalars is to use the presumed shape PDF approach. The presumed PDF method takes into account the effects of turbulent fluctuations on the passive scalar transport process and the chemical reaction rates while avoiding the prohibitively enormous computation costs. By presumed shape PDF approach, means of any quantity that depends only on the mixture fraction can be calculated.

$$\widetilde{\psi_i}(x,t)=\int_0^1\psi_i(Z,t)\tilde{P}(Z;x,t)dZ \tag{66}$$

The beta function PDF is widely used for the Favre PDF in turbulent diffusion flames.

$$\tilde{P}(Z;x,t)=\frac{\tilde{Z}^{\alpha-1}(1-\tilde{Z})^{\beta-1}}{\Gamma(\alpha)\Gamma(\beta)}\Gamma(\alpha+\beta) \tag{67}$$

α and β are calculated as

$$\alpha=\tilde{Z}\gamma \qquad \beta=(1-\tilde{Z})\gamma \qquad \gamma=\frac{\tilde{Z}(1-\tilde{Z})}{\widetilde{Z''^2}}-1\geq 0 \tag{68}$$

If we parameterize χ by χ_{st} and use the presumed shape PDF approach for both mixture fraction and scalar dissipation rate, together with statistical independence, the joint Favre PDF of Z and χ becomes [16]:

$$\widetilde{P}(Z,\chi_{st};x,t)=\widetilde{P}(Z;x,t)\widetilde{P}(\chi_{st};x,t) \tag{69}$$

If one knows the fluctuation of mixture fraction and the scalar dissipation rate in the physical space, by using this knowledge and presumed shape PDF approach, one can determine the mean quantities of species mass fractions.

$$\widetilde{Y}_i(x,t)=\int_0^1 \underbrace{\widetilde{Y}_i(Z,\chi_{st},t)}_{\text{Mixture Fraction Space}}\ \underbrace{\widetilde{P}(Z;x,t)\widetilde{P}(\chi_{st};x,t)}_{\text{Physical Space Solution}}dZ\,d\chi_{st} \tag{70}$$

The information on fluctuations of scalar fields in the physical space are computed in the turbulent flow field solver and the species mass fractions in mixture fraction space are solved using laminar flamelet equations and stored in the steady or transient libraries. The probability distribution of scalar dissipation rate should be a log-normal PDF as argued in Peters [36].

$$\widetilde{P}(\chi)=\frac{1}{\chi_{st}\sigma\sqrt{2\pi}}\exp\left\{-\frac{1}{2\sigma^2}\left(\ln(\chi_{st})-\mu\right)^2\right\} \tag{71}$$

where the mean and variance of the scalar dissipation rate are related to the parameters $\sigma(x,t)$ and $\mu(x,t)$ by

$$\widetilde{\chi_{st}}=\exp\left(\mu+0.5\sigma^2\right)\ \text{and}\ \widetilde{\chi_{st}''^2}=\widetilde{\chi_{st}}^2\left[\exp\left(\sigma^2\right)-1\right] \tag{72}$$

Experimental data suggest that $2\le\sigma\le4$. Effelsberg [37] used the parameter $\sigma=1$ leading to

$$\frac{\sqrt{\widetilde{\chi_{st}''^2}}}{\widetilde{\chi_{st}}}=1.31 \tag{73}$$

The log-normal distribution has been found in numerical experiments to provide an accurate description of gradient magnitude and dissipation rate fluctuations of conserved scalars in fully developed turbulence [39], although the most appropriate value for sigma is still an open question. The detailed review can be found in literature [16, 17, and 38].

Chapter III

The Model Study

The objective of the thesis is to introduce an easily implemented transient laminar flamelet model coupled with Large Eddy Simulation in order to capture thermo-chemical dynamics of highly turbulent reacting flow fields. This model validation study was designed to investigate local extinction and re-ignition effects especially for the lift-off flames. Thus the piloted partially premixed methane/air diffusion flames (Sandia flames D, E and F) are selected for the model validation. The detailed discussion of the model validation is in the chapters 4 and 5. The governing equations and their interactions with laminar flamelet libraries used in this study are discussed in detail in the following section.

3.1. The Governing Equations

The Navier-Stokes equations to which involve the continuity, momentum and energy equation for unsteady incompressible viscous flows read;

Continuity equation

$$\frac{\partial \rho}{\partial t} + \frac{\partial (\rho u_i)}{\partial x_i} = 0 \qquad (1)$$

Momentum equation

$$\frac{\partial \rho u_i}{\partial t} + \frac{\partial (\rho u_j u_i)}{\partial x_j} = \frac{\partial}{\partial x_j}\left(\mu \left(\frac{\partial u_i}{\partial x_j} + \frac{\partial u_j}{\partial x_i} \right) - \frac{2}{3}\mu \delta_{ij} \frac{\partial u_k}{\partial x_k} \right) - \frac{\partial p}{\partial x_i} + \rho b_i \qquad (2)$$

Energy equation

$$\frac{\partial \rho e}{\partial t}+\frac{\partial\left(\rho e u_j\right)}{\partial x_j}=\rho \dot{q}+\frac{\partial}{\partial x_j}\left(k \frac{\partial T}{\partial x_j}\right)-\frac{\partial\left(u_j p\right)}{\partial x_j}+\frac{\partial\left(u_i \tau_{ij}\right)}{\partial x_j}+\rho b_i u_i \quad (3)$$

Where e represents energy, $\dot{q}$ the heat flux and k the thermal conductivity coefficient, b is the body force and it was neglected in this study. The LES model splits the quantities into filtered and fluctuating parts such as.

$$u=\bar{u}+u' \quad (4)$$

where $\bar{u}$, the large scale part, is defined through volume averaging as:

$$\bar{u}(x_i,t)=\int_V G(x_i-x_i')u(x_i',t)dx_i' \quad (5)$$

This filter is a top hat filter that filters all scales smaller than a user defined length scale. In this study it was selected as the average cell size expressed in the previous chapter. Therefore LES resolves only turbulent structures that are greater than the cell size determined by the user. All of the smaller turbulent structures compared to the selected filter size are modelled. This modelling method is called sub-grid scale modelling and is discussed in chapter 2.

Using predefined filtering method, the Navier-Stokes equations are re-written for continuity and momentum equations.

$$\frac{\partial \rho}{\partial t}+\frac{\partial\left(\rho \bar{u}_i\right)}{\partial x_i}=0 \quad (6)$$

$$\frac{\partial}{\partial t}\left(\rho \bar{u}_i\right)+\frac{\partial}{\partial x_j}\left(\rho \bar{u}_i \bar{u}_j\right)=-\frac{\partial p}{\partial x_i}+\mu \frac{\partial^2 \bar{u}_i}{\partial x_j \partial x_j}-\frac{\partial \tau_{ij}}{\partial x_j} \quad (7)$$

It has to be noted that $\overline{u_i u_j} \neq \overline{u}_i \overline{u}_j$. The closure term in momentum equation, τ_{ij}, is the sub-grid scale stress (SGS) tensor and must be modeled. The comprehensive discussions are made in chapter 2.

3.2. The Transient Laminar Flamelet Model (TLFM)

The transient laminar flamelet model (TLFM) was developed by Ferreira [37] for the applications for non-premixed flames subjected to high strain rates in unsteady turbulent flow field. The main advantage of the model comes from an additional parameter, reaction progress variable, in order to predict the reignition of flame after the local extinction regimes. This parameter mimics the partially premixing effects in unsteady flow fields. The unsteady flamelet equations for the species mass fraction and the temperature read;

$$\frac{\partial \phi_i}{\partial t} = \frac{\chi}{2}\frac{1}{Le}\frac{\partial^2 \phi_i}{\partial Z^2} + \frac{\dot{\omega}_i}{\rho} \tag{8}$$

$$c_p \frac{\partial T}{\partial t} = c_p \frac{\chi}{2}\left(\frac{\partial^2 T}{\partial Z^2}\right) - \sum_{n=1}^{N} \frac{h_i \dot{\omega}_i}{\rho} + 2\frac{\chi}{2}\frac{\partial T}{\partial Z}\frac{\partial c_p}{\partial Z} \tag{9}$$

where c_p is the specific heat at constant pressure, h_i is the enthalpy of the species, $\dot{\omega}_i$ is the chemical source term, χ is the scalar dissipation rate, which is defined as:

$$\chi = 2D\left(\partial Z/\partial x_i\right)^2 \tag{10}$$

and Lewis number , Le , is defined as:

$$Le = \lambda/\rho c_p D_i \tag{11}$$

The Lewis number for each species is calculated by CHEMKIN software. The Eqs. (8) and (9) are solved in the FLATRA code [40]. The finite difference method (VODPK) is used to discretize the equations in time and space. The solver features backward differentiation

methods for stiff ODEs and implicit Adams methods for non-stiff ODEs [41]. It combines features of the earlier codes EPISODE and LSODE. Both use a fixed-leading coefficient version of the variable step BDF and Adams methods. VODE uses LU factorization, allows banded and dense Jacobians, and has an option that lets the user keep a copy of the full Jacobian matrix, as well as the LU factored Newton matrix. For many problems this can increase performance considerably. VODPK uses a preconditioned Krylov method for the numerical linear algebra [42].

3.3. Discussions on The Flamelet Assumption

Before implementing some additional parameters to the classical flamelet approach and improving its capabilities to solve extended problems like partially premixing cases and lifted diffusion flames, it is important to further discuss the flamelet idea in addition to those made in chapter 2. Flamelet equations are originally built on the assumption of very large Damköhler number, or infinitely fast chemistry [36]. The Damköhler number, Da, is the measure of the competition between chemical reaction and strain rate, which is induced by turbulent flow field. The reaction zones are deteriorated at low Da. Peters defines the local Da number as:

$$Da \equiv \frac{1 - Z_{st}}{Z_{st}} \frac{A_f}{\chi_{st}} \tag{12}$$

where A_f is the reaction rate constant.

If one argues that $\frac{\partial^2 \phi_i}{\partial Z^2}$ value is very large compared to the time derivative in Eqn. (8), the time derivative term is negligible. This argument has already been used to derive the flamelet equations by neglecting the contribution of curvature effects i.e. contribution of the gradients lying on the stoichiometric mixture fraction iso surface ($Z = Z_{st}$). Therefore the steady state laminar flamelet equation (SLFM) reads

$$-\frac{\chi}{2} \frac{1}{Le} \frac{\partial^2 \phi_i}{\partial Z^2} = \frac{\dot{\omega}_i}{\rho} \tag{13}$$

The argument underlying the large $\frac{\partial^2 \phi_i}{\partial Z^2}$ value is the thin reaction zone assumption. The thin reaction zone is defined as

$$\mu_R \sim \left(\frac{Z_{st}}{1-Z_{st}} \frac{\chi_{st}}{A_f} \right)^{1/3} \ll 1 \tag{14}$$

This formula and the argument are supported by a small scalar dissipation rate, χ_{st}, and large chemical reaction rate, A_f. On the other hand, Mell et.al. [43] discussed the asymptotic solution of SLFM and ended with the following

$$\left(\chi \frac{\partial^2 \phi}{\partial Z^2} \right)_{Z_{st}} \sim \chi_{st}^{2/3} \left(A_f \frac{1-Z_{st}}{Z_{st}} \right)^{1/3} \tag{15}$$

This equation contains a contradiction against the thin reaction zone assumption. As discussed above this assumption argues that a decrease in χ supports the thin reaction zone due to the largeness of $\frac{\partial^2 \phi_i}{\partial Z^2}$. But as it is seen in Eqn. (15) decreased χ causes lower values in $\frac{\partial^2 \phi_i}{\partial Z^2}$. Therefore the order of the magnitude of this value may be closer to the time derivative in Eqn. (8).

Mell has also showed that decreasing values of scalar dissipation rate leads thinner reaction zones in mixture fraction space, Z, but thicker in physical space. Three dimensional effects may have more relevance for reaction zones in which χ_{st} is smaller rather than the one dimensional. Therefore the thinness in Z space alone (i.e. $Da \gg 1$) is not sufficient to justify neglecting the curvature effects in Eqns. (8 and 9). The extended version of the temperature equation is rewritten here including these curvature effects.

$$\rho \left(\frac{\partial T}{\partial \tau} + u_2 \frac{\partial T}{\partial Z_2} + u_3 \frac{\partial T}{\partial Z_3} \right) - \frac{\partial (\rho D)}{\partial x_2} \frac{\partial T}{\partial Z_2} - \frac{\partial (\rho D)}{\partial x_3} \frac{\partial T}{\partial Z_3}$$

$$-(\rho D)\left[\left(\frac{\partial Z}{\partial x_\alpha}\right)^2\frac{\partial^2 T}{\partial Z^2}+2\frac{\partial Z}{\partial x_2}\frac{\partial^2 T}{\partial Z\partial Z_2}+2\frac{\partial Z}{\partial x_3}\frac{\partial^2 T}{\partial Z\partial Z_3}+\frac{\partial^2 T}{\partial Z_2^{\,2}}+\frac{\partial^2 T}{\partial Z_3^{\,2}}\right]$$

$$=-\frac{1}{\rho c_p}\sum_{i=1}^{n} h_i \dot{m}_i+\frac{q_R}{c_p}+\frac{1}{c_p}\frac{\partial P}{\partial t} \qquad (16)$$

This phenomenon encourages us to introduce another parameter to regain the lost information due to lack of the surface gradients knowledge lying on the iso-surfaces of mixture fraction in the flamelet equations (8) and (9). This subject will be discussed while introducing the new parameter, a progress variable.

The steady flamelet assumption based on thinness of reaction zones in Z spaces may not be justified for many cases such as simulation of partially premixed and lifted flames. Due to this fact the transient laminar flamelet equations must be used.

3.4. Unsteadiness Nature of Scalar Dissipation Rate and Its Interaction with Strain Rate

Scalar dissipation rate introduces influences of turbulent flow field into the flamelet equations and it is originally defined as in Eqn. (10). It represents the rate of reducing scalars in turbulent flow field (see Eqn. (17)). In this equation J is a scalar in the turbulent flow field. Its dimension is [1/s] and it may be used to define a characteristic diffusion time. Peters [36] and Bilger [44] argue that the structure of the reaction zone is strongly coupled to the underlying strain rate field through the influence of fluctuating strain rate on the scalar dissipation rate.

$$\chi=-\left(\frac{\partial}{\partial t}+u.\nabla-D\nabla^2\right)\frac{1}{2}J^2=-D\nabla J.\nabla J \qquad (17)$$

The studies have showed that for $Sc \geq 1$ fluids, regions of high scalar dissipation rates are concentrated in sheet-like structures [46, 97, and 99]. The Schmidt number, $Sc = \frac{\nu}{D}$ represents the competition between momentum and molecular diffusion. The thickness of a sheet-like scalar dissipation structure is set by the competition between the thinning effect of compressive strain acting in the direction of scalar gradient and extensive strain acting orthogonal to the scalar gradient, and the thickening effect of mass diffusion in figure 3.1 [45].

Experimental studies have showed that the largest scalar gradients tend to be aligned with the principal compressive strain axis, and the dissipation sheets are oriented orthogonal to this axis (see Fig. 3.2) [102,103]. The regions of high scalar dissipation are sometimes, but not always, associated with high strain rates. This lack of a strong correlation between strain rate and sheet thickness is most likely a direct result of flow unsteadiness. This argument was enhanced by recent studies [46]. It was shown that the strain rate profiles didn't tend to reach a peak at the same location as the scalar dissipation rate. Kothnur and Clement have showed that it was not possible to model scalar dissipation sheets in a turbulent flow as an ensemble of 1-D quasi-steady, strained laminar diffusion sheets [46, 103]. An unsteady 1-D strained laminar diffusion layer model should be implemented to be more successful in the modelling study. The importance of the unsteadiness terms in physical and mixture fraction spaces comes out as a fact of the nature of the problem.

The scalar dissipation may occur at the finest mixing length scales of the flow. The resolution of LES computations may be selected by concerning the thickness of the dissipation layers. As a result of unity approximation in the Schmidt number ($Sc \approx 1$) for the gas-phase fluids, the scales of velocity gradients are almost the same order of magnitude with scalar gradients. This scale concerned resolution selection may be vital for diffusion flames because the local flame extinction might be explained by the scalar dissipation rate exceeding the critical quenching value. The local quenching is a typical consequence of smaller diffusion time scales compared to the chemical time scales at that local surface.

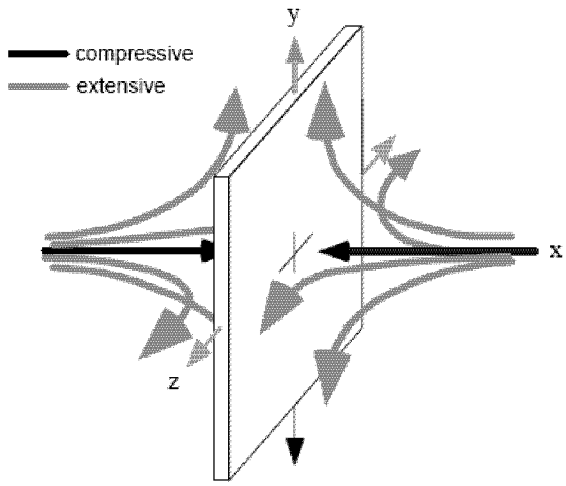

Figure 3.1: Sheet-like dissipation layer (or reaction zone) resulting from principal strain rates that are compressive in one direction (x, defined as being normal to the layer) and extensive in the two orthogonal directions (y and z).

Batchelor [47] has introduced the length scale for the scalar dissipation as a function of Schmidt number and the finest, Kolmogorov, length scale,

$$\lambda_B \equiv \lambda_K Sc^{1/2} \qquad (18)$$

In other words, the ratio of the smallest length scale in the velocity to the scale for scalar gradient fields in turbulent mixing is of the order of $Sc^{1/2}$. This definition justifies the pervious argument on velocity and scalar gradients in the gas phase flows. Nevertheless, Dowling [48] has found that the smallest dissipation scales observe Batchelor scaling based on time-resolved single point scalar field measurements. He has suggested that the regions of highest dissipation observe Taylor scaling. As a consequence of these discussions, the determination of filters plays an important role in investigating local extinction, re-ignition and stabilization.

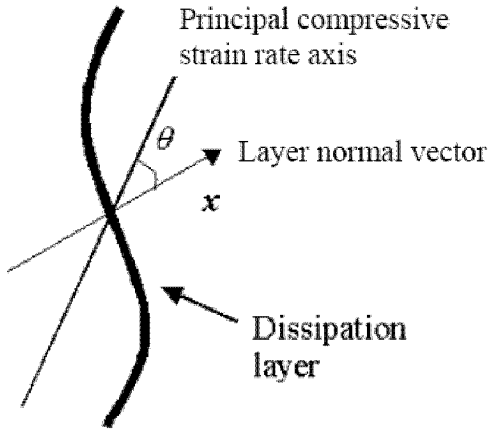

Figure 3.2: The orientation of the highest-dissipation layer with respect to the 2-D principal compressive strain rate axis.

3.5. The Additional Variable

A flamelet spends only a finite residence time in a region of interest in the turbulent flow field, and therefore it may not be able to adjust to the local conditions and reach a steady state structure. Therefore the local flamelet structure can be somewhere between initial burning state and a quasi-steady state. Several studies [49, 50-58] have showed that the instantaneous unsteady laminar flame structure was a function of the time integrated strain rate history rather than a strong function of the instantaneous flow kinematics. In summary, the unsteady model is crucial and apart from this, an integrated time history should be implemented into the model to adjust the local conditions.

The instantaneous kinematics is not adequate alone to express the unsteady laminar flame structures. Another variable must be introduced into the model to overcome the limitation of the kinematic approach for the dissipation rate, and to parametrize the flamelet evolution. This new variable should not only provide an unsteady response to the changes in dissipation rate but also transport a thermo-chemical history in its nature.

All unsteady problems need specified initial conditions to solve the equation of interest and the final solution in the transient regime depends on these initial conditions. Therefore under the guidance of previous discussions the flamelet should start from an initial condition that is

not only defined by a kinematic property, scalar dissipation rate χ, but also a new variable which transports the information of probability of ignition to that specific local position such as a dynamic property can be the progress variable c. Then the flamelet evolves starting from this specified initial condition in the unsteady turbulent flow field with time.

3.6. The Initial Conditions for Flamelet Equations

The initial conditions for flamelet equations are specified in terms of mixture fraction, scalar dissipation rate, progress variable and time. It is regarded as a composition of unburnt and fully burnt mixtures according to the BML model. Using the presumed PDF of the progress variable in the BML model [104] the initial conditions for the unsteady flamelet equation (8), reads;

$$\phi_i(Z,\chi,c,\tau=0)=(1-c)\ \phi_{i_{unb}}(Z)+c\,\phi_{i_b}(Z) \qquad (19)$$

where $\phi_{i_{unb}} = \phi_i(Z,\chi,\tau=0)$ and $\phi_i = \phi_{i_b}(Z,\chi,\tau=\infty)$ are the species of completely unburnt state of the pure mixing problem and the fully burnt state respectively and c is the reaction progress variable. For burnt conditions the steady state flamelet solutions for the given scalar dissipation rate were used as initial condition to build the transient libraries with an appropriate progress variable definition [54]. The solutions of Eqs. (8) and (9) were written in transient libraries for certain values of mixture fraction, scalar dissipation rate, residence time and reaction progress variable.

3.7. Different Library Approaches for Flamelet Equations

The flamelet equations (Eqns. (8 and 9)) are solved for the pure diffusion flame and the partially premixed flame conditions for methane-air combustion. The evolutions of the flamelets with time are depicted in figures 3.3(a-b) for non-premixed and partially premixed libraries at different scalar dissipation rates. The lower temperatures are read at the stiochiometric point for a partially premixed case in figure 3.3b where the relatively higher dissipation rate ($\chi = 1.0\ s^{-1}$) is imposed by the flow field. On the contrary, there is no

significant difference between non-premixed and partially premixed libraries in figure 3.3a that is initiated by a lower dissipation rate ($\chi = \mathbf{0.01}\ s^{-1}$). The value of temperature gradient shows the tendency to local extinction. The higher gradients lead to increased extinction because of the heat loss out of the reaction zone. Although there is a similarity in the gradients for fuel lean mixtures of both cases, the higher gradients are observed in the fuel rich parts for partially premixed flamelets as expected.

The evolution of the different mass fractions is investigated in the mixture fraction space by time dependent CO_2 and CO mass fraction values for the same set of parameters (Fig. 3.4(a-b)). The mixture fraction space is shown for the partially premixed boundary conditions because of the convenient comparison of these two cases.

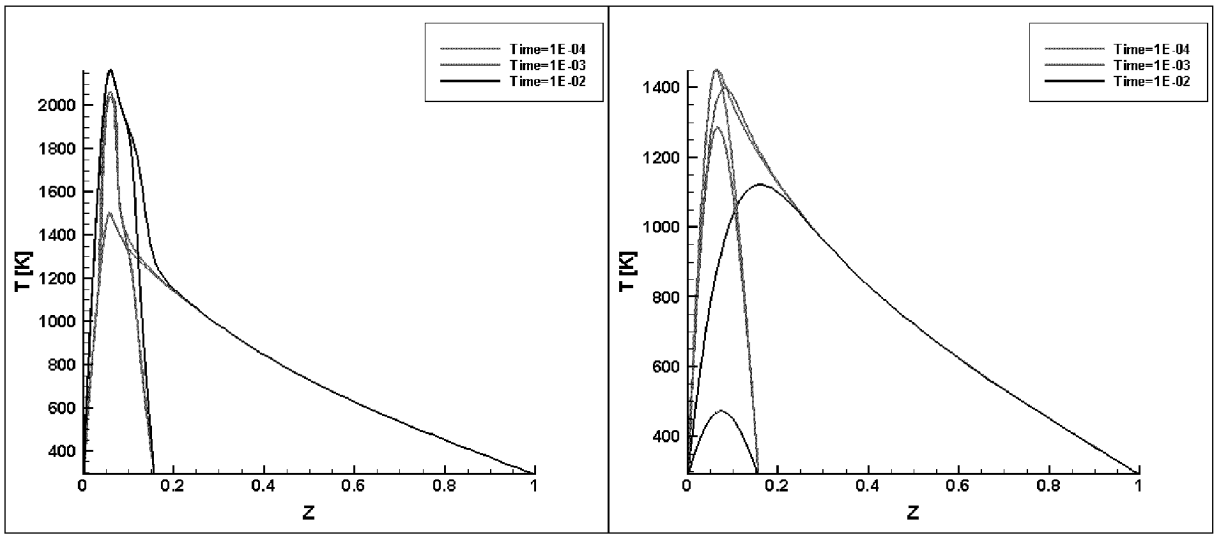

a) at $\chi = \mathbf{0.01}\,[\mathbf{1}/s]$ & $c = \mathbf{0.5}$ b) at $\chi = \mathbf{1}\,[\mathbf{1}/s]$ & $c = \mathbf{0.5}$

Figure 3.3(a-b): Time evolution of temperature in transient flamelet libraries for the given scalar dissipation rate and progress variable both for non-premixed and partially premixed mixtures.

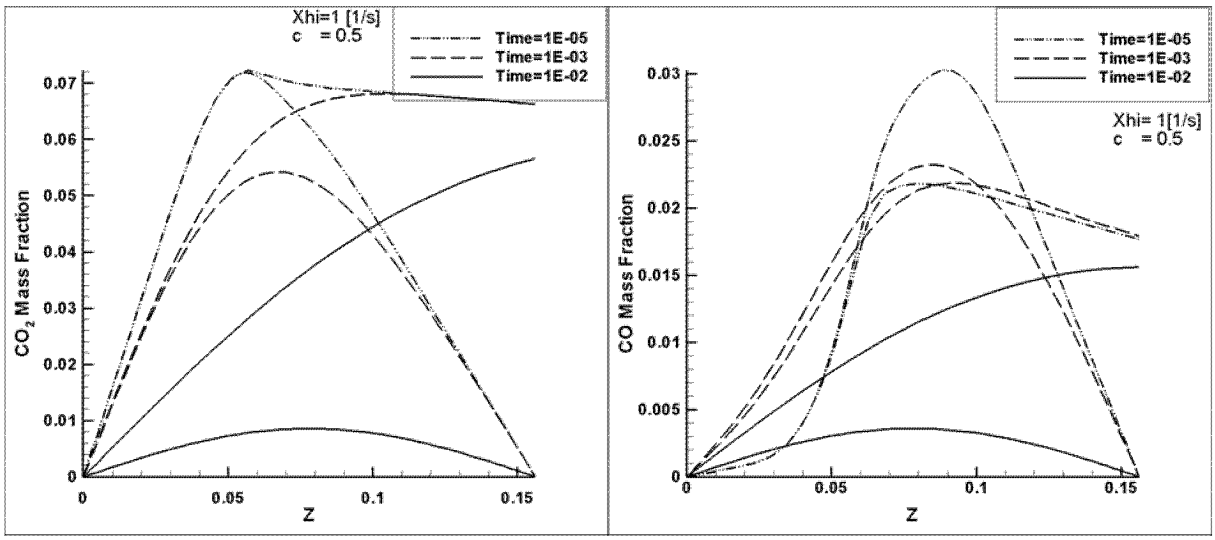

a) CO_2 mass fraction b) CO mass fraction

Figure 3.1(a-b): Time evolution of species in transient flamelet libraries for the given scalar dissipation rate and progress variable both for non-premixed and partially premixed mixtures.

The mass fraction of CO_2 follows almost the similar trend as the temperature. As the product species are related to the amount of released heat, the stable species are directly correlated with the temperature. As it is seen in figure 3.4a (evolution of flamelet from $\tau = 1e-4$ to $\tau = 1e-2$) time dependence (or response to the unsteadiness imposed by the turbulence in partially premixed flames) of the partially premixed flamelets is stronger than the pure diffusion flamelets. Due to the effects of partial premixing, CO mass fraction values are higher throughout the transient period (see Fig. 3.4b).

Figure 3.5a shows the dependence of temperature on the scalar dissipation rate at a constant residence time ($\tau = 0.001$) and progress variable ($c = 0.5$). Due to the local extinction in the flame structure, the flame temperature has lower values for the higher values of scalar dissipation rate. Because of the boundary conditions in the laminar flamelet solution of partially premixed and diffusion flames, they have different gradients in the fuel rich fields for temperature. The similar trends may be observed for CO_2 and CO mass fractions in figure 3.5(b-c). The mass fraction of minor species (CO) is detected at higher values in partially premixed libraries for the non-equilibrium conditions as expected. The CO mass fraction has a lower value for partially premixed flame compared to the pure diffusion flame at very low values of the scalar dissipation rate.

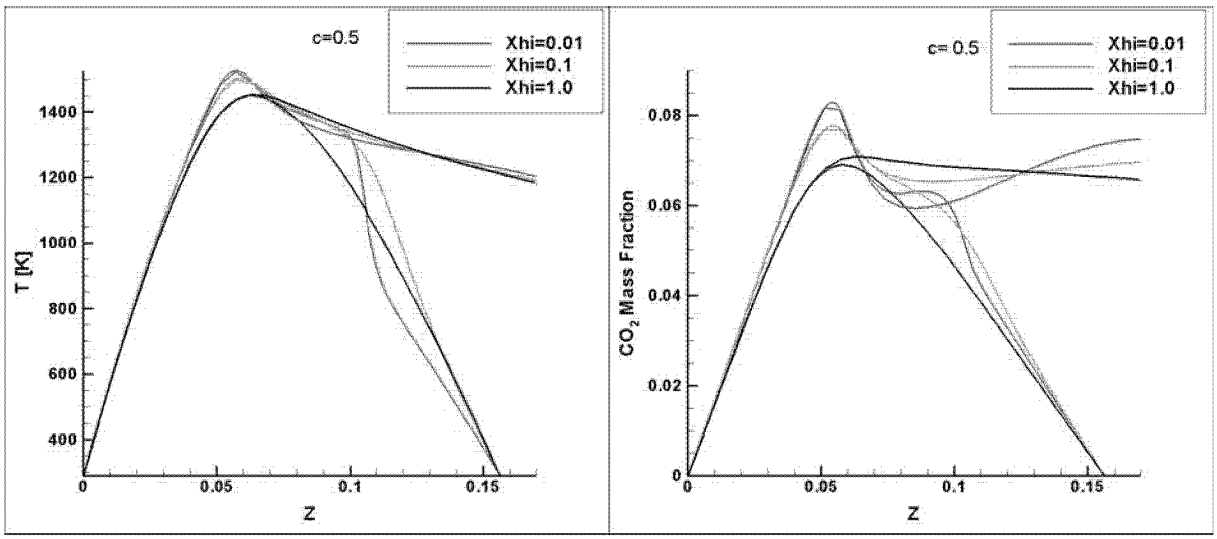

a) Temperature b) CO_2 mass fraction

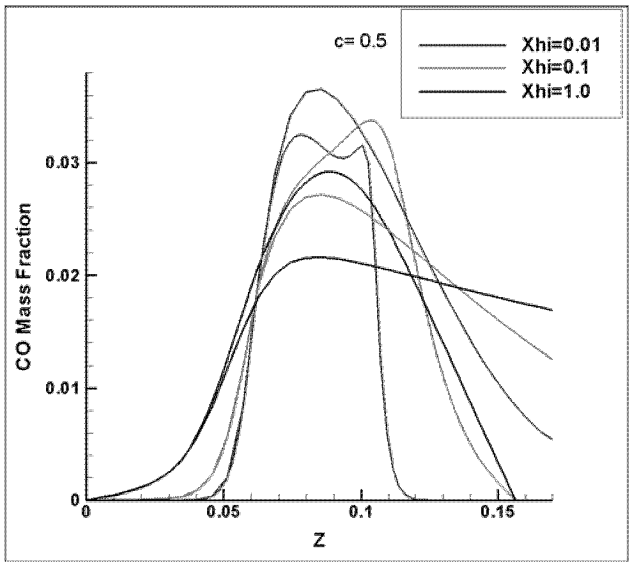

c) CO mass fraction

Figure 3.5(a-c): Effects of scalar dissipation rate changes on the scalar field in the transient flamelet libraries both non-premixed and partially premixed mixtures for the given progress variable.

Figure 3.6(a-c) shows the dependence on the progress variable of temperature and species mass fractions at a certain residence time ($\tau = \mathbf{0.0001}$). The progress variable defines the starting point of the following of the possible reactions. Temperature and product mass fraction increase with higher values of progress variable for both partially premixed and pure

diffusion libraries. Figure 3.6(b-c) shows that, non-ignited partially premixed fluid particles have a high probability to ignite in the presence of stable and unstable species. This is the idea behind the partially premixed phenomenon and it can be illustrated truly by using a transported progress variable.

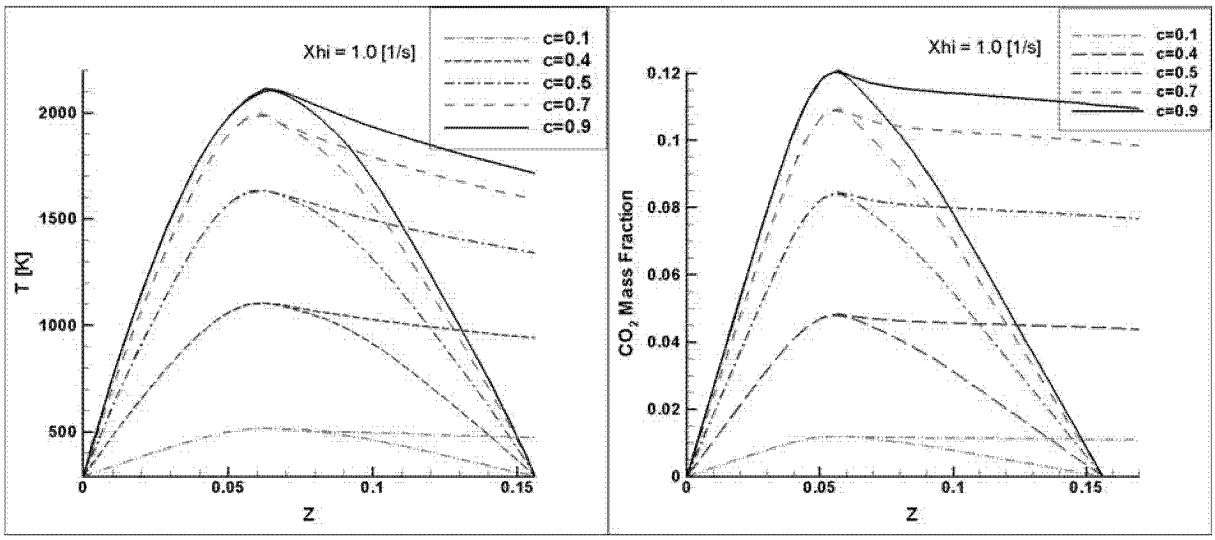

a) Temperature b) CO_2 mass fraction

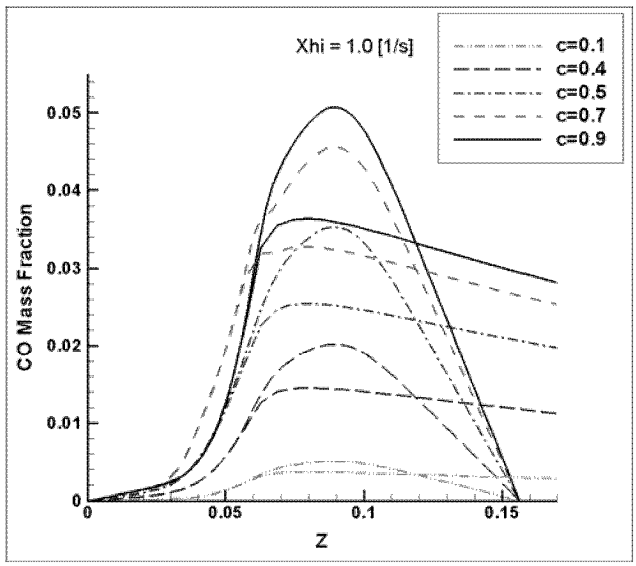

c) CO mass fraction

Figure 3.3(a-c): Effects of the progress variable changes on the scalar field in the transient flamelet libraries both non-premixed and partially premixed mixtures for the given scalar dissipation rate.

3.8. The Coupling Strategy

In this study a finite volume commercial fluid solver, CFX5.7, was used to solve the conservation equations [56] and the interface routines for coupling the TLFM were implemented into this software. Hence, the required information was passed via this software between flow solver and the flamelet libraries. The scheme of the coupling method is given in figure 3.7.

In addition to the Navier-Stokes equations, two additional transport equations for mixture fraction and the progress variable were solved in the flow solver. Therefore the solver provides vectorial and scalar data at each node in the transient turbulent flow field. Then the resolved variables were used to extract the required information such as, scalar dissipation rate, flamelet residence time, and presumed PDF shape in order to read species concentrations from the laminar flamelet libraries via the interface routines. The four variables were used with the 5^{th} order interpolation among the libraries to find the mass fractions at each node [41]. These new species mass fractions result in a different composition of the mixture; therefore, the new density field may be calculated using the ideal gas assumption. Ideal mixture properties can be calculated directly from the properties of the components and their proportions in the mixture.

An arbitrary constitutive fluid property, α, may be calculated from

$$\alpha = \sum_{i=1}^{n} \phi_i \, \alpha_i \qquad (20)$$

where α_i is the property value for the fluid component i. If the specific volume, $1/\langle \rho_i \rangle$, is used as α_i. Thus the mixture density, ρ, may be calculated from the mass fractions, ϕ_i, and the thermodynamic density, $\langle \rho_i \rangle$, of each component.

$$\frac{1}{\rho} = \sum_{i=1}^{n} \frac{\phi_i}{\langle \rho_i \rangle} \qquad (21)$$

The new density field will affect the solution of the transport equations in the next iteration step and the iteration continues until reaching the convergence. The calculations of the variables used in interface routines to interpolate the mass fractions in the flamelet libraries are described in the following sections.

3.8.1. Mixture Fraction Variable and Its Variance

The mixture fraction field is solved by a filtered scalar transport equation.

$$\frac{\partial \bar{\rho}\tilde{Z}}{\partial t}+\frac{\partial}{\partial x_j}\left(\bar{\rho}\tilde{u}_i\tilde{Z}\right)=\frac{\partial}{\partial x_j}\left\{\left(\bar{\rho}\mu_{eff}\right)\frac{\partial \tilde{Z}}{\partial x_j}\right\}-\frac{\partial}{\partial x_j}\left(\bar{\rho}(\widetilde{u_i Z}-\tilde{u}_i\tilde{Z})\right) \tag{22}$$

The unclosed term in this equation is expressed by using an Eddy Viscosity Model. So the sub-grid scale fluxes in the mixture fraction transport equation is given by

$$\bar{\rho}(\widetilde{u_i Z}-\tilde{u}_i\tilde{Z})=-\bar{\rho}D_t\nabla\tilde{Z} \tag{23}$$

where D_t is the turbulent eddy diffusivity. D_t can be determined from turbulent viscosity and a constant turbulent Schmidt number.

$$D_t=\frac{\upsilon_t}{S_{c_t}} \tag{24}$$

Turbulent eddy viscosity is defined by subgrid model in terms of filter size, Δ, strain rate, and a Smagorinsky model constant, C_s.

$$\nu_t=(C_s\Delta)^2(2\bar{S}_{ij}\bar{S}_{ij})^{1/2} \tag{25}$$

The presumed shape PDF method used to obtain mean species mass fraction values in this study requires the mean value and the sub-grid scale variance of the mixture fraction variable. Solving the transport equation for the mixture fraction variance causes an extra computational

expense. Hence, no transport equation for the mixture fraction variance is solved; this value is modelled. The sub-grid scale mixture fraction variance can be expressed as;

$$\rho\widetilde{Z''^2} = C_s\Delta^2\rho\left|\nabla\widetilde{Z}\right|^2. \tag{26}$$

3.8.2. Scalar Dissipation Rate

In the classical RANS models the scalar dissipation rate is modeled using the turbulent kinetic energy, its dissipation rate and the variance of the mixture fraction;

$$\widetilde{\chi} = C_\chi \frac{\tilde{\varepsilon}}{\tilde{k}}\widetilde{Z''^2} \tag{27}$$

where the time scale ratio C_χ is assumed to be constant. The suggested values are $C_\chi = \mathbf{1.0}$ or $C_\chi = \mathbf{2.0}$ by Jones [57] and Janika [58] respectively.

In the present study a sub-grid scale model is introduced for the instantaneous scalar dissipation rate in non-premixed turbulent reacting flows. The scalar dissipation and its dependence on laminar and turbulent fields are described by using scalar and vectorial quantities estimated locally from the Favre-filtered field. The instantaneous scalar dissipation rate is generally defined as in Eqn. (10). In the proposed method the diffusivity has been described by molecular and turbulent diffusivities of the species.

$$\widetilde{\chi} = 2\left(D_m + D_t\right)\left(\nabla\widetilde{Z}\right)^2 \tag{28}$$

where D_m and D_t represent molecular and turbulent diffusivities respectively. In this study, the molecular diffusion dependence of scalar dissipation is predicted based on well-known Chapman-Enskog kinetic theory by using the empirical relation [59]. In this formula, the molecular diffusion coefficient is expressed in terms of temperature, pressure, molecular

weight of species, M_i, and diffusion volumes of molecules, V_i. This theory is accurate to an average of about eight percent [59].

$$D_m = 10^{-3} \frac{T^{1.75}\left(1/\tilde{M}_1 + 1/\tilde{M}_2\right)^{1/2}}{p\left[\left(\sum_i V_{i1}\right)^{1/3} + \left(\sum_i V_{i2}\right)^{1/3}\right]^2} \tag{29}$$

In order to define the turbulent part of the scalar dissipation equation a sub-grid diffusivity equation is proposed. The sub-grid diffusivity can be determined from equations (24) and (25).

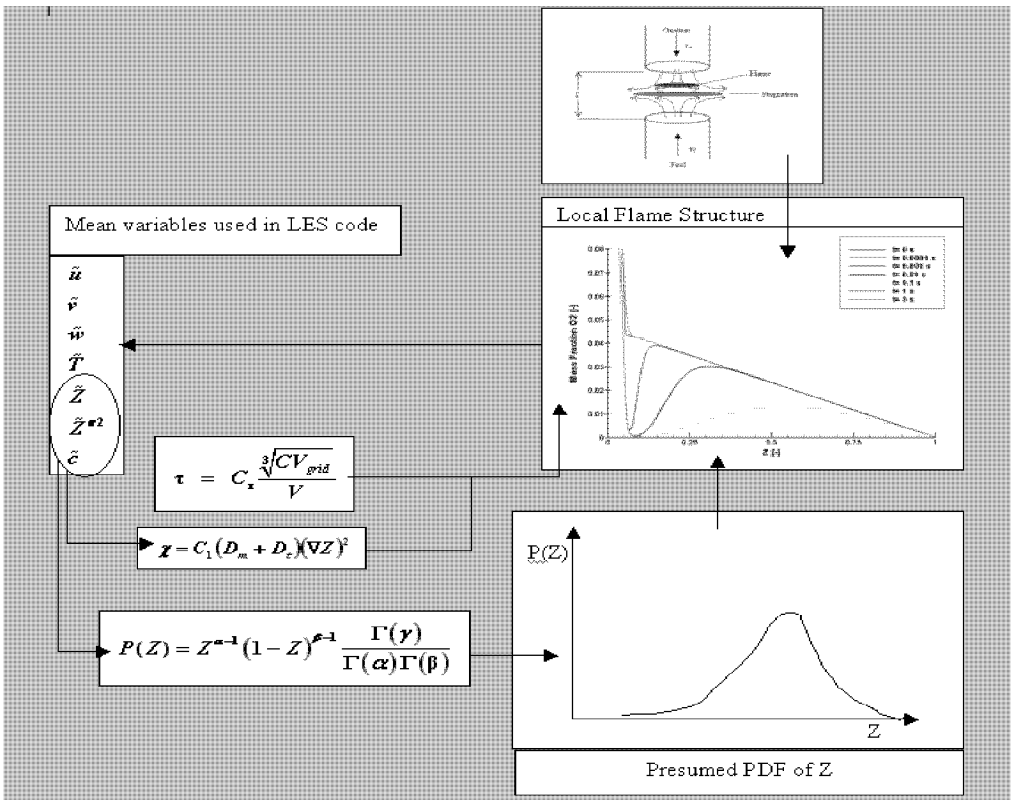

Figure 3.1: Flow chart of coupled TLFM/LES model

3.8.3. The Residence Time

The introduced residence time of the fluid particles in the turbulent flow field is assumed to be statistically independent from the local mixture fraction. The residence time of a fluid particle in the computational grid cell is introduced as:

$$\tau_r = C_\tau \frac{\sqrt[3]{(\Delta_1 \Delta_2 \Delta_3)}}{V} \tag{30}$$

with $C_\tau = 1.0$, where $\Delta_1, \Delta_2, \Delta_3$ are increments in the spatial directions and V is the velocity. The post processing results show that turbulent time scales of RANS calculations such as; $\tau \propto \tilde{k}/\tilde{\varepsilon}$ are greater than the residence time by two orders of magnitude. Actually, this is the inherent advantage of using instantaneous residence time definition instead of the turbulent time scales of RANS.

3.8.4. Progress Variable

In order to complete the intrinsic information about the chemical reactions and to account for the finite rate chemistry variations within iso-surfaces of the mixture fraction field, a last variable introduced to the model is the reaction progress variable. The mixture fraction cannot account for chemical variations in the directions perpendicular to gradient of mixture fraction even though assumptions such as fast chemistry or steady flamelet state relationships are needed to associate a chemical state with the mixture fraction. So the chemical variations must be mimicked and tracked by a new non-conserved variable, the progress variable, which is defined independently from the mixture fraction. It is obtained from an additional scalar transport equation with a source term designed to capture the local re-ignition states.

$$\frac{\partial \bar{\rho}\tilde{c}}{\partial t} + \frac{\partial \bar{\rho}\tilde{u}_j\tilde{c}}{\partial x_j} = \frac{\partial}{\partial x_j}\left\{\left(\bar{\rho}D + \frac{\mu_t}{Sc_t}\right)\frac{\partial \tilde{c}}{\partial x_j}\right\} - \frac{\partial}{\partial x_j}(\bar{\rho}(\widetilde{u_i c} - \tilde{u}_i\tilde{c})) + \bar{S}_c \tag{31}$$

The unclosed term is modelled as it is in the mixture fraction transport (Eqn. (23)).

$$\bar{\rho}(\widetilde{u_i c} - \tilde{u}_i \tilde{c}) = -\bar{\rho} D_t \nabla \tilde{c} \tag{32}$$

The source term is defined so as to imitate the competition between extinction and re-ignition states [60].

$$\begin{aligned} \bar{S}_c &= 1/\tau \cdot (c_{fl} - \tilde{c}) \qquad \text{if} \quad c_{fl} - \tilde{c} > 0 \\ \bar{S}_c &= 0 \qquad\qquad\qquad\quad \text{if} \quad c_{fl} - \tilde{c} \leq 0 \end{aligned} \tag{33}$$

where c_{fl} is a given state of reaction progress, which is evaluated from the transient library.

$$c_{fl} = 1 - \frac{Y_F(\tilde{Z},\chi,\tilde{c},\tau)}{Y_{F,unb_{max}}} \tag{34}$$

where F, and unb_{max} denote fuel, and maximum mass fraction of the unburned state at the inlet respectively. The source term in Eqn. (31) has the function to make the transported value of c equal to the local value c_{fl}, Eqn. (34).

3.8.5. The Presumed PDF Method

The presumed shape PDF method is used to obtain mean values of the reactive scalars, $\widetilde{\phi_i}$. The mean of any scalar quantity, which depends on the mixture fraction, may be calculated as

$$\widetilde{\phi_i}(x,t) = \int_0^1 \phi_i(Z)\widetilde{P}(Z;x,t)dZ \tag{35}$$

Using the previously defined four variables instead of the mixture fraction variable alone, Eqn. (35) can be extended to Eqn. (36).

$$\tilde{\phi}_i = \int_0^1 \int_0^1 \int_0^\infty \int_0^\infty \phi_i(Z,c,\chi,\tau)\tilde{P}(Z,c,\chi,\tau)\,dZ\,dc\,d\chi\,d\tau \tag{36}$$

The joint probability density functions of the four variables are considered to be independent of each other. Therefore, it is assumed that the probability density functions of them are not

correlated [36]. This assumption seems a priori very crude. In fact, statistical independence is verified very well in direct numerical simulations. The mixture fraction **Z** measures the reactants mixing and is mainly related to large-scale flow motions. On the other hand, χ is linked to the local flame structure and corresponds to a local **Z** gradient and measures the local diffusion zone thickness and is governed by small-scale features. The progress variable, **c**, tracks the non-conserved scalars and transports the information of thermo chemical history. It also shows the probability of possible reactions. The residence time, τ, reflects the unsteady feature of the interactions between strain rate, which is imposed by the turbulent flow field, and thermo chemical effects. The new form of the equation reads:

$$\widetilde{\phi}_i = \int_0^1 \int_0^1 \int_0^\infty \int_0^\infty \phi_i(Z,c,\chi,\tau).P(Z).P(c).P(\chi).P(\tau)dZ\ dc d\chi\ d\tau \qquad (37)$$

P(Z) represents the fluctuations of the mixture fraction and is assumed as a β-distribution function. The scalar dissipation rate, χ, and the reaction progress variable, **c**, and the residence time, τ, are represented by a delta function. The mass fractions of the species are computed locally at each node by applying an interpolation algorithm among the unsteady flamelet libraries of the FLATRA code [41].

3.9. The Alternative Coupling Strategy

The introduced alternative coupling strategy is different from the normally used flamelet coupling models. The disadvantage of the classical method is the computational expenses due to the integration of the presumed shape PDFs. The transported values of turbulent flow variables are solved and model parameters are calculated at each node. These variables and parameters are firstly interpolated between flamelet libraries and then the findings of these interpolation processes are integrated at each node using Eqn. (37). These interpolations and following integration steps which depend on mixture fraction variance only take most of the computational time and make the computation very expensive.

Because of the vast number of processes at each node, the number of the species and that of nodes are limited in the classical coupling strategy to keep the computation time in reasonable limits. The introduced alternative coupling method is a good solution to reduce computational costs while increasing the number of nodes and species used in the simulation study. Apart from that, this method creates a great opportunity to increase the nodes in discretization of the parameters such as as, Z, Z''^2, χ, c and τ. In this new method, several hundred thousand different artificial solutions are created for the discretized interface parameters. The detailed schematic description of the coupling strategy is given in the figure 3.8.

In this method the user determines the discretized data points for the interface parameters with respect to the requirements of the problem. The user can select as many data as he wants according to his own criteria. There is no limit for the amount of data points. It might be only limited by the maximum size of the data set, which can be stored in the memory of that specific machine. The number of the discretized data for the interface parameters do not create extra load during the computational process. The discretized parameters within the selected ranges defined for the problem such as in table 3.1 are combined with each other. Then, using these combinations, interpolations between the flamelet libraries and the integration of those interpolated parameters have been calculated in Eqn. (37). In this study, $70x9x11x13x9 = 810810$ artificial possible solution sets are created and stored in the pointers for the different combination of the parameters, which are listed in table 3.1, to find the mass fractions of the species corresponding to those discretized values. This work is completed before starting to solve Navier-Stokes (NS) equations in the flow solver.

The flow solver solves NS equations with additional two scalar transport equations for mixture fraction and reaction progress respectively and creates the interface variables to the libraries such as, Z, Z''^2, χ, c and τ at each nodal position. Then, using these variables the solution field is determined and a 6^{th} order interpolation is applied to get mass fractions of the species at that node (see Appendix A). The mass fraction of these new species results in a different composition of the mixture. Therefore, the new density field may be calculated using ideal gas assumption. The new density field will affect the solution of the transport equations in the next iteration step and the iteration is continued until reaching the convergence.

Variable Name	Selected Range	Total number of values
Mixture Fraction (Zmix)	[0, 0.1563]	70
Mix. Frac. Variance (Zvar)	[5E-5, 1E-3]	9
Progress Variable (c)	[0, 1]	11
Scalar Dissipation Rate (χ)	[1E-3, 15]	13
Residence Time (τ)	[1E-5, 0.1]	9

Table 3.1: The combination of the variable in the artificial solution field.

Our simulation studies show that the new method considerably increases the speed of the simulation up to 30 times compared to the classical method. The saving of the computational time gives the possibility to invest more computation time in finer grids. The filter size of the LES is the grid size in this study. Eddies which have smaller turbulent length scale than the filter (grid) size are modelled, whereas the bigger size eddies are solved directly. So the finer mesh makes the simulation more reliable while solving the turbulent flow field equations in LES. The alternative coupling strategy offers this opportunity to its users.

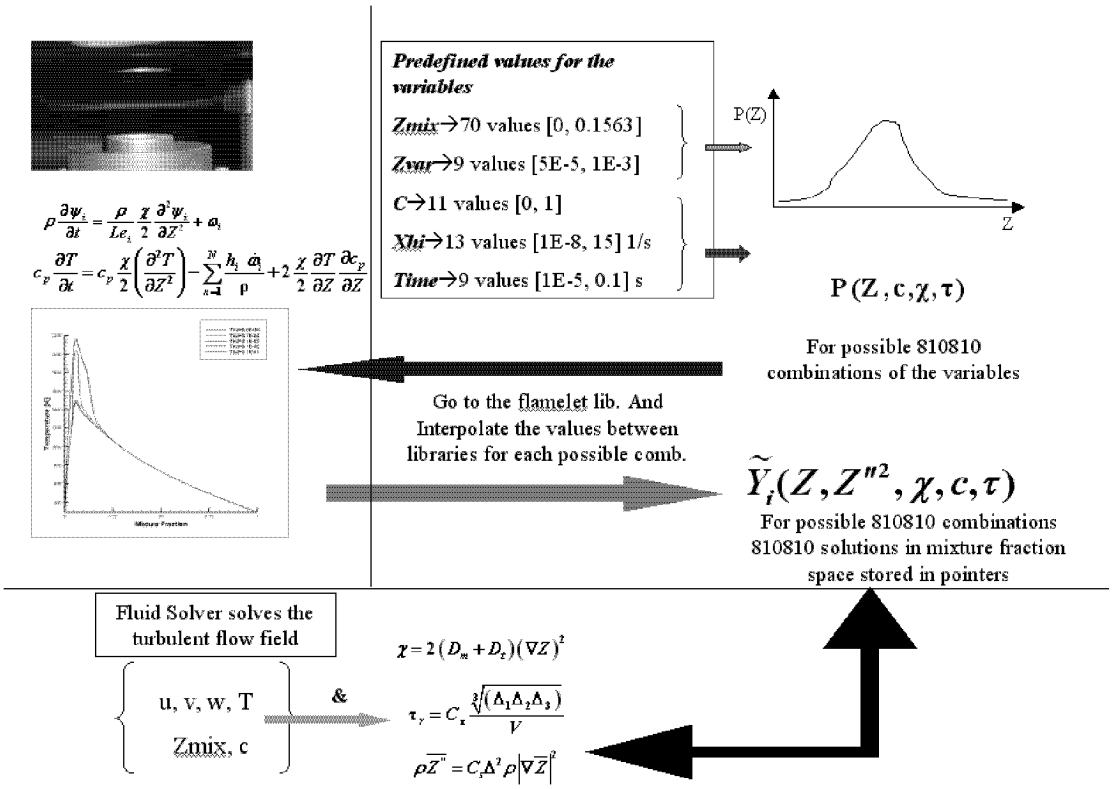

Figure 3.8: The new flow chart of coupled TLFM/LES model using pre-calculated solution fields.

Chapter IV

Analysis of the Sandia Flames (D, E, F)

4.1. Burner Types

Turbulence, chemical kinetics, thermal radiation and pollutant formation interact simultaneously with spaces of complex geometries and boundary conditions inside a combustor. The burners used in the combustion research studies tend to simplify these complex geometry and boundary condition problems. Various burner types used to study turbulent diffusion flames are described in this section. These are jet burner, pilot-stabilized burner and bluff-body burner.

The jet burner is the simplest have been performed most common burner on which the original studies of turbulent non-premixed flames. It consists of a simple stream of fuel surrounded by a co-flowing stream of air. There are several studies with this type of burners to investigate transition to turbulence and associated instabilities [61-63]. This burner has been also used to study the effects of differential diffusion on the flame structure [64]. The jet burner is used to study soot formation and thermal radiation if the jet velocity is small enough to create laminar flames. If the jet velocity is very high, it is possible to reach blow off conditions and study the lifted flame stabilizations [65].

The piloted jet burner produces a simple streaming flow. The stabilization of the main jet is issued using a heat source from a set of premixed flames. The burner consists of an axisymmetric jet centered in an annulus in which a number of premixed flames are stabilized on a flame holder. The burner is centered in an unconfined co-flowing stream of air. This type of burners is useful for studying the effects of the interaction between turbulence and chemistry in flames without added complications of soot formation and thermal radiation. Very high main jet exit velocities force the flames to be extincted in certain downstream

regions where turbulent mixing time scales become the same order of magnitude as in the chemical time scales. Further downstream of the extinction zone reignition of the flame may occur due to less intense turbulent mixing rates.

Bluff-body burners show a great similarity to practical combustors used in industrial applications. This type of burner provides a flame suitable for the study of turbulence chemistry interactions. The burner is centered in a co-flowing stream of air and usually consists of a circular bluff-body with an orifice at its center for the main fuel. The recirculation zones provide stabilization of the flame. These recirculation zones are created by the turbulent flow field inside the burner due to the configuration of burner boundaries and inlet velocity profiles. The length of the recirculation zones is about one bluff body diameter. As it was discussed in piloted jet flames, extinction and re-ignition states in the flame may also be detected in the bluff body burners.

4.1.2. Experimental Details

A detailed understanding of the combustion mechanisms requires an accurate diagnosis of the combustion system with well-organized measurement techniques. Techniques which have been used to generate extensive time-resolved data in flames include: Laser-Doppler Velocimetry (LDV) for velocity; Absorption and Phase-Doppler methods for measuring particle number density and size distribution; Raman-Rayleigh scattering for mixture fraction, temperature and the concentration of major species; and Laser Initiated Fluorescence (LIF) for the concentration of radicals and some minor species.

Under the enlightment of the previous discussions in order to capture unsteady thermo chemical dynamics of highly turbulent flow fields and investigate local extinction and re-ignition states, a set of piloted flames provided by Sandia Laboratories were selected in this work. The model validation study for the introduced model was performed on the Sandia D, E and F flames (see table 4.1). These partially premixed methane/air flames have different velocities in the main jet and pilot. The possibility of local extinction increases from flame D to F. Selected flames have significant probability of local extinction above the pilot region, with flame F being close to global extinction of the downstream part of the flame [66]. The measured scalars in the Sandia flames include temperature, mixture fraction, N_2, O_2, H_2O, H_2,

CH_4, CO, CO_2, OH, and NO concentrations. The data set includes axial and radial profiles of Reynolds- and Favre-average mass fractions and rms fluctuations, conditional statistics at each streamwise location, and complete single-shot data for all measured scalars. Two component laser-Doppler anemometry (LDA) measurements in flames D, E, and F were performed at the Technical University of Darmstadt [67].

The burner geometry is the same as used in numerous previous investigations of piloted flames at Sydney University and Sandia Laboratories [66,68]. It is given in figure 4.1. The jet fluid is a mixture of three parts air and one part CH_4 by volume. Partial premixing with air also reduces the flame length and produces a more robust flame than the pure CH_4 or the nitrogen-diluted CH_4. The equivalence ratios are high enough for these flames to burn as diffusion flames, with a single reaction zone near the stoichiometric mixture fraction and there is no indication of significant premixed reaction in the fuel-rich CH_4/air mixtures. Flame D (Re=22400) has a small degree of local extinction [66]. Flame F is close to global extinction of the downstream part of the flame. The pilot is a lean (ϕ=0.77) mixture of C_2H_2, H_2, air, CO_2, and N_2 with the same nominal enthalpy and equilibrium composition as methane/air at this equivalence ratio.

The piloted burner has a main jet diameter of d_j=7.2 mm and a pilot jet diameter of d_p=18.2 mm (see Figs 4.(1-2)). The detailed flow parameters are given in table 4.1. The measurements provide the users with the axial profiles of scalar measurement in these three flames includes locations x/d = 5, 10, 15,…,75. The radial profiles were obtained at x/d = 1, 2, 3, 7.5, 15, 30, 45, 60, and 75 in each flame.

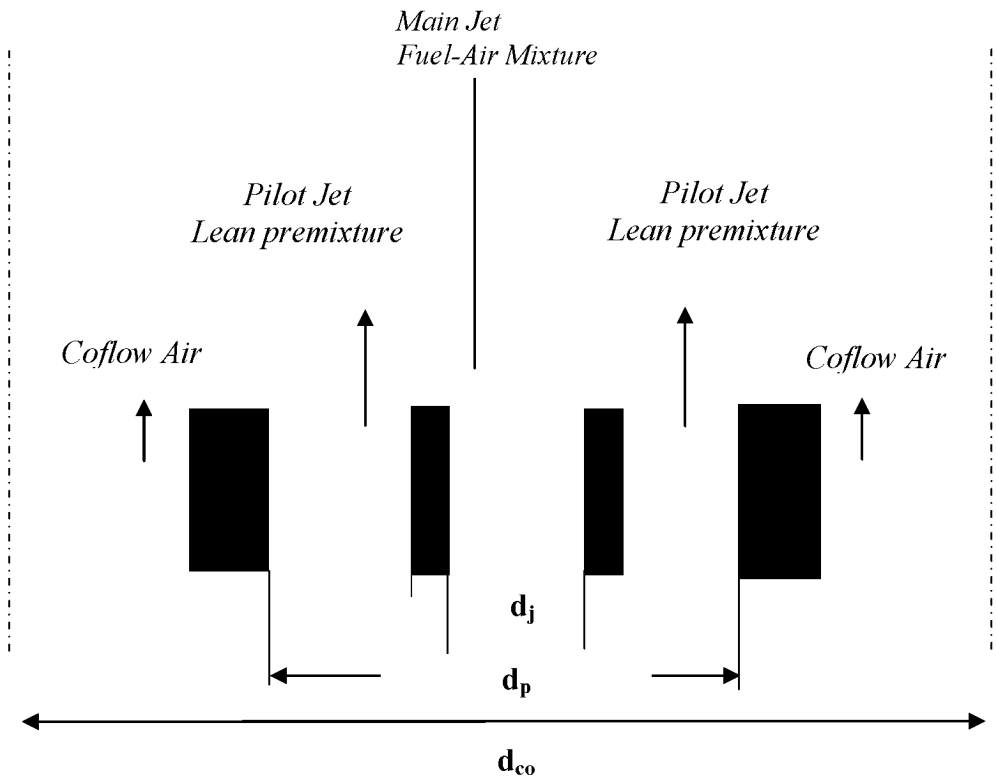

Figure 4.1: Schematic configuration of piloted jet flames (d_j: main jet diameter, d_p: pilot jet diameter, d_{co}: coflow diameter).

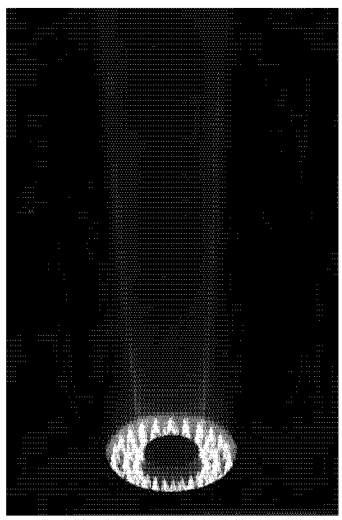

Figure 4.2: The picture of Sandia piloted jet flames.

Flame Name	$Re_{mainjet}$	$U_{mainjet}$(m/s)	U_{pilot} (m/s)	$U_{co\text{-}flow}$ (m/s)
D	22400	49.6(+/- 2)	11.4(+/- 0.5)	0.9(+/- 0.05)
E	33600	74.4(+/- 2)	17.1(+/- 0.75)	0.9(+/- 0.05)
F	44800	99.2(+/- 2)	22.8(+/- 1.0)	0.9(+/- 0.05)

Table 4.1: Sandia flames flow parameters.

4.2. Computational Domain

4.2.1. Initial and Boundary Condition Setup

The computational domain covers a cylindrical area with a radius of $20d_j$ (20d) in radial direction and length of 70d in axial direction (see Fig. 4.3). The challenge in the Sandia E and F flames is the simulation of high gradient regions. The orthogonality in the computational domain is guarantied by using O-grid [100]. In the selected geometry, the main and the pilot jet regions are considered as critical regions that cover a circular area of (~10d). Therefore the square of the O-grid is placed in this region and 51 uniform nodes divide the edges of the square. The co-flow region is meshed with coarser grids relative to main and pilot jets. Two hundred nodes are distributed parabolically along the centerline.

Several steps have been followed while generating the initial conditions. Firstly, the commercial codes flamelet model based on the classical flamelet approach and RANS model is used with all additional reactive and non-reactive scalars. The central difference advection scheme is not selected at the early stages of the simulation because of the convergence criteria. A varying blend between upwind and central difference schemes is chosen using a blending factor. In flow regions with low gradients, the blend will be close to second order advection scheme for accuracy. In areas where the gradients change sharply, the blend will be closer to first order advection scheme to prevent overshoots and undershoots to maintain robustness. After the robustness is established, the result of the last time step is used as an initial condition in the final simulation. The transient scheme is defined by the second order backward Euler transient scheme. The simulation is started with 1.0e-4 second constant time step and then it drops to the level adjusted to the CFL conditions given in Eqn. (1).

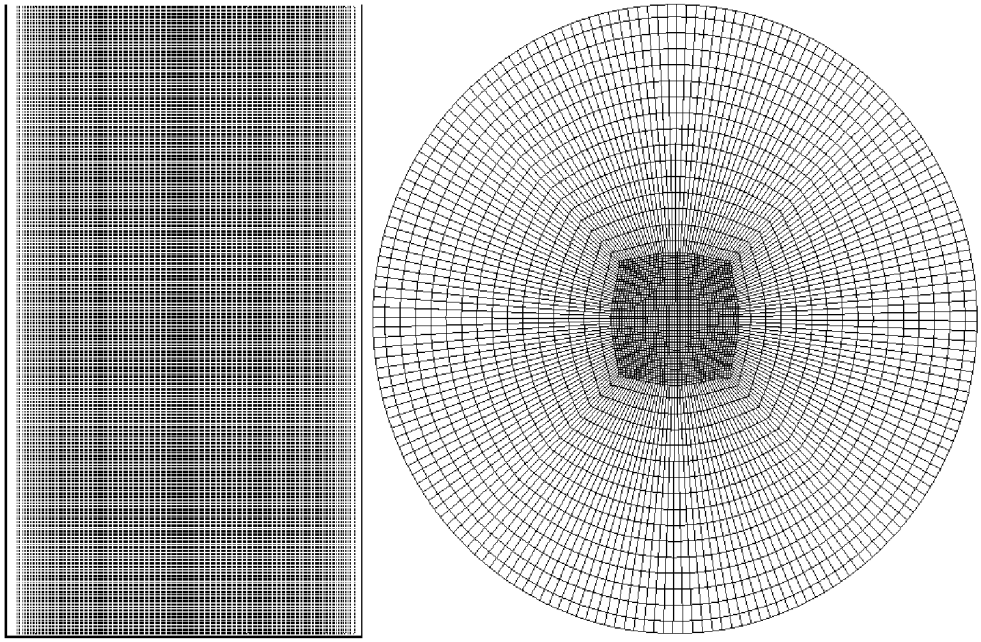

Figure 4.3: The front and bottom views of the computational domain.

$$CFL = \frac{u\,\Delta t}{\Delta x} + \frac{\nu\,\Delta t}{\Delta x^2} \qquad (1)$$

The inflow boundary is introduced by using mean quantities according to the experimental data field given in the Sandia database [68]. Superposing random perturbations on individual mean velocity component mimics the stochastic components of the flow at the velocity inlet boundaries. Similar calculations are repeated without the stochastic components and only slight changes in the flow field are noted as discussed in [14]. The stochastic components of the flow at the velocity-specified inlet boundaries are accounted for by superposing random perturbations on individual velocity components as:

$$\overline{u_i} = <\overline{u_i}> + \mathrm{I}\psi\left|\overline{u}\right| \qquad (2)$$

where I is the intensity of the fluctuation, ψ is a Gaussian random with $\overline{\psi} = 0$, and $\sqrt{\overline{\psi}} = 1$.

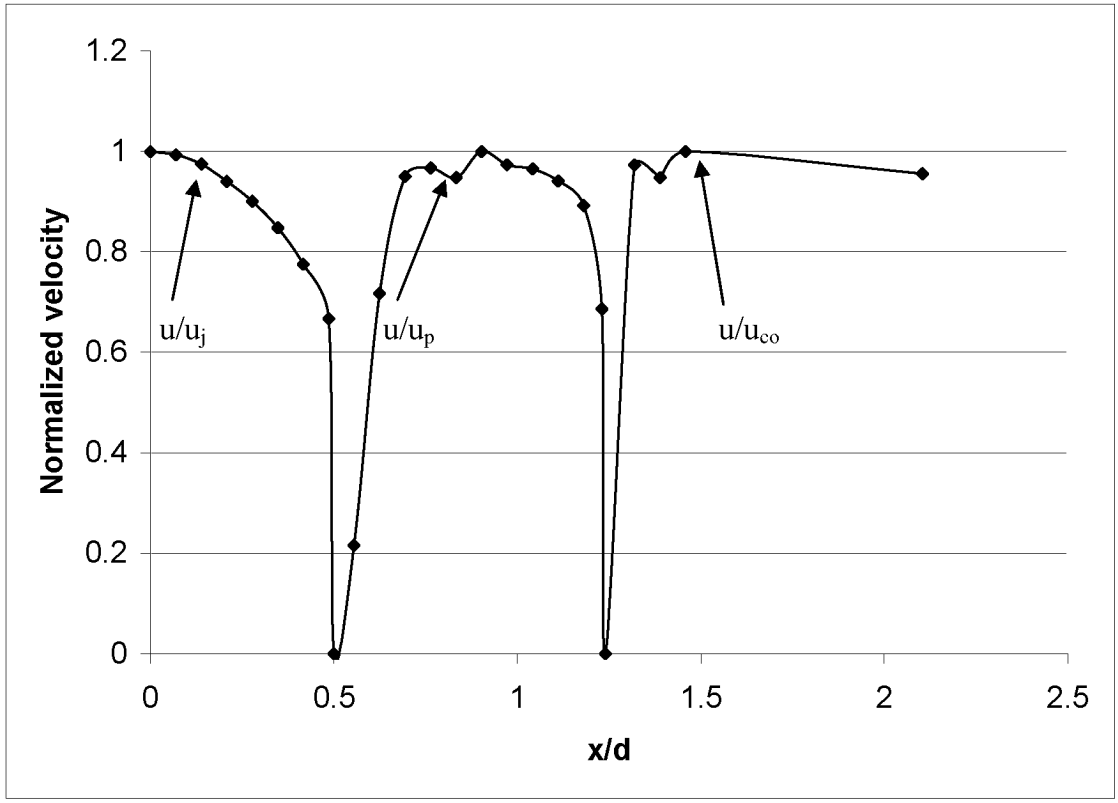

Figure 4.4: Normalized inlet velocity profiles.

The Reynolds normal stresses $\widetilde{u'u'}$ and $\widetilde{v'v'}$ are inferred from experimental data of 2D-LDV measurements [67], the other normal stress is taken to be equal to $\widetilde{u'u'}/2$. Figure 4.4 presents the inlet boundary conditions normalized by their local centreline velocities (u_j, u_p, u_{co}) and main jet diameter, d. The co-flow air boundaries are set wide enough (20d) to be sure that the boundary specifications do not influence the main jet profile. The constant pressure gradient is applied at the exit plane as it is described in the experiment [66]. The detailed inflow boundary conditions are presented in table 4.2 for the scalar variables.

Boundary conditions other than the inlet conditions include non-reflective boundaries with zero inflow and free slip boundaries, which are implemented at the outlet and the sides respectively.

Scalars	Main Jet stream	Pilot stream	Co-flow stream
Temperature [K]	294	1880*	291
Pressure [atm]	0.993	0.993	0.993
CH_4**	9.7472E-3	0.0	0.0
O_2**	6.1407E-3	1.6997E-3	7.3718E-3
N_2**	2.3101E-2	2.6220E-2	2.7053e-2
H_2O**	0.0	5.2311E-3	3.4773E-4
CO_2**	0.0	2.4960E-3	0.0
CO**	0.0	1.4506E-4	0.0
H_2**	0.0	6.4026E-5	0.0
H**	0.0	2.5010E-5	0.0
OH**	0.0	1.6507E-4	0.0

Table 4.2: Specification of inlet boundary conditions for D, E and F flames.

* The main jet inlet temperature for F flame is given as 1860 [K].

** Specific mole numbers $\left(Y_i / W_i\right)$.

The same geometry and mesh are used for all the flames worked on in this thesis. The different time steps are selected by considering CFL numbers and the main jet velocities of each flame. These time steps are $\Delta t = 1x10^{-4}\ s$, $\Delta t = 0.67x10^{-4}\ s$ and $\Delta t = 0.5x10^{-4}\ s$ for flames D, E, and F respectively. The CFL number was computed based on axial convection and diffusion in Eqn. (1). The runs were performed in HP Superdomes Stardust and Pegasus machines. These machines have Itanium-2 processors at 1.5GHz speed and totally 96 processors. Because of user limitations we could not exceed 14 processors at a time. So, one iteration for a simulation with 917,420 nodes takes almost six minutes depending upon the load of the machines.

4.3. Results and Discussions

Time averaged results of the simulation are discussed and compared with the experimental data in the following sections. The comparison studies are summarized under two topics, the first pertains to the the axial profiles and the second to the the radial profiles. The averages have been calculated from the instantaneous flow field solutions by sampling over two flow-

through times, where the flow-through times is defined as the time a fluid particle travelling along the centerline would reside within the flow field [14].

Mixture fraction is also a conserved scalar that is representative of other conserved scalars in the flow. Almost all of the experimental data sets are configured in terms of the normalized mixture fraction instead of the transported one. The Sandia piloted jet flames data fields contain mixture fraction data in terms of Bilger mixture fraction definition [68]. This mixture fraction is normalized for the partially premixed situation. They use a bit different form of mixture fraction rather than the classical Bilger mixture fraction definition by adding the elemental mass fractions of hydrogen and carbon into the equation. In the case of neglecting differential diffusion, as it is in our study, hydrogen and carbon based mixture fraction presents the same results compare to the original definition introduced by Bilger [68].

$$F = \frac{0.5(Y_H - Y_{H,2})/W_{TH} + 2(Y_C - Y_{C,2})/W_{TC}}{0.5(Y_{H,1} - Y_{H,2})/W_{TH} + 2(Y_{C,1} - Y_{C,2})/W_{TC}} \qquad (3)$$

where

Y_H = H element mass fraction in the measured sample

Y_C = C element mass fraction in the measured sample

$Y_{H,1}$ = H element mass fraction in main jet stream

$Y_{C,1}$ = C element mass fraction in main jet stream

$Y_{H,2}$ = H element mass fraction in co-flow stream

$Y_{C,2}$ = C element mass fraction in co-flow stream and

$W_{TH} = 1.008$, $W_{TC} = 12.011$ are atomic weights.

The stochiometric value for the given mixture fraction definition lies at $F = 0.351$.

4.4. Flame D

4.4.1. Centerline Axial Profiles

The mean axial velocity profile along the centerline is given in figure 4.5a. The good agreement of the velocity flow field has also aided the prediction of the conserved scalar, the mixture fraction. This is a clear advantage of LES approach. The mixture fraction has the ability to account for turbulent advection in diffusion flames (Fig. 4.5b). The mixture fraction is a conserved scalar that is representative of other conserved scalars in the flow such as total enthalpy or the mass fraction of a particular chemical element. Therefore the quality of the prediction of the mixture fraction field strongly affects the temperature and mass fraction of the species in the far downstream field region of the jet. At this region ($x/d > 45$) the important phenomenon is mainly turbulent mixing rather than the chemical kinetics. Because most of the reactions have been completed, the mixture fraction and dissipation rate control the mixing process and the temperature in the far downstream flow field. Actually good agreement in the mixture fraction field gives an early indication of better prediction in the mixing dominated part, the far downstream region, for temperature and the main stable species, CH_4, O_2, CO_2, and H_20. On the other hand, to map the partially premixed process in the fuel rich part of the domain ($x/d < 40$), an extra parameter has to be taken into account, herein the progress variable. The progress variable can account for chemical variations in directions perpendicular to mixture fraction gradient [98]. Because of the lack of detailed information of reaction progress or the information of transported burned and unburned structures in the flame front, the classical flamelet libraries, which are determined by mixture fraction and scalar dissipation rate alone, may not reflect the partially premixed and partially reacted processes [14, 69]. The model, which is used in this study, can be viewed as a remedy to mimic the partially premixed effects in the fuel rich zones (see Fig. 4.5c).

Figures 4.5b and 4.5c present the calculated scalar fields both from our simulation and Pitsch's flamelet model. The results of Pitsch's simulation are scanned from his paper [14] by using free software WinDig [101]. The predictions of the mixture fraction field along the centerline are almost the same for these two models. The near downstream results of Pitsch's model for the mixture fraction show a better agreement as compared to our model (see Fig. 4.5b). When two calculated temperature data are compared with the experiment, it is very

clear that the near downstream region temperature predictions are in agreement with the presented model. Although the mixture fraction field is predicted better in Pitsch's model, the partial premixing phenomenon is captured better in our coupling model. This is mainly due to the additional chemically dynamic parameter which is called progress variable in our model.

A new definition is introduced in our model for post-processing of the study of chemical dynamics: the reactedness parameter. This parameter gives a measure of reaction progress as a composition of reactive scalars in Eqn. (4). This parameter may follow the chemical dynamics and show their deviations from the quasi equilibrium state. It should be noted that the classical steady state flamelet models assume that this parameter is always equal to one.

$$\mathbf{R} = 1 - \left\{ \frac{\min\left(\frac{Y_{O_2}}{s}, Y_{CH_4} \right)}{Y_{CO_2} + \min\left(\frac{Y_{O_2}}{s}, Y_{CH_4} \right)} \right\} \qquad (4)$$

The reactedness of a mixture is defined in terms of mass fraction of main stable species and it varies between zero for frozen and one for fully burnt mixtures. Therefore a proper way of tracking interactions between the turbulent flow field and chemical dynamics is implemented into the model as a part of post process study. There are similar studies in the literature to detect the locally extinct fluid parcels [70, 71]. However, they mainly focus on a kind of progress variable definition based upon the premixed combustion theory and the conditional PDFs of this defined variable. Detailed studies on those definitions are made in chapter 5.

Figure 4.5d presents the reactedness both for calculated from simulation and inferred from experimental data. Our model tracks the chemical dynamics very well at the near downstream region mainly up to x/d < 25. This behavior is also observed for the temperature field (Fig. 4c). The overprediction of fuel, CH_4, may cause the underprediction of the products at the near downstream region, (Fig. 4.5e). The correlation between experiment and simulation data field is observed at the far downstream region, x/d > 45, where the main reactions have been completed.

All flamelet models are based upon the thin reaction zone assumption. It implies a fast chemistry in the reaction dynamics. So the radicals, or unstable species, such as CO may not be predicted in a perfect sense. These species are produced and consumed during relatively very slow reactions. One way to capture these reactions can be to solve separate transport equations for these species as a post processing procedure. On the other hand, the mass fractions of the interim species are predicted at higher values than the experimental results in Reynolds average models [41]. This is mainly due to definition or modeling approach of scalar dissipation rate and the residence time. The scalar dissipation rate is expressed in terms of the instantaneous scalar gradients in LES unlike to combination of the averaged scalar variance and turbulent time in RANS. Our post-process studies show that the ratio between those two scalar dissipation rate definitions is the order of 100. The higher dissipation rates in LES pick up lower minor species mass fraction values from the libraries (see Fig. 3.5c).

The calculated higher interim species mass fraction values may also be observed in LES simulations [14], if one uses a conditional residence time definition or a kind of integrated time definition along the line of stiochiometric mixture fraction values such as in Eqn (5).

$$\tau = \int_0^x \frac{1}{\left\langle \tilde{u}_{\tilde{Z}} \middle| \tilde{Z}_{st} \right\rangle (x',t)} dx' \qquad (5)$$

This type of time definitions tracks the flamelets in the physical space only along with the stoichiometric mixture fractions. The stoichiometric mixture is found inside the piloted jet region at the downstream zone not along the centerline (Fig. 4.5h). The higher velocities are expected and observed along the centerline rather than the radial directions. This method implies much lower velocities in the formula, Eqn. (5), than reality. So the model assumes longer residence time and as a consequence of this longer residence time it promotes the slower reactions to produce interim species. One of the drawbacks of this type of model may be observed in terms of overprediction of temperature along the centerline at near downstream region due to the estimation of a longer residence time.

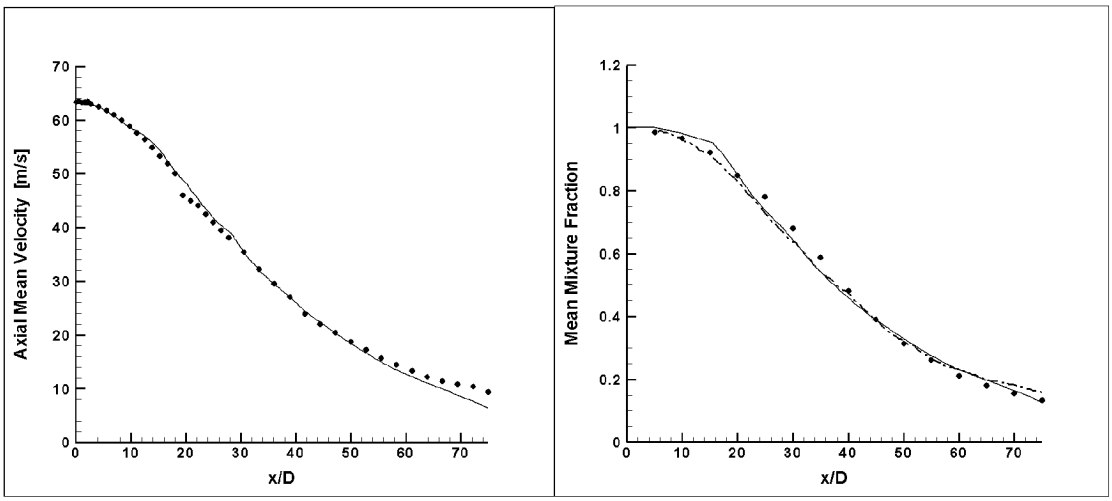

a) Velocity b) Mixture fraction

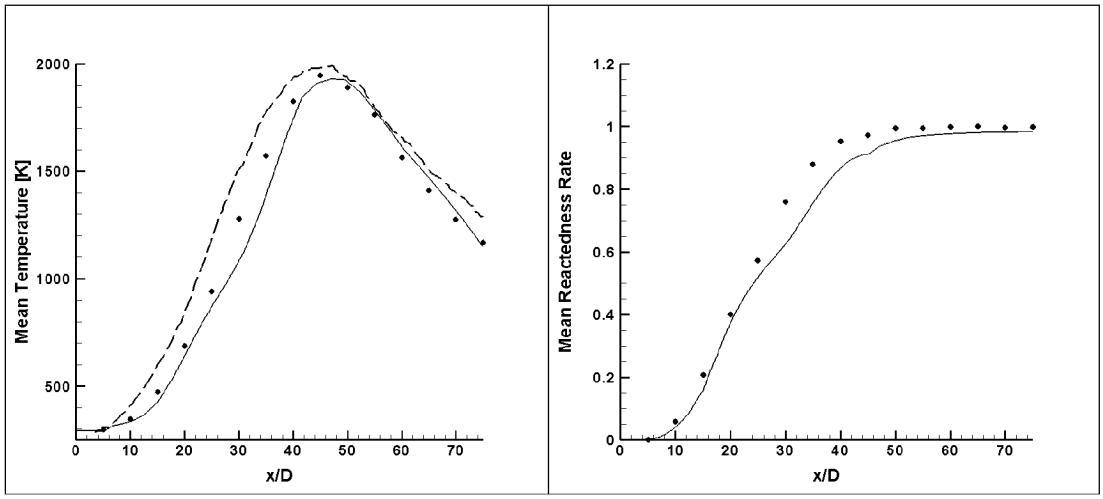

c) Temperature d) Reactedness

Figure 4.5(a-d): Mean values of scalars along the centreline (lines: simulation; symbols: experiments; long dash lines: Pitsch's simulation for b and c [14]).

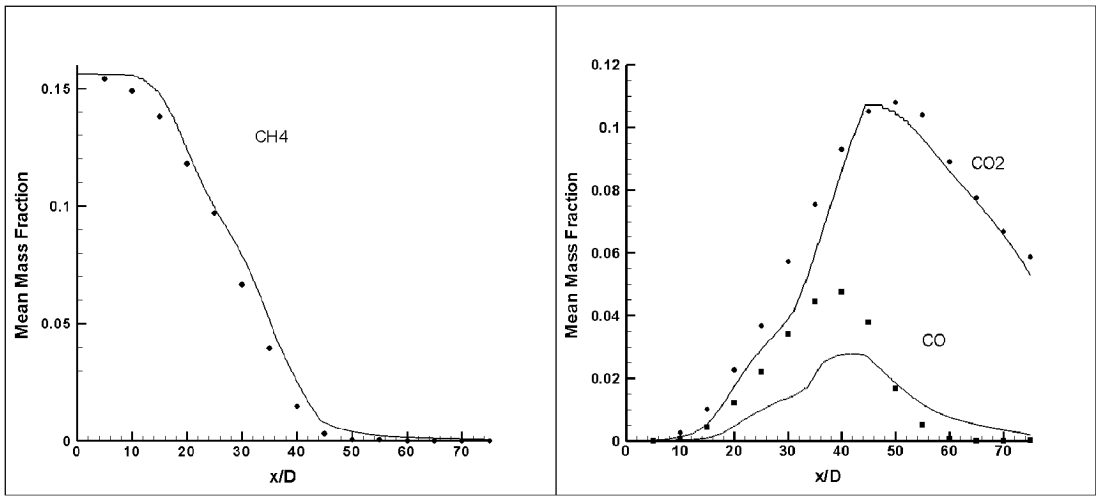

e) CH_4 mass fraction

f) CO_2 and CO mass fractions

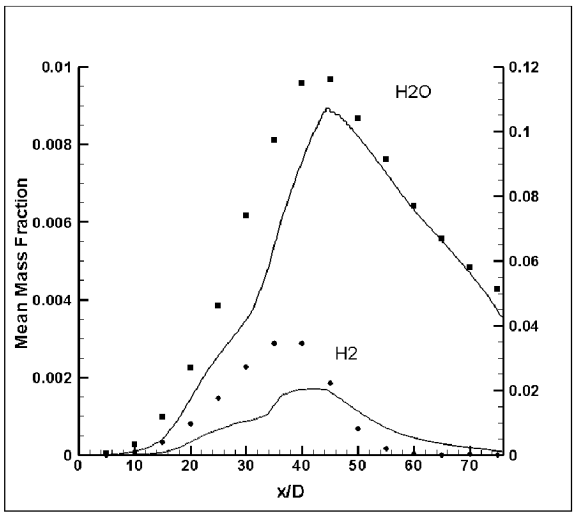

g) H_2O and H_2 mass fractions

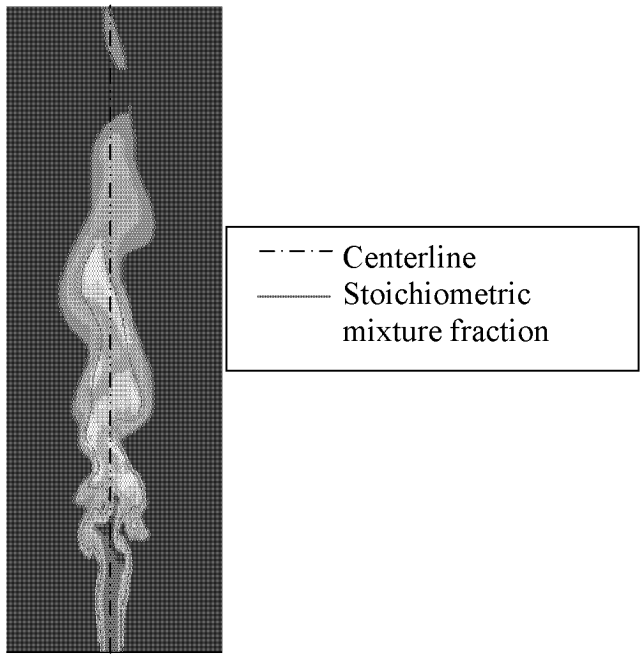

h) Plane sketch of mixture fraction

Figure 4.5(e-h): Mean values of scalars along the centreline (lines:simulation; symbols:experiments).

4.4.2. Radial Profiles

The comparison between radial profiles of the mean values of simulated scalars and the experimental data are presented and discussed in the following paragraphs. The comparison of the radial profiles at x/d=15 for the species mass fractions and temperature with experimental data shows good agreement in figures 4.6(a-d). There is an overprediction in temperature profile around its peak value in figure 4.6a. However, if the fuel, CH_4, mass fraction curve is checked in figure 4.6b, the calculated CH_4 mass fraction reaches its minimum value at exactly the same radial location where the temperature peak occurs. Apart from this, there are not enough experimental data points in the neighborhood of these maximum and minimum values in figure 4.6a and 4.6b respectively. The mass fractions for the minor species were under predicted on the fuel rich side because of the reasons discussed previously.

Figures 4.7(a-f) present the radial profiles at x/d=30 both for simulation and experiments. The partial premixing starts to affect the chemical dynamics in this region and leads to the classical flamelet models to predict higher temperature profiles especially in the fuel rich region [14, 68, and 72]. On the other hand, the models considering partial premixing phenomena may predict the temperature field on the fuel rich side (Fig. 4.7a). Except the interim species, H_2 and CO, the quality of the predictions for other scalars in the fuel rich part is in agreement with the experiment. This is not only the effect of the progress variable definitions used to mimic the partial premixing process, but also the definition of residence time individually for each cell to reflect the unsteady feature of the interactions between strain rate and thermo chemical effects.

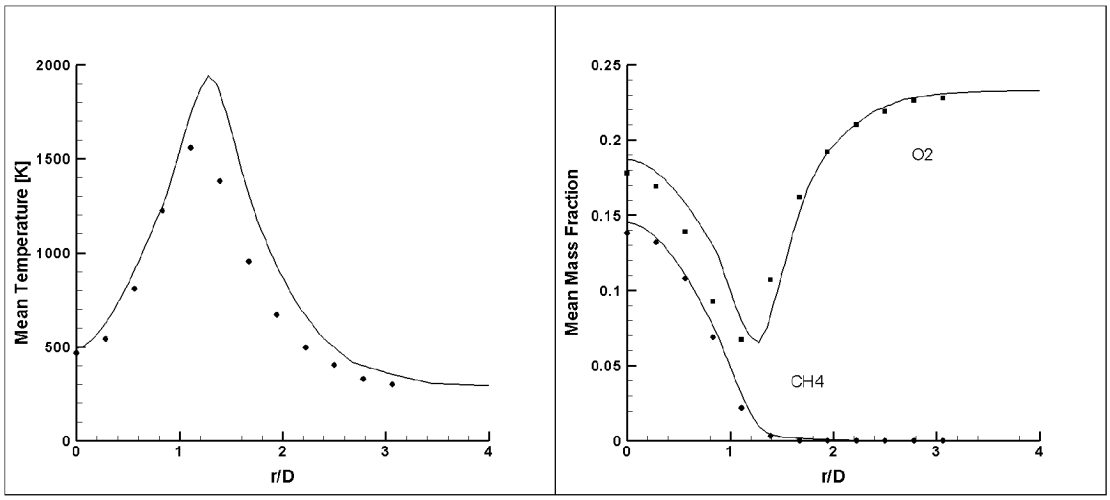

a) Temperature

b) CH_4 and O_2 mass fractions

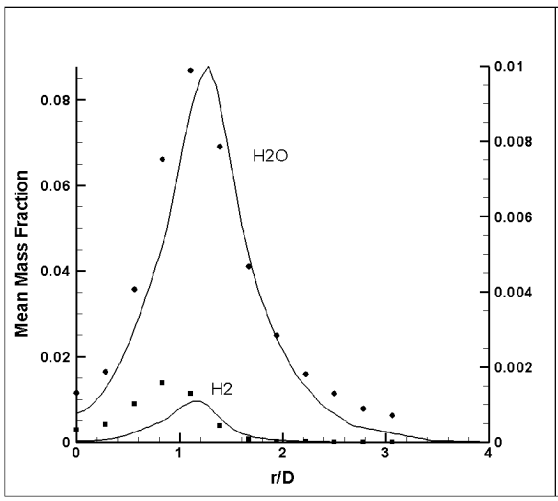

c) H_2O and H_2 mass fractions

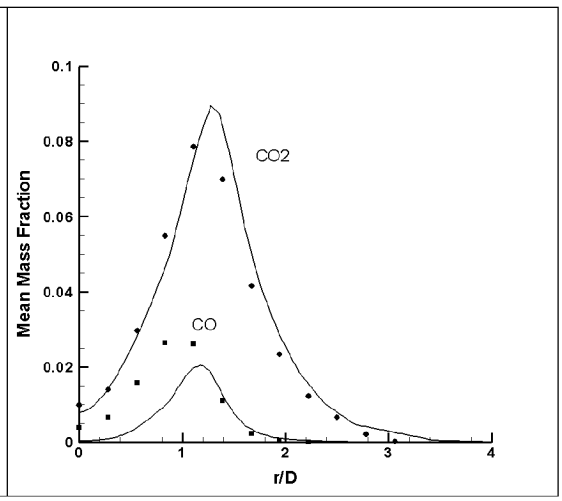

d) CO_2 and CO mass fractions

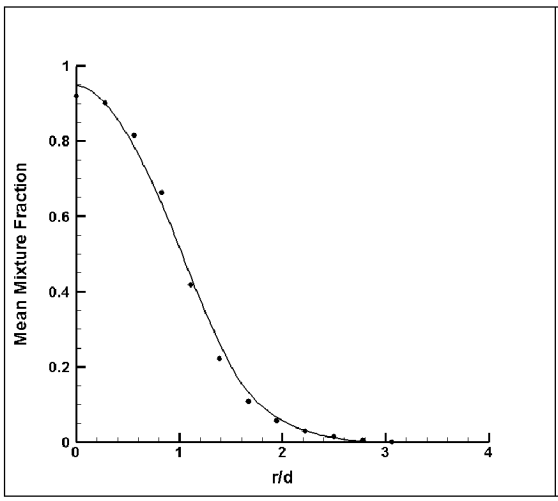

e) Mixture fraction

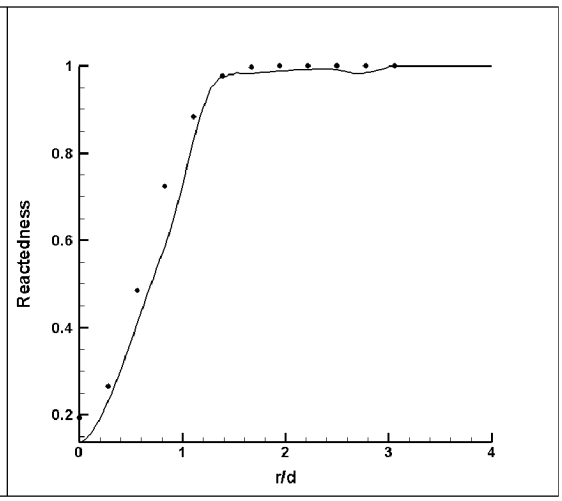

f) Reactedness

Figure 4.6(a-f): Radial distribution of mean values of scalars at x/d=15 (lines: simulation; symbols: experiments).

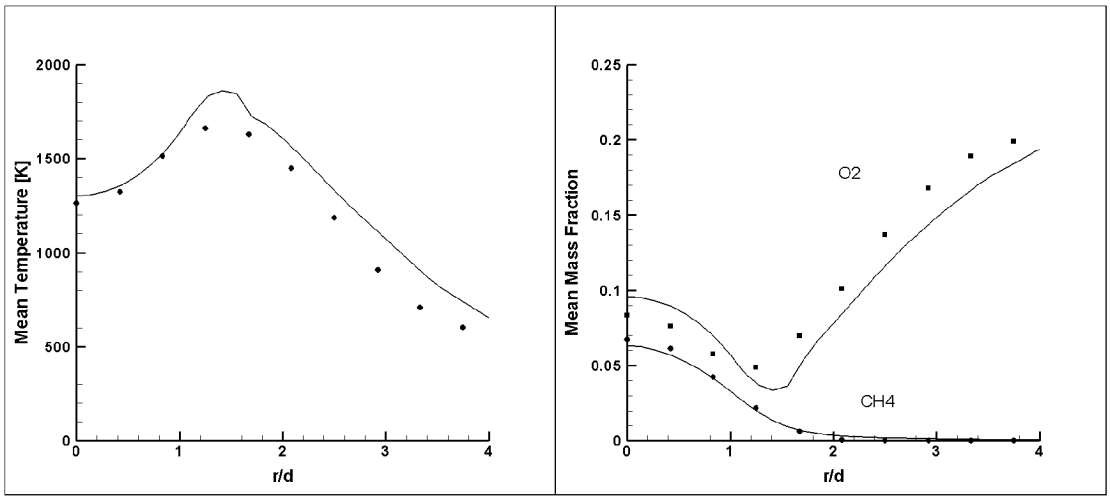

a) Temperature

b) CH_4 and O_2 mass fractions

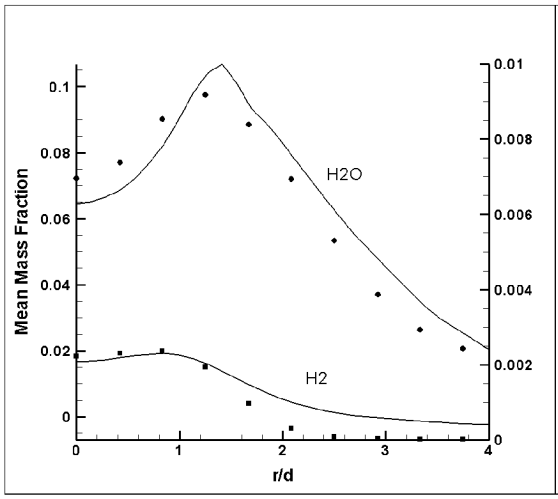

c) H_2O and H_2 mass fractions

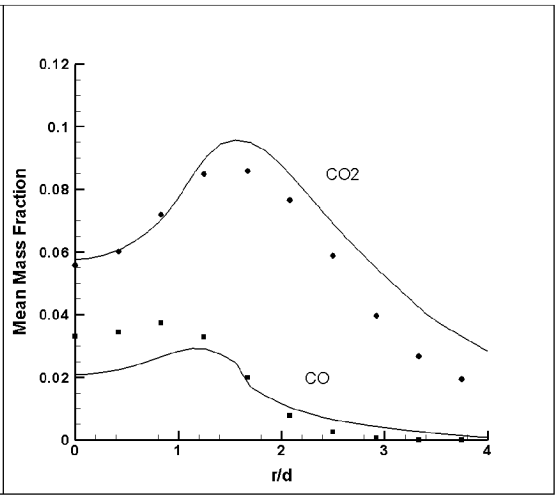

d) CO_2 and CO mass fractions

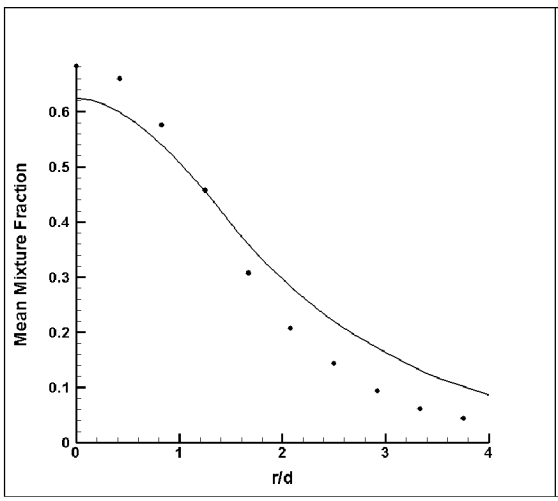

e) Mixture fraction

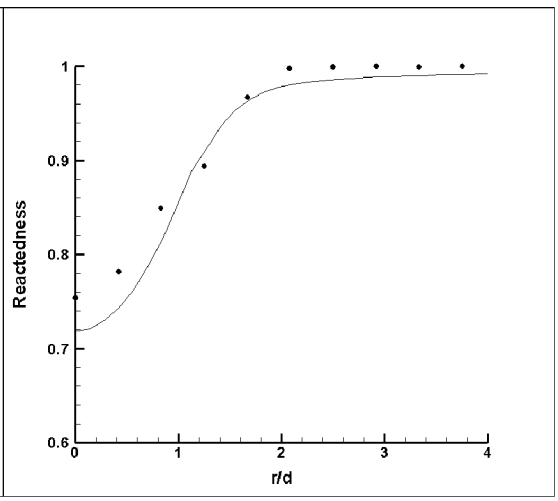

f) Reactedness

Figure 4.7(a-f): Radial distribution of mean values of scalars at x/d=30 (lines: simulation; symbols: experiments).

The radial profiles at x/d=45 are depicted in the figures 4.8(a-d). The partial premixing still affects the species distribution due to the diffusion of the species. The effect of the diffusion process compared to convective transport becomes stronger when the fluid parcels travel downstream. This phenomenon is discussed in bimodality analysis in the chapter 5. It is obvious that the quality of the predictions along the centreline affects the radial profiles directly. The higher and lower time averaged values in mean scalar quantities at this radial profile are the main consequence of over and under predictions of those scalar quantities at x/d=45 axial distance (see Fig. 4.5(a-h)).

4.4. Flame E

4.4.1. Centerline Axial Profiles

The same post processing methods used in the flame D are followed for the analysis of the flame E. There are two differences between the models used for the simulation of those two flames. These are the definition of progress variable and reactedness. Apart from this, the flamelet libraries used in the simulation of E and F flames are designed for the partially premixed flames unlike to diffusion flamelet libraries used in flame D. All changes have been done to improve the prediction of scalars in the fuel rich mixtures where the partial premixing, local extinction and reignition phenomena are frequently observed. The dynamic analysis of local extinction and reignition phenomena are comprehensively investigated in the next chapter.

The definition of progress variable is replaced by a new definition based upon the reactedness (Eqn. (6)). The definition of reactedness used in the post process study of flame D, is replaced by the definition in Eqn. (6) for the analysis of the flame E and F.

$$\mathbf{R} = \mathbf{1} - \left\{ \frac{\mathbf{min}\left(\frac{Y_{O_2}}{s}, Y_{CH_4} \right)}{Y_{CO_2} + Y_{H_2O} + Y_{H_2} + Y_{CO} + \mathbf{min}\left(\frac{Y_{O_2}}{s}, Y_{CH_4} \right)} \right\} \qquad (6)$$

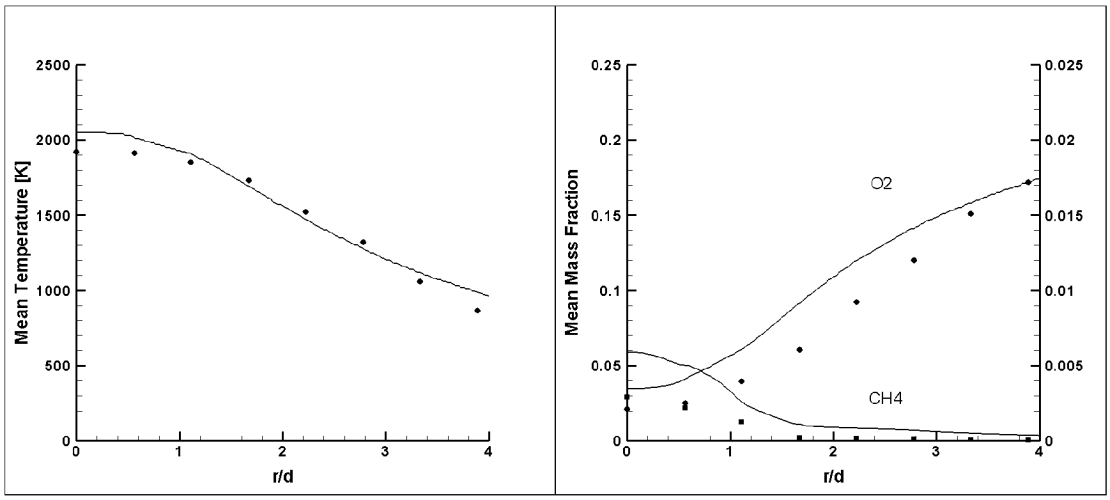

a) Temperature

b) CH_4 and O_2 mass fractions

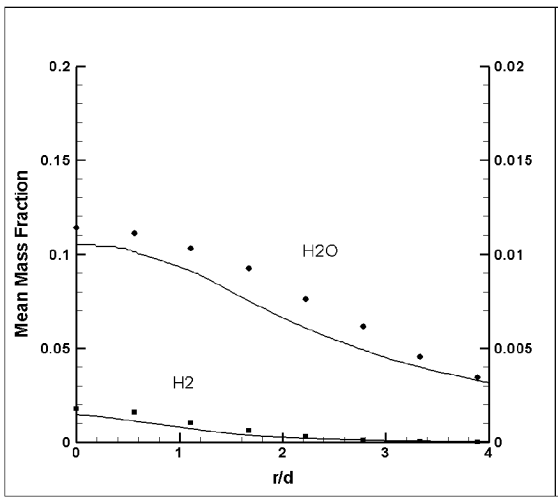

c) H_2O and H_2 mass fractions

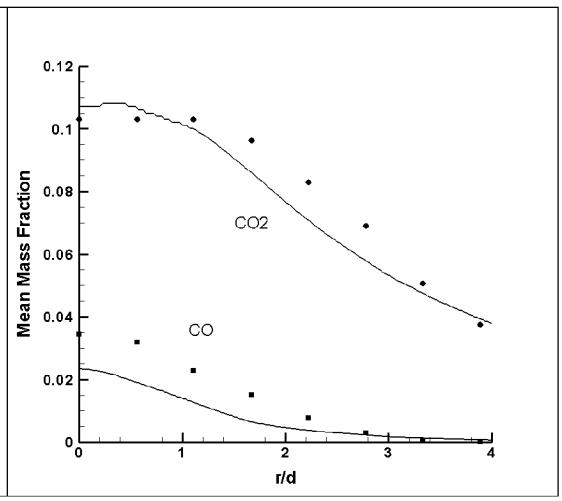

d) CO_2 and CO mass fractions

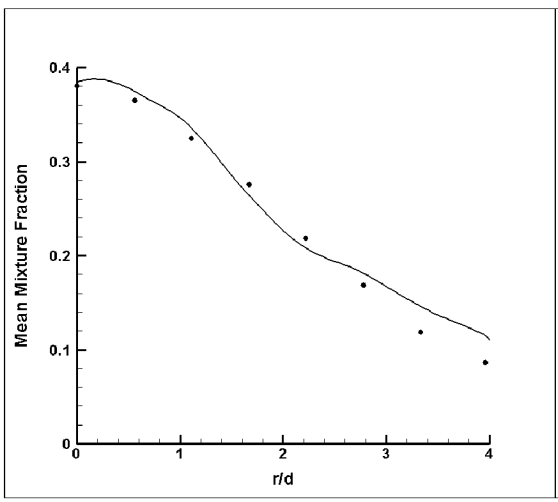

e) Mixture fraction

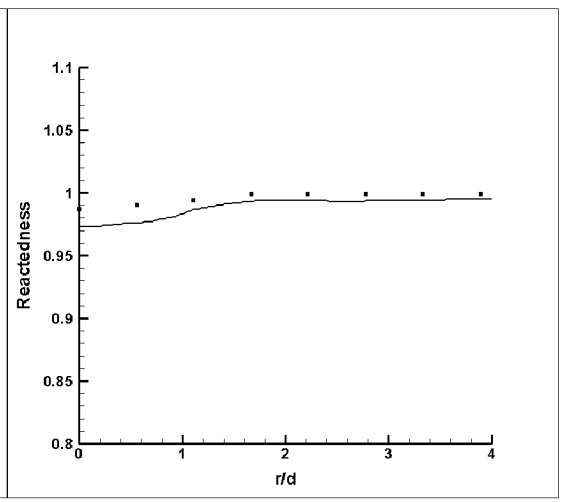

f) Reactedness

Figure 4.8(a-f): Radial distribution of mean values of scalars at x/d=45 (lines: simulation; symbols: experiments).

This new definition for both reactedness and progress variable is more complex and includes more information due to the addition of minor species in the denominator. It might be a better way to track the partially premixing of stable and interim species in the unsteady reacting turbulent flow field.

The time-averaged results calculated from reacting turbulent flow field are compared with the experimental data along the centerline. The same method described in the post processing study of the flame D is applied here. The mean axial mixture fraction profile along the centerline is given in figure 4.9a. It presents a good agreement with the experimental data. There are slight underpredictions at around x/d=10 and 45. The agreement between experimental and calculated data fields for mixture fraction variable along the centerline increases the quality of prediction of the other scalar fields such as temperature in figure 4.9b. The overpredicted temperature at far downstream region correlates with the overprediction of mixture fraction at the same region.

The agreement between calculated and experimental data for reactedness parameter along the centerline demonstrates the quality of the tracking of reaction kinetics in the partially premix region (Fig 4.9c). Due to the mismatching of the mixture fraction at very near downstream location x/d=10, the CH_4 mass fraction is underpredicted in the same region. The consumption of the fuel is generally captured well along the centerline (Fig 4.9d). The other main products CO_2 and H_2O are estimated very well except the underestimated H_2O mass fraction around the stoichiometric mixture in figure 4.9(e-f).

The improvements in the quality of the prediction of scalar fields may be due to the combined effects of the changes in the reactedness, the progress variable, and especially the changes in the flamelet libraries. The detailed discussions on different types of libraries were made in chapter 3. Very clear indication of the effects due to the changes in the flamelet libraries from pure diffusion to partially premixed may be observed in the prediction of interim species, CO and H_2 in figure 4.9(e-f). So the under-estimated interim species along the centerline in the flame D (Fig.4.5(f-g)) may be due to the lack of the true information of higher scalar gradients in the pure diffusion laminar flamelet libraries for the fuel rich side (Fig. 3.4, chapter 3).

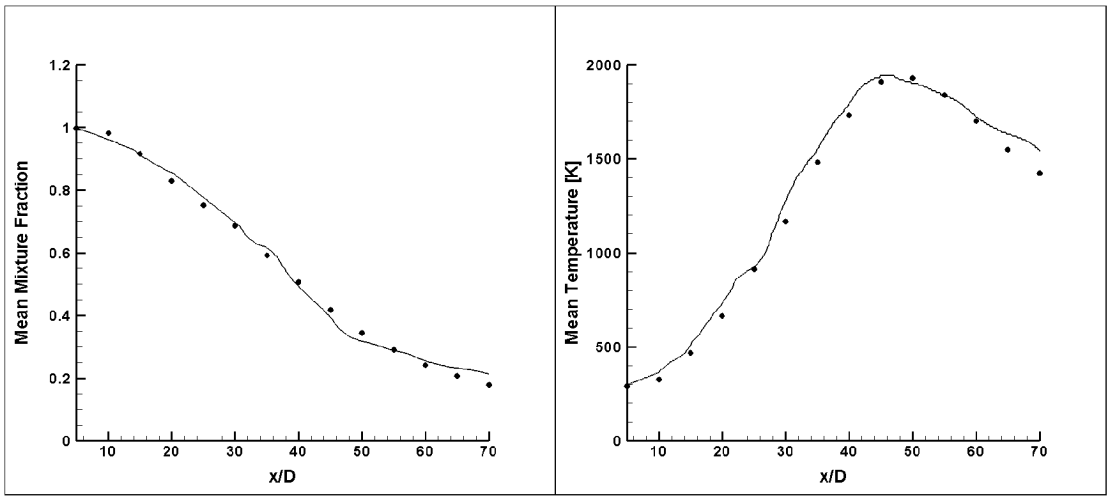

a) Mixture fraction

b) Temperature

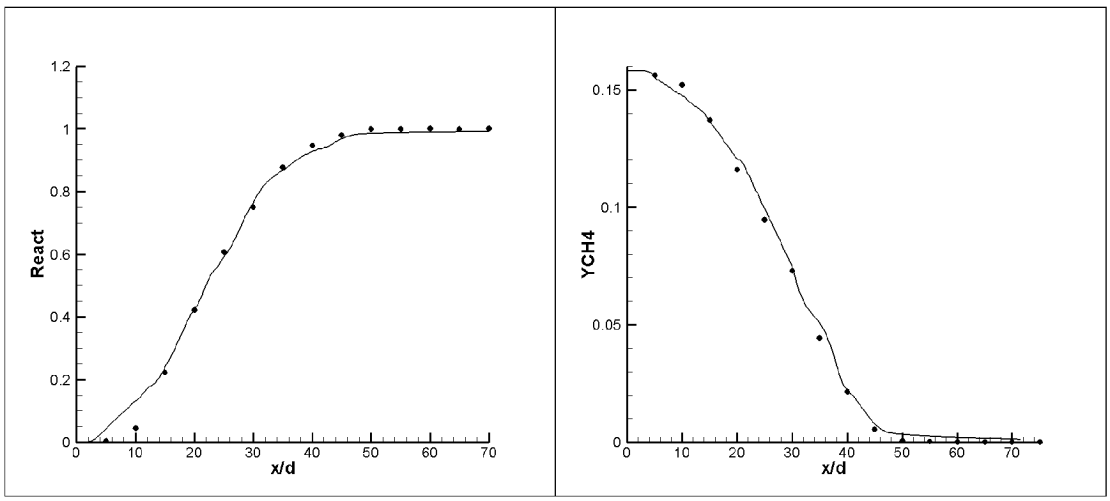

c) Reactedness

d) CH_4 mass fraction

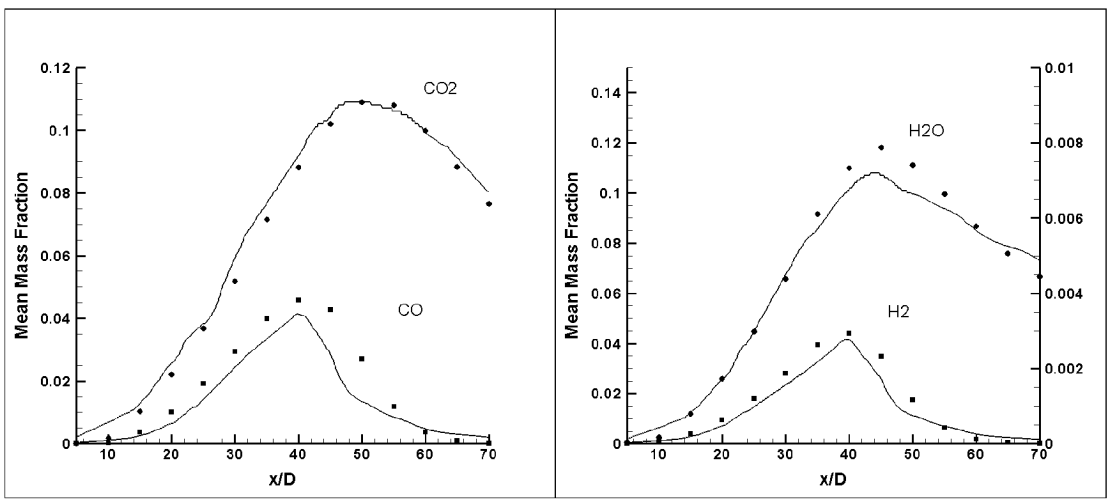

e) CO_2 and CO mass fractions

f) H_2O and H_2 mass fractions

Figure 4.9(a-f): Mean values of scalars along the centreline (lines: simulation; symbols: experiments).

4.5. Flame F

4.5.1. Centerline Axial Profiles

The coupling method and the definitions used in the simulation of the flame F are the same as in the flame E. The existence of a turbulent field with high Reynolds number (Re=44000) offers a challenging study in the simulation of the flame F. One of the main challenges in this study is to capture the local extinction and reignition regions in the unsteady reacting turbulent field. In order to capture those regions the partial premixing feature of the species should be simulated truly. Although the stable species, or main products, may be expressed using the kinematic parameters, the flame radicals may exhibit some flame history. Thus the flamelet history should be tracked down using dynamic parameters such as progress variable or reactedness parameter.

The axial mean velocity along the centerline is in agreement with the experimental data (Fig. 4.10b). The overpredicted region near to the nozzle is due to the selected inlet boundary conditions in the simulation. For this simulation study, the inlet velocity profile was calculated and selected by multiplying the inlet velocity profile of the flame D with factor two. Except for the far downstream region, estimation of the mean mixture fraction values along the centerline presents a very good agreement (Fig. 4.10a). The overpredicted mixture fraction values further downstream affect the quality of the prediction for main stable species and temperature in figure 4.10(c-g).

The calculated axial main temperature may be investigated in two different parts (Fig. 4.10c). The first overestimated mean temperature values at certain downstream region between x/d=10&35 may be expressed due to the overpredicted CO_2 production in those regions (Fig 4.10f). The second overestimated region is placed in the far downstream region due to the overpredicted mixture fraction value in figure 4.10a. The reactedness, or progress variable, follows the chemical dynamics perfectly at $x/d > 25$ region (see Fig. 4.10d). The main products CO_2 and H_2O are predicted well in the region of $x/d < 40$. In other words, stable species are estimated well in the fuel rich side compare to the fuel lean side (Fig. 4.10(f-g)). The discrepancies in the estimation of main scalars for the fuel lean side may be due to the overprediction of mixture fraction values far downstream region.

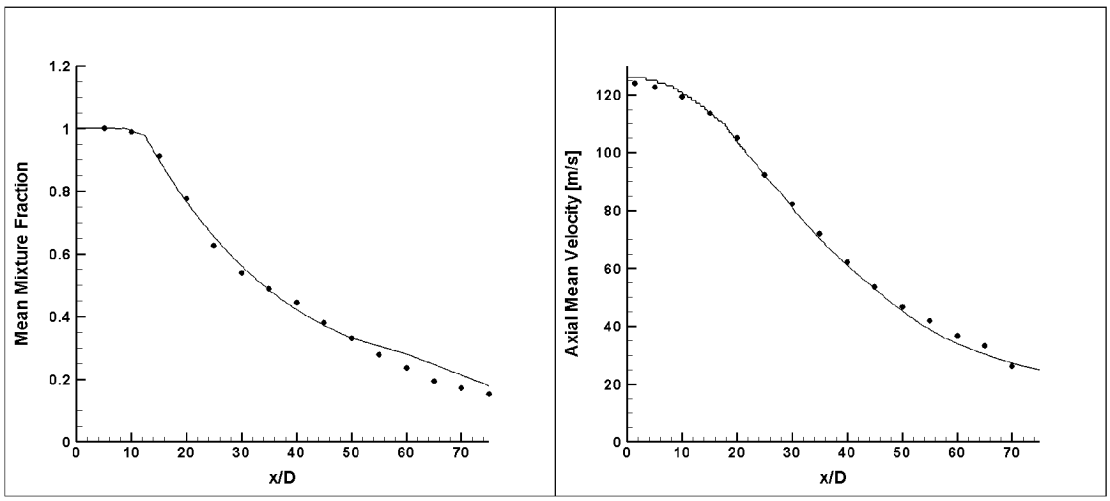

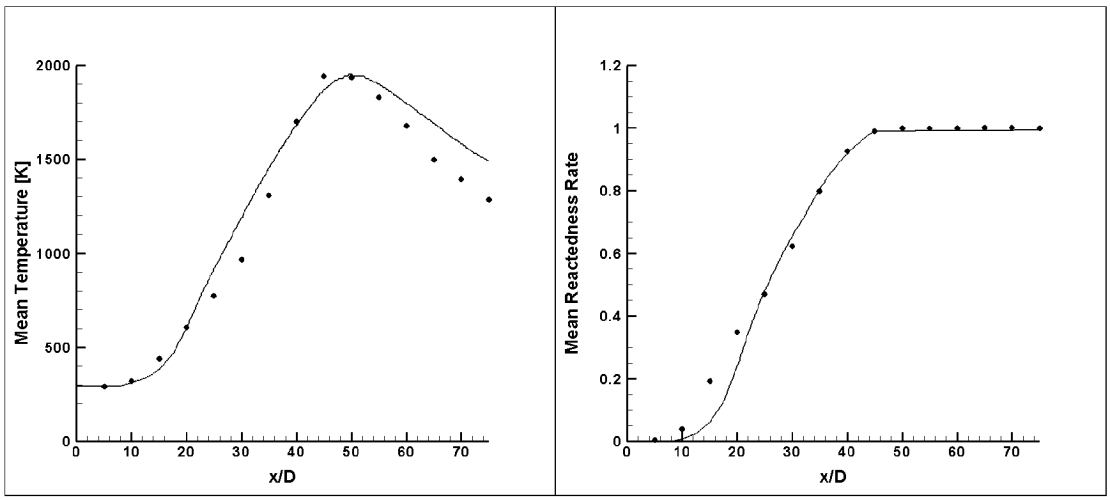

Figure 4.10(a-d): Mean values of scalars along the centreline (lines: simulation; symbols: experiments).

The stoichiometric length of the flame F is given approximately as 47.5d in the experimental documents based on the interpolation of axial profile of Favre average mixture fraction [68]. The stoichiometric mixture fraction value equals to 0.351 for the piloted Sandia flames. The error level in this estimation for the stoichiometric flame length is around 4% in the flame F.

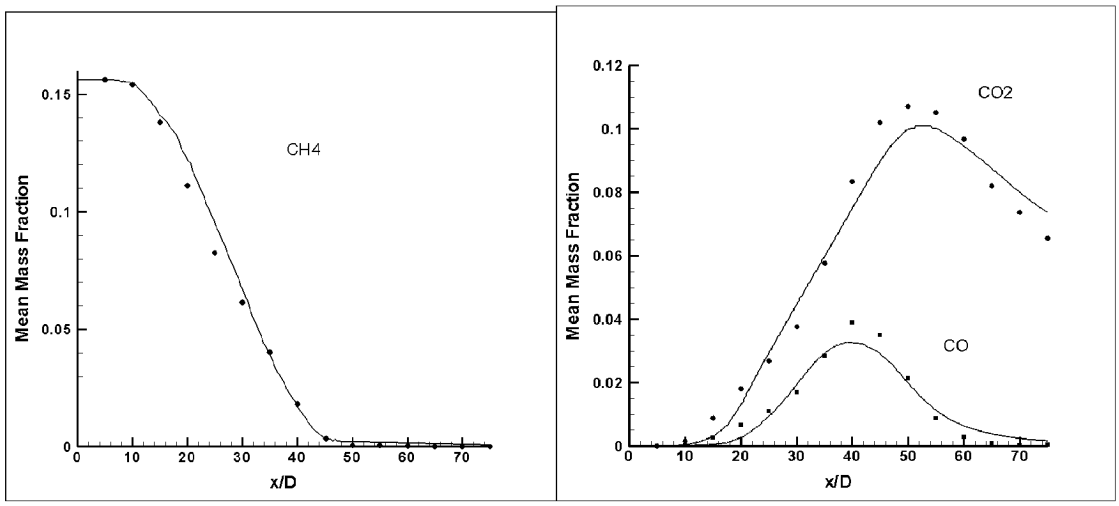

e) CH_4 mass fraction

f) CO_2 and CO mass fractions

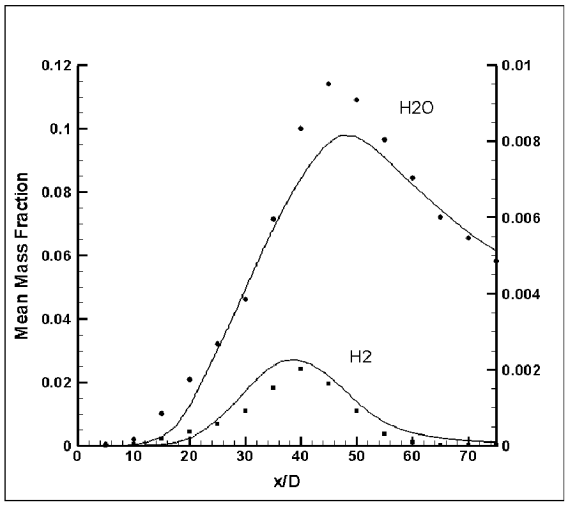

g) H_2O and H_2 mass fractions

Figure 4.10(e-g): Mean values of scalars along the centreline (lines: simulation; symbols: experiments).

4.5.2. Radial Profiles

The calculated and the experimental data are compared in the following figures regarding to the radial distribution of different scalars. Although the nature of the flame F shows higher turbulent features as compared to the other flames, the prediction of the scalar fields is in better agreement not only for the main species but also for the interim species in figures 4.(11-13). So, one should focus on the changes against the flame D made for modeling of E and F flames.

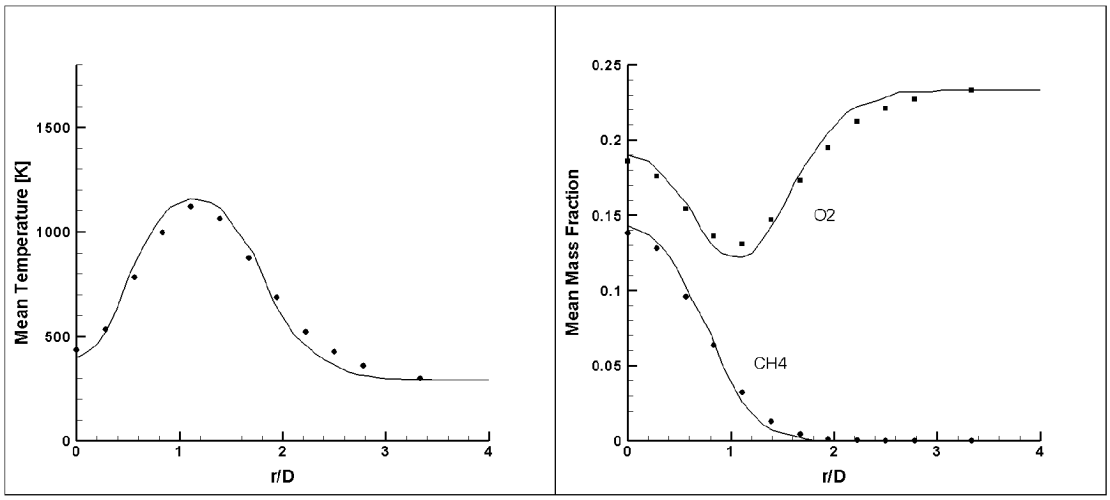

a) Temperature

b) CH_4 and O_2 mass fractions

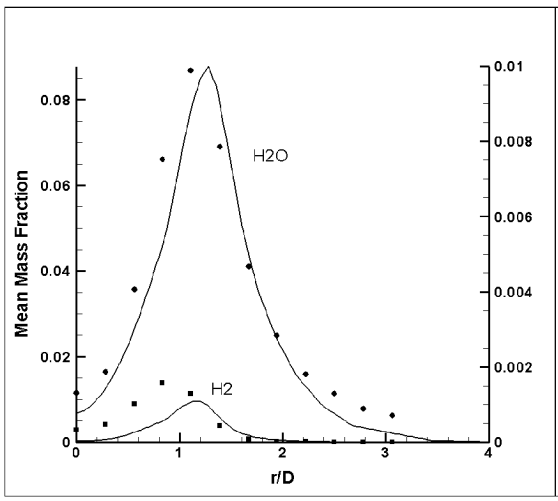

c) H_2O and H_2 mass fractions

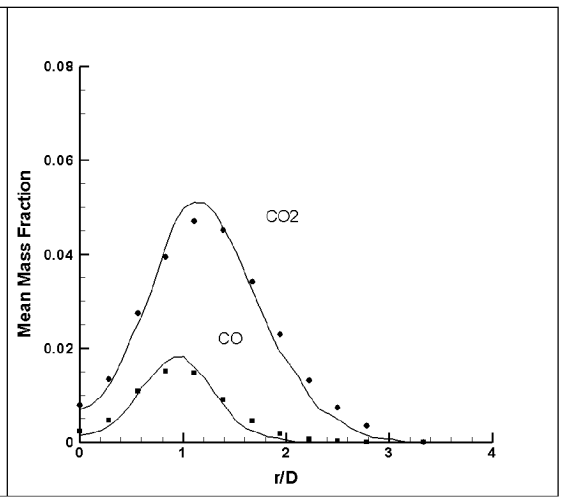

d) CO_2 and CO mass fractions

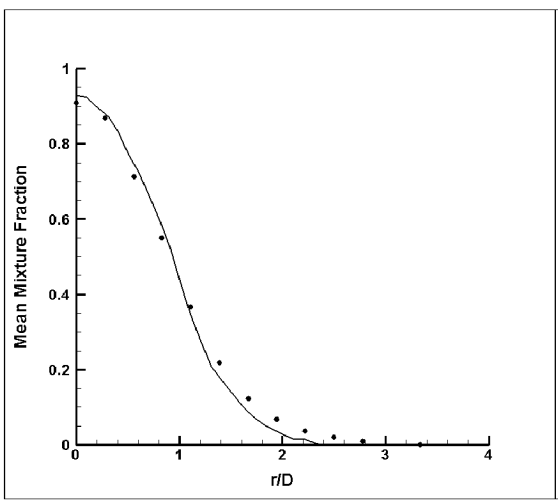

e) Mixture fraction

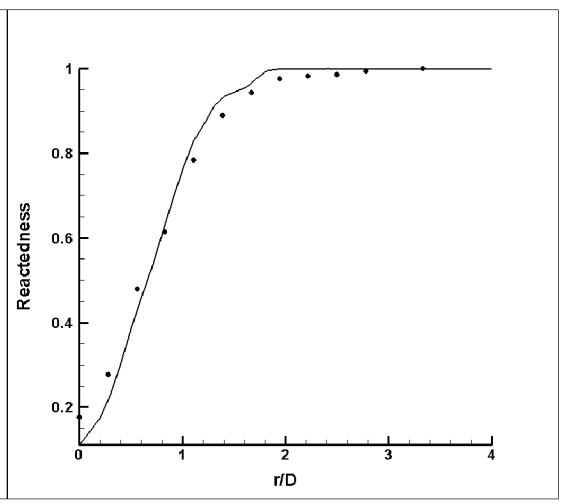

f) Reactedness

Figure 4.11(a-f): Radial distribution of mean values of scalars at x/d=15 (lines: simulation; symbols: experiments).

There are two main differences between the models used in the simulation of the flames D and F. The first difference is in the definition of progress variable and the second difference is the modification in the flamelet libraries. Instead of the pure diffusion laminar flamelet libraries used in flame D, the partially premixed flamelet libraries bounded with the inlet boundary conditions are used in the simulation of the flame F.

Figure 4.11a shows experimental and calculated radial profiles of temperature at x/d=15. The agreement between the experimental and the calculated data fields is the consequence of the true calculation of the mass fractions of main and minor species shown in figure 4.11(b-d). The only discrepancy in these figures appears the in the prediction of H_2 at the fuel rich side (Fig 4.11c).

The temperature and mass fractions of main products are slightly overpredicted at x/d=30 in figure 12(a, c-d). These overpredicted values are related with the overpredicted values along the centerline. The agreement between experimental and calculated mass fractions of minor species is noticeable in figure 4.12 (c-d).

Due to the overpredicted scalar fields along the centerline, the predictions of the scalars at x/d=45 exhibit various level of deviations from the experimental values (Fig. 4.13).

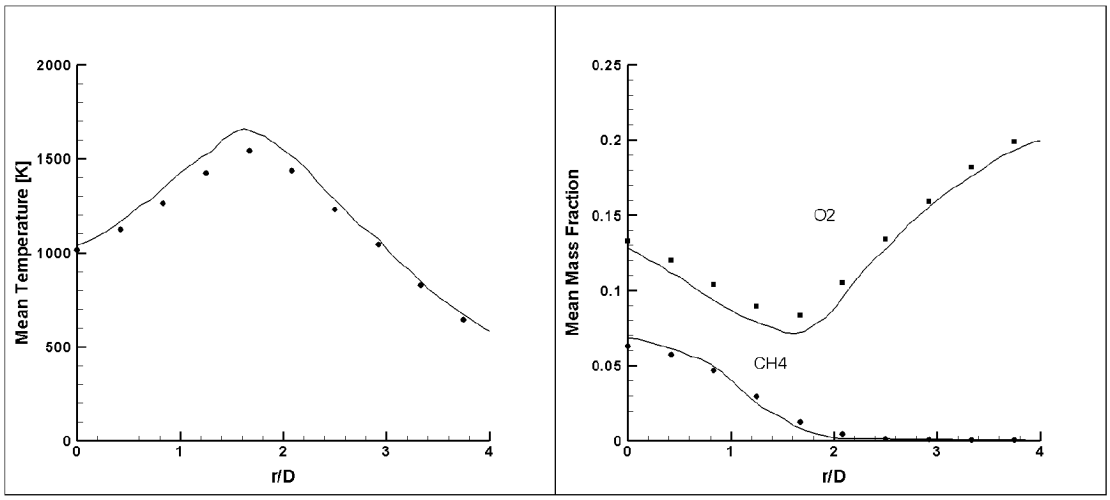

a) Temperature

b) CH_4 and O_2 mass fractions

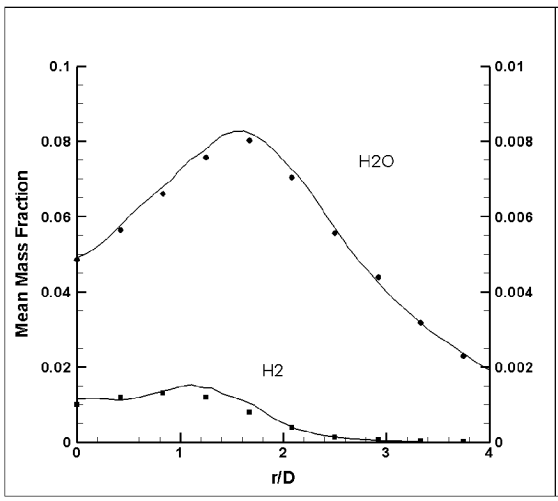

c) H_2O and H_2 mass fractions

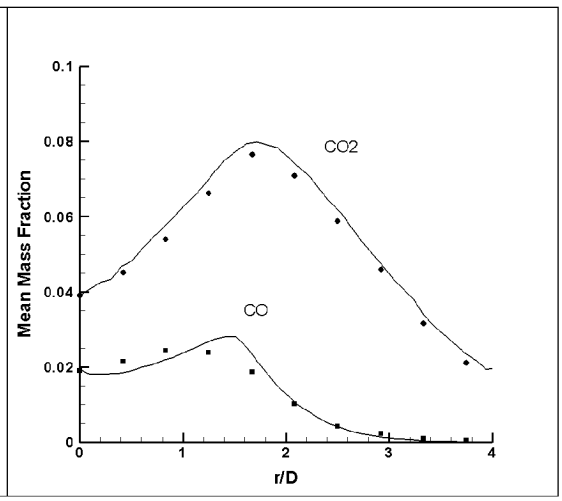

d) CO_2 and CO mass fractions

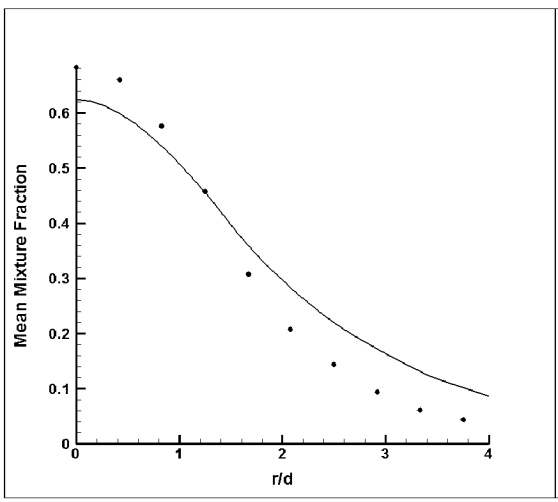

e) Mixture fraction

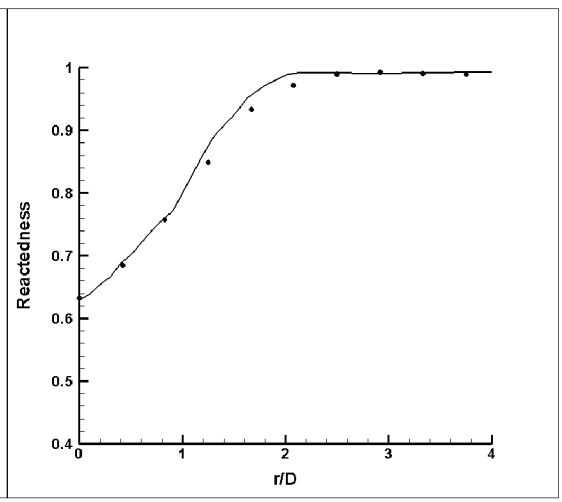

f) Reactedness

Figure 4.12(a-f): Radial distribution of mean values of scalars at x/d=30 (lines: simulation; symbols: experiments).

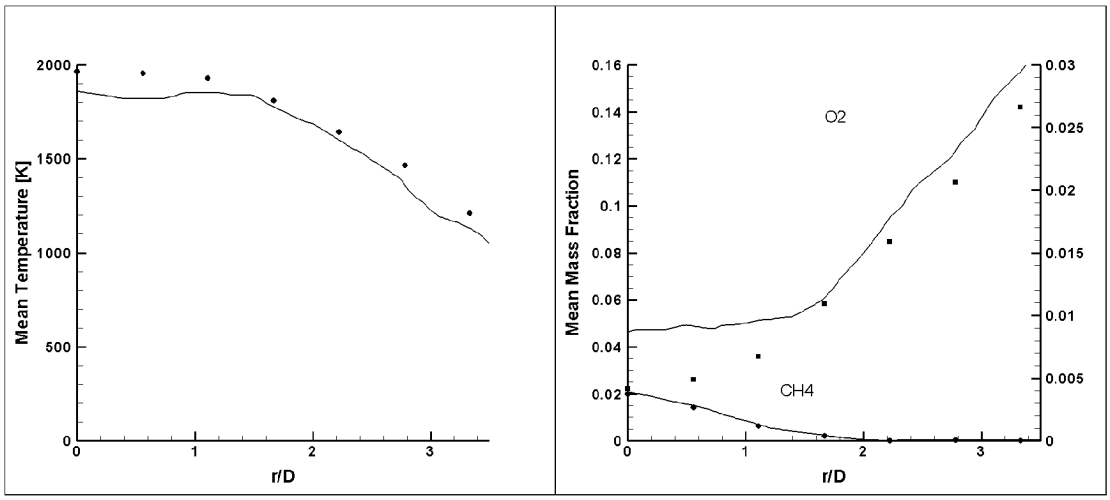

a) Temperature

b) CH_4 and O_2 mass fractions

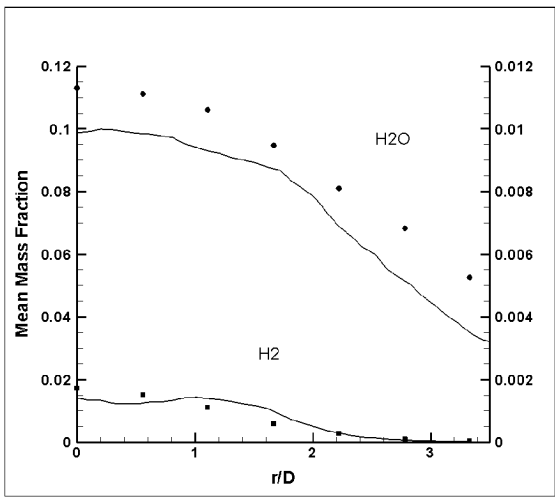

c) H_2O and H_2 mass fractions

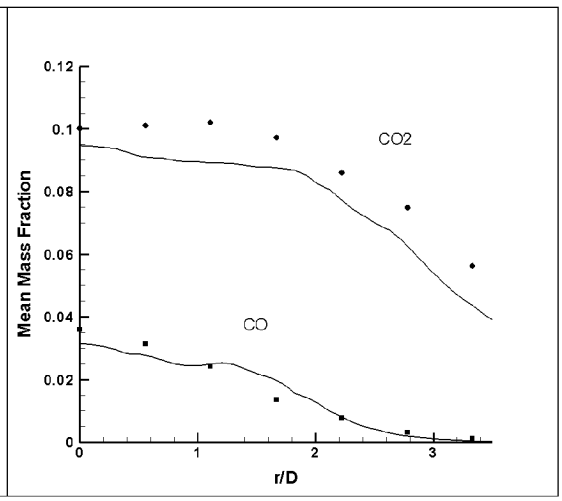

d) CO_2 and CO mass fractions

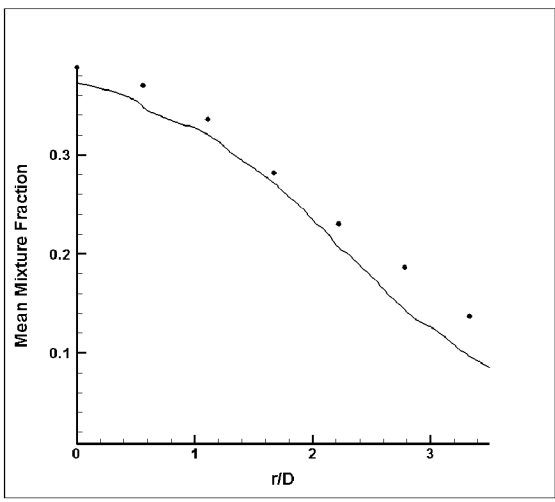

e) Mixture fraction

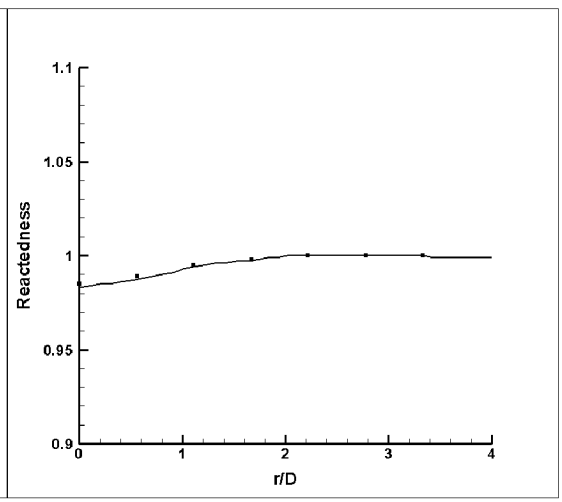

f) Reactedness

Figure 4.13(e-f): Radial distribution of mean values of scalars at x/d=45 (lines: simulation; symbols: experiments).

Chapter V

Dynamic Analysis of the Flames

5.1. Extinction and Reignition

Extinction and reignition phenomena in the investigated flames are discussed in this chapter. As the jet velocity is increased, extinguished parcels appear more frequently in the region of high mixing rates. One of the clear indications of existence of extinguished fluid parcels in the reaction zones is the high probability of low temperatures (see Fig. 5.2). There would be some experimental error in these graphs as usual, but the points indicating extinguished fluid parcels, at 1200 [K] and less, can be regarded as reliable because of low chemiluminescence at low temperatures [66,72]. After the local extinction regimes, the flame reignites further downstream where the mixing rate is more relaxed. Reignition can occur if there are burnt fluid parcels convected from the intense mixing region.

Figure 5.1 presents the stoichiometric mixture fraction iso-surfaces colored for different scalars. The following sets of figures depict different scalars and species mass fractions attached on the stoichiometric mixture fraction. In figure 5.1a the local extinguished regions may be identified by high quenching scalar dissipation rates. The red colored regions are subjected to the local extinction due to the high mixing rates. Those extinguished layers might be identified by low temperature values observed at the regions subjected to intense turbulence. These low temperatures correspond to increases in mass fractions of the minor species in the mixture (Fig. 5.1e). Excess amount of the minor species indicates a delay in the reaction. The higher CO levels coincide mainly with the lower temperature regions and are observed at high mixing rates due to the low residence time at those regions (Fig. 5.1d).

The combustion at fast chemistry limits is a local phenomenon and depends on the local stable compositions of the mixture regardless of the fluid's history [58, 62]. On the other hand minor species, such as CO, do not seem to correlate well with the mixture fraction and exhibit some history effects (Fig 5.1e). The level of the reactedness value shows not only the rate of partial premixing in the specified turbulent flow field but also the level of local kinetic reactions (Fig. 5.1f). The transported progress variable integrates the dynamic reaction rates and carries the reactive turbulent flow field history (Fig 5.1c). By using only kinematic parameters such as scalar dissipation rate and local reactedness value, the regions containing relatively high CO concentration cannot be truly identified. So the transported progress variable and its competition with a kinematic parameter, local reactedness value, would be a better approach for this problem.

When the flames approach extinction, the data points are highly populated at the domain between the flamelet profiles and the frozen limits. It is not clear whether fluid parcels are partially burnt or simply mixed with hot combustion products in this region. Figure 5.2 illustrates the scatter plots of three Sandia flames (D, E, and F) which exhibit local extinction.

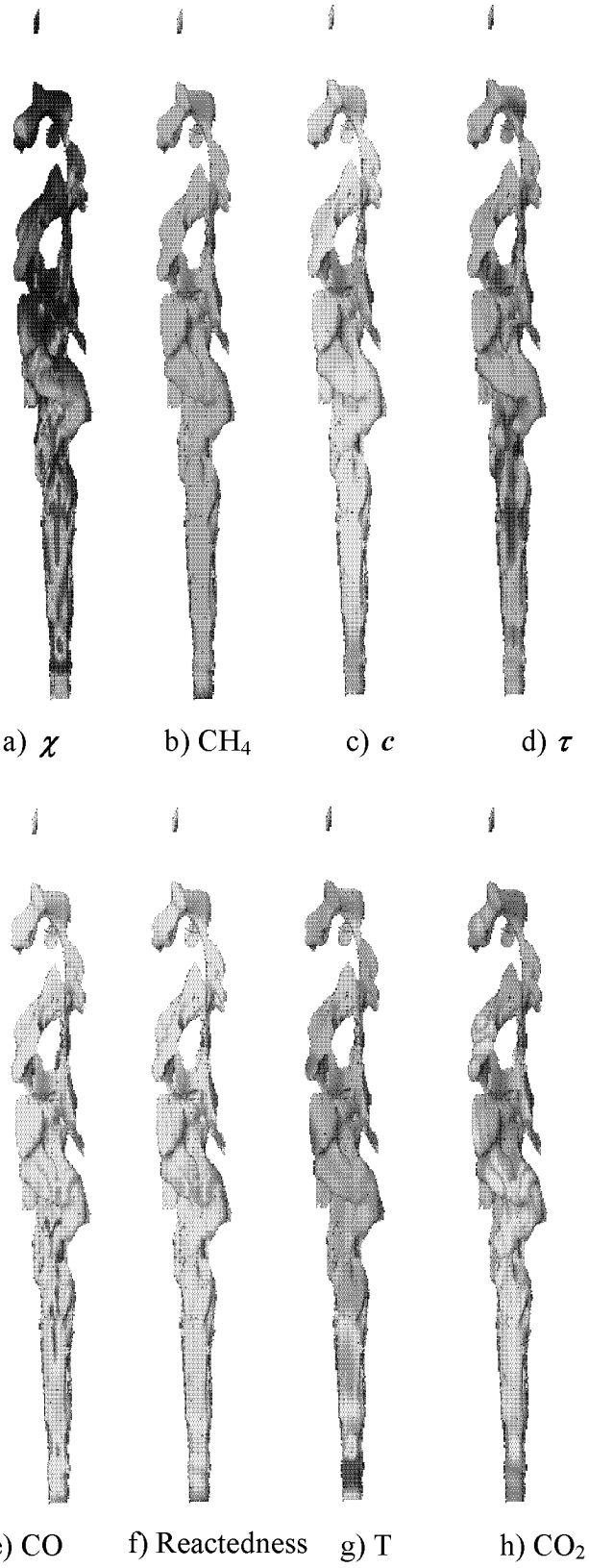

Figure 5.1: The instantaneous variations of the scalars on the stoichiometric mixture fraction iso-surface.

The scatter plots at 15d for Sandia flames in figure 5.2a indicate the probability of the local extinction, which is characterized by the depressed temperature samples. Although the flame D has small local extinction probability, other two flames E and F have a high level of extinction at 15d (see Fig.5.2a). Though the local extinction is still an important phenomenon for the flame F at 30d, the scatter plots show low extinction probability for the flames D and E at the same radial position (see Fig.5.2b). At far downstream region, say 45d, the scatter plot of the flame F presents very low level of probability for extinguished fluid parcels (Fig.5.2c). This might be due to the reignition process following local extinction at near downstream regions.

In this study, we used three different approaches to investigate the partial premixing, the local extinction and the reignition phenomena. Bimodality and conditional probability function are the ones most commonly used to express extinction and reignition regimes [14, 61, 72, and 73]. The reactedness parameter can be also used for the same purposes [70, 72].

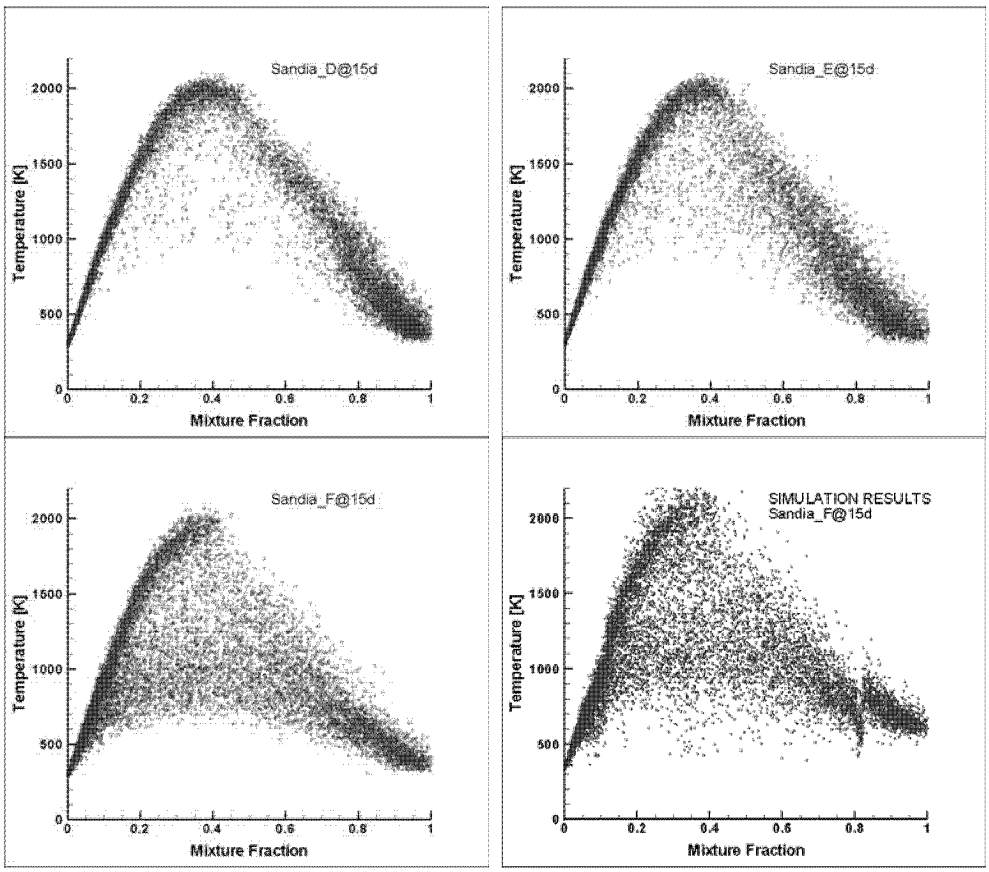

Figure 5.2a: Scatter plots of experimental and simulation temperature fields for Sandia flames at x/d=15.

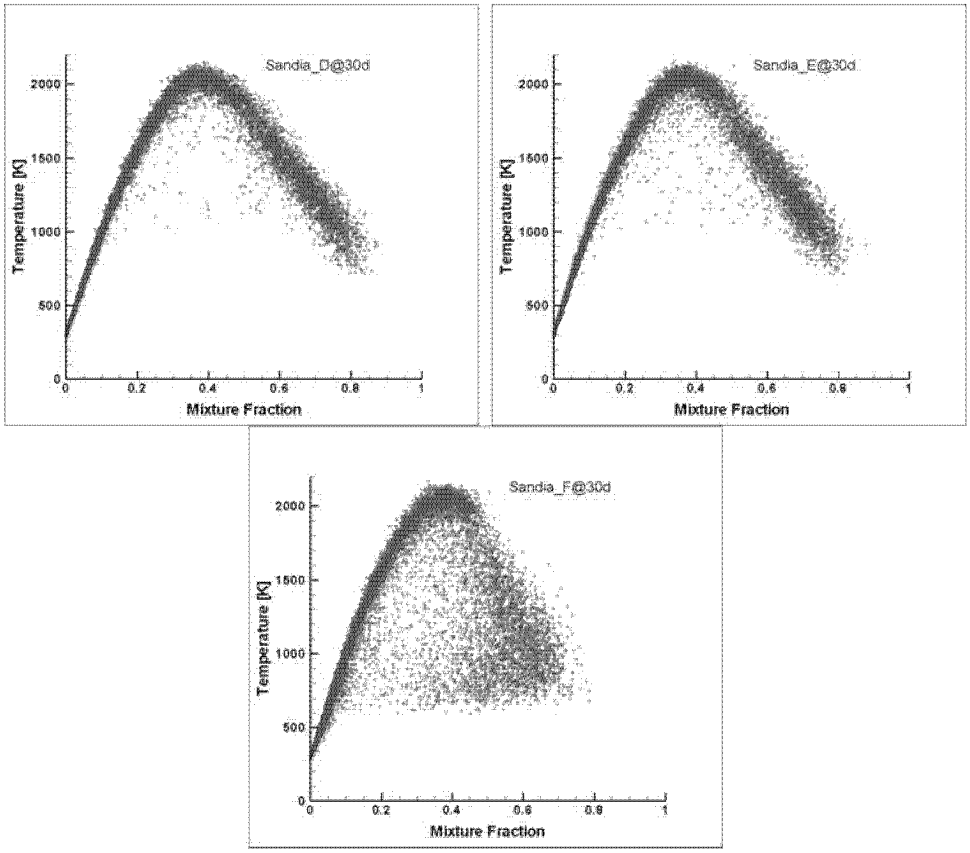

Figure 5.2b: Scatter plots of experimental temperature field for Sandia flames at x/d=30

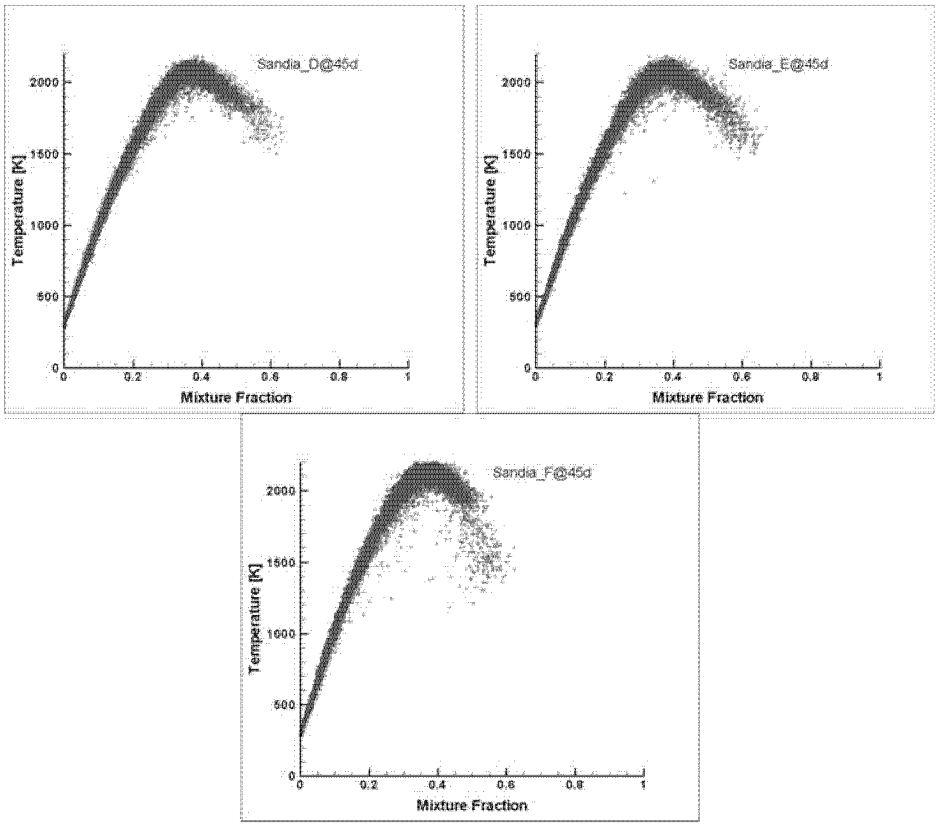

Figure 5.2c: Scatter plots of experimental temperature field for Sandia flames at x/d=45

5.2. Bimodality

Several studies have been done to express locally extinguished fluid parcels and following reignition processes [14, 71-78]. Locally extinguished fluid parcels and following reignition processes are expressed by indicating the interactions between frozen (unburned) or burned fluid structures. Therefore characteristic bimodality of the temperature distribution can be created in lean and near stoichiometric samples [71].

We carried out the bimodality analysis for different mixture fraction intervals as indicating in table 5.1.

Mixture Type	**Normalized interval (Zmix/Zstoic.)**
Very Lean	[0.5, 0.7]
Lean	[0.7, 0.9]
Stoichiometric	[0.9, 1.1]
Rich	[1.1, 1.3]
Very Rich	[1.3, 1.5]

Table 5.1: The classified mixture fraction intervals for bimodality analysis.

In this study, we followed the similar method employed by Masri [70] for the analysis of our simulated reacting turbulent flow field. The definition of the reactedness in Eqn. (1) is not the same definition used in the previous chapter 4 (Eqn. (4)). Hence, we demonstrated this reactedness with a different symbol, $\mathfrak{R}$. However, both definitions give a measure of reaction progress in one way or other.

$$\mathfrak{R}_i = \frac{P_i - P_{unb,i}}{P_{b,i} - P_{unb,i}} \qquad (1)$$

Reactedness, $\mathfrak{R}_i$, can be calculated for any scalar at any data point depending on reaction in the computational domain. P_i is the calculated scalar and represents temperature or species

mass fractions. $P_{unb,i}$ and $P_{b,i}$ are unburned and fully burnt values of the scalar which fall into the specified mixture fraction interval, (Table 5.1). The steady state flamelet values were chosen as the fully burnt limit in each selected mixture fraction interval.

The values of $\mathfrak{R}_i$ vary between zero for unburnt and one for fully burnt mixtures. For any data point, differences in the values of $\mathfrak{R}_i$ calculated from the two different scalars reflect a variation due to turbulence interaction in the progress of the reactions related to that scalar. All scalar data fields used in this study were conditioned with respect to mixture fraction intervals given in table 5.1. The calculated $\mathfrak{R}$ values using Eqn. (1) were allocated for each selected mixture fraction interval. The conditional probabilities of those $\mathfrak{R}$ values were calculated using Eqn. (2). The probability of $\mathfrak{R}$ at the interval bounded by x and y was calculated as follows:

$$p(x \le \mathfrak{R} \le y) = \frac{1}{\Delta \mathfrak{R}_{x,y}} \frac{n_{\mathfrak{R},x,y}}{N} \qquad (2)$$

where $n_{\mathfrak{R},x,y}$ is the number of data points falling in the range $x \le \mathfrak{R} \le y$ and N is the total number of data points sampled in the mixture fraction range. The width of the interval bounded by x and y is $\Delta \mathfrak{R}_{x,y}$. The area under each conditional probability density function (cpdf) curve bounded by the horizontal axis is equal to one when computed over the whole range of $\mathfrak{R}$ for which $p(\mathfrak{R})$ is defined as;

$$\sum_{\mathfrak{R}} p(\mathfrak{R})\, \Delta \mathfrak{R} = 1.0 \qquad (3)$$

The data collected in the simulation at certain radial positions for the flames E and F were used in this study to identify and express the bimodality features of these flames. More than 100 data points were found in each mixture fraction interval. The cpdfs were calculated for temperature and CO_2 mass fraction in each mixture fraction range using the equations (1) and (2).

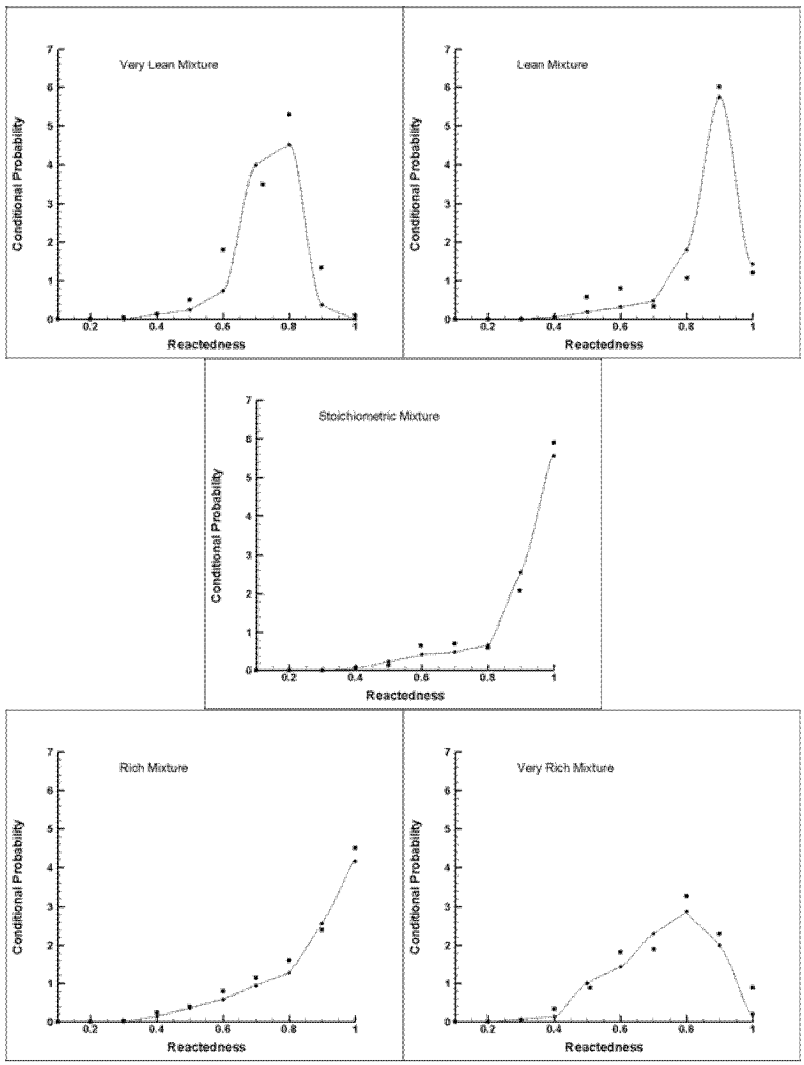

Figure 5.3: Conditional probability density function of the reactedness calculated from temperature for the flame E at x/d=15 (lines: simulation; symbols: experiments).

Figure 5.3 and 5.4 illustrate the cpdfs reactedness as a function of temperature at x/d=15 for the flames E and F in the predefined mixture fraction intervals respectively. Initially, it can be considered that the reactedness of temperature for the flame F exhibits clear bimodality from very lean mixture to stoichiometric mixture (Fig. 5.4). This trend is less distinct on the fuel rich side. However, the cpdf is still broad due to the existence of the partially premixed flamelets. Although we expect similar bimodality feature in the flame E, there is no clear evidence of bimodality for this flame (Fig. 5.3).

The reactedness of temperature for the flame E is accumulated around fully burnt state ($\mathfrak{R}=1$) from lean to very rich fuel mixtures in figure 5.3. There is a certain level of partial

premixing in all selected mixing intervals except the stoichiometric mixture. On the other hand, the different levels of mixing show a clear indication of partial premixing in figure 5.4 for the flame F.

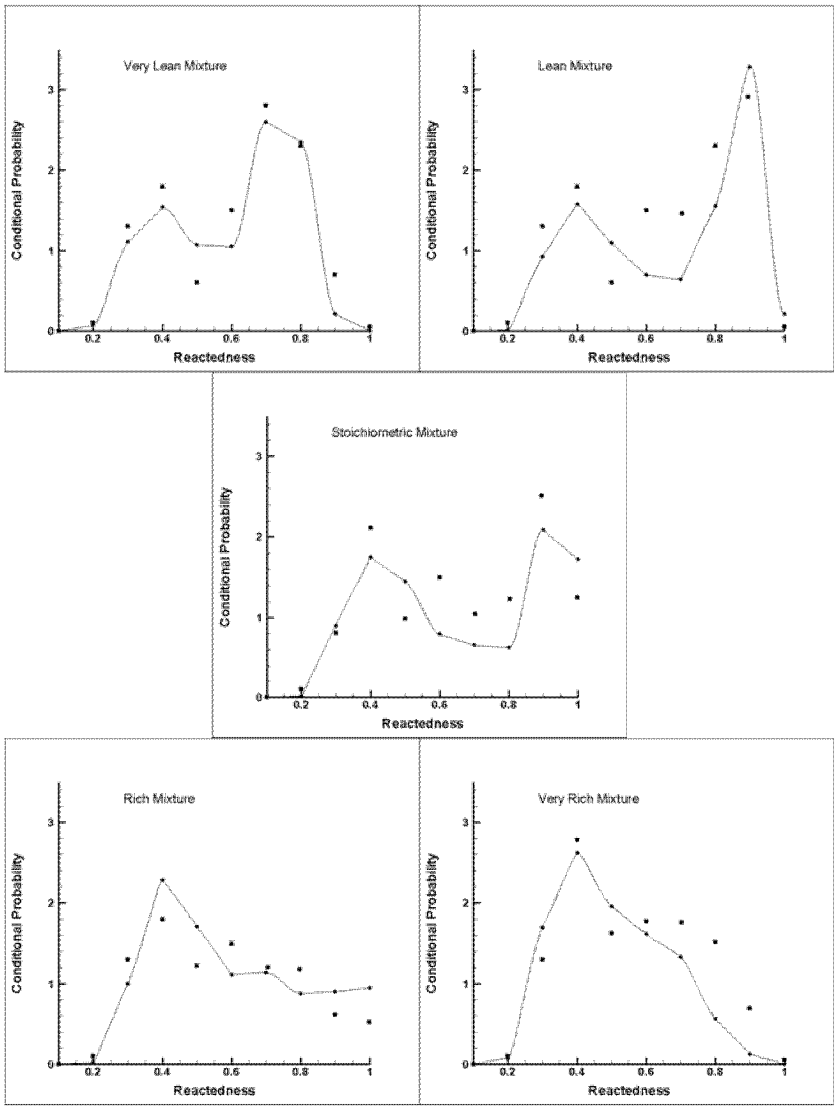

Figure 5.4: Conditional probability density function of the reactedness calculated from temperature for the flame F at x/d=15 (lines: simulation; symbols: experiments).

The other radial profiles (x/d=30 & 45) of the flame E do not show any distinct bimodality and the partially premixing trend throughout the lean and the rich mixtures. Because of the clear bimodality trends in figure 5.4 it would be worthwhile to discuss the other radial profiles (x/d=30 & 45) of the flame F. The reactedness of temperature at x/d=30 is given in figure 5.5 for the flame F. Except for the very lean mixture, there is still a probability for unburnt or

partially burnt states. Very lean and very rich mixtures show dominant partially premixing features compare to the other three. The reactedness of temperature for lean, stoichiometric and rich mixtures concentrated around the fully burnt state

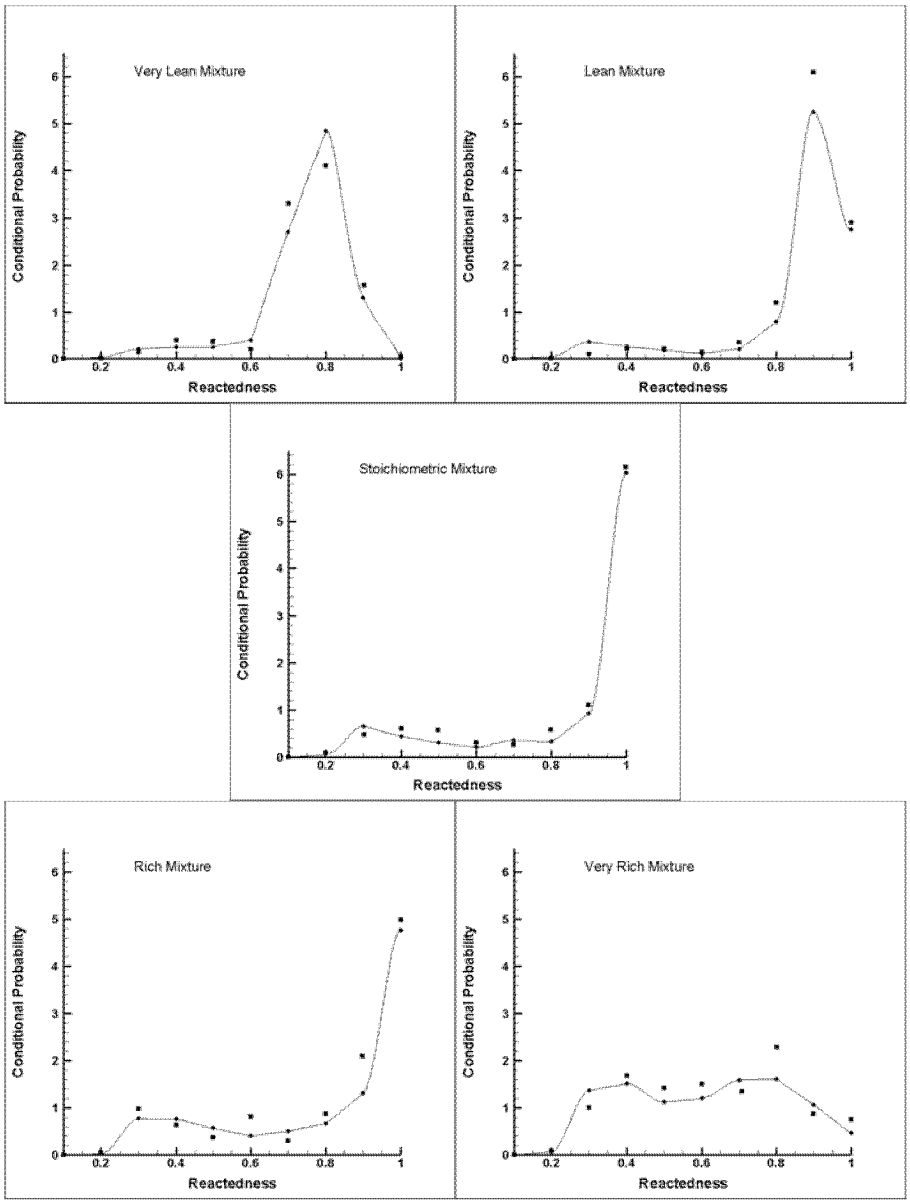

Figure 5.5: Conditional probability density function of the reactedness calculated from temperature for the flame F at x/d=30 (lines: simulation; symbols: experiments).

The characteristic shape of the bimodality is lost further downstream (x/d=45) (see Fig.5.6). Apart from this, there is no more dominating partial premixing in any mixture fraction interval for the reactedness of temperature except for very lean mixtures. All reactedness values fall into the range of $\mathfrak{R} \geq \mathbf{0.8}$. This means that the main reactions have already

completed at this point. This behaviour is also very clear in the time averaged temperature distribution along the centerline (see Fig.4.10c). Based on the previous discussion, one may conclude that the feature of bimodality shifts from the unburnt to the burnt side when the fluid parcels flow to the further downstream regions in the unsteady turbulent field.

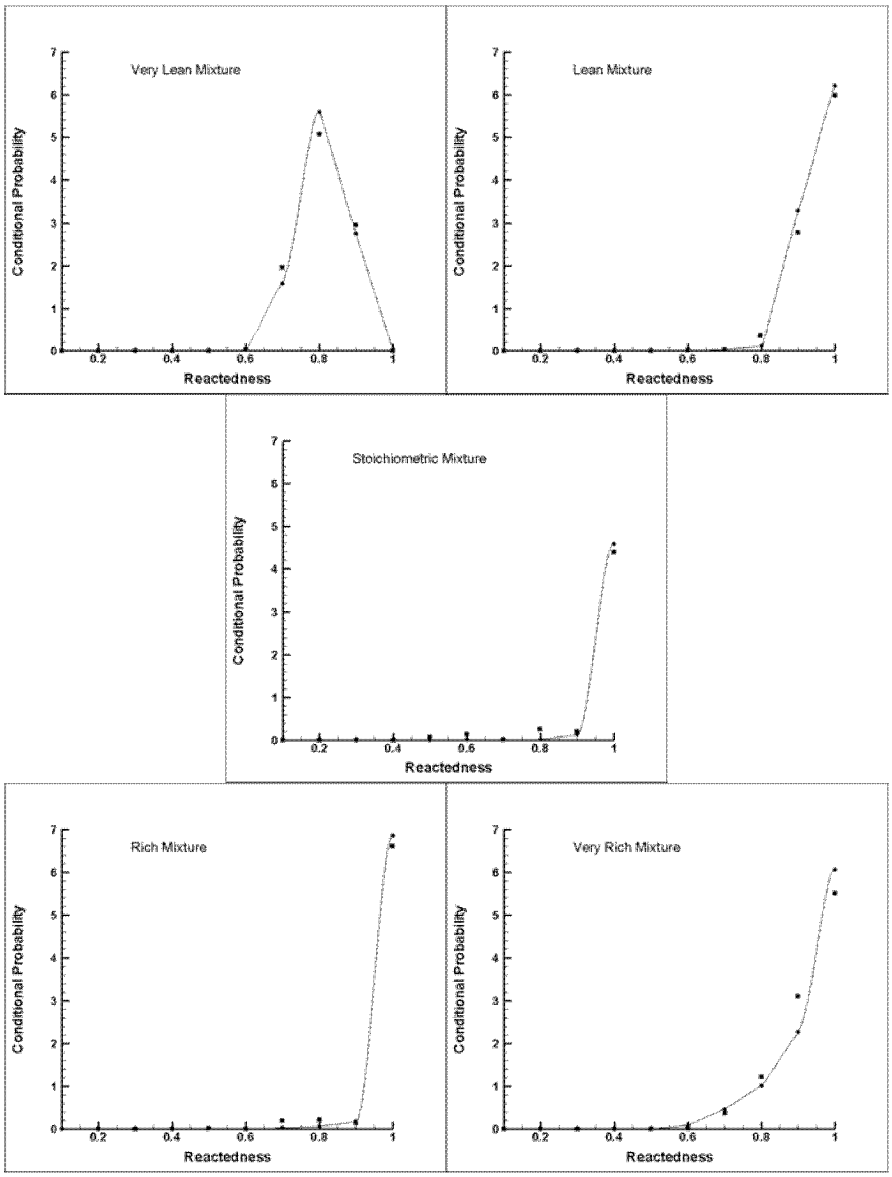

Figure 5.6: Conditional probability density function of the reactedness calculated from temperature for the flame F at x/d=45 (lines: simulation; symbols: experiments).

The reaction progresses of various species present different bimodality characteristics. Here, we take sample specie, CO_2, to represent the final products. As it is discussed above, the flame F exhibits more bimodality than the other flames. So the flame F is selected to create the characteristic bimodality figures of the selected specie.

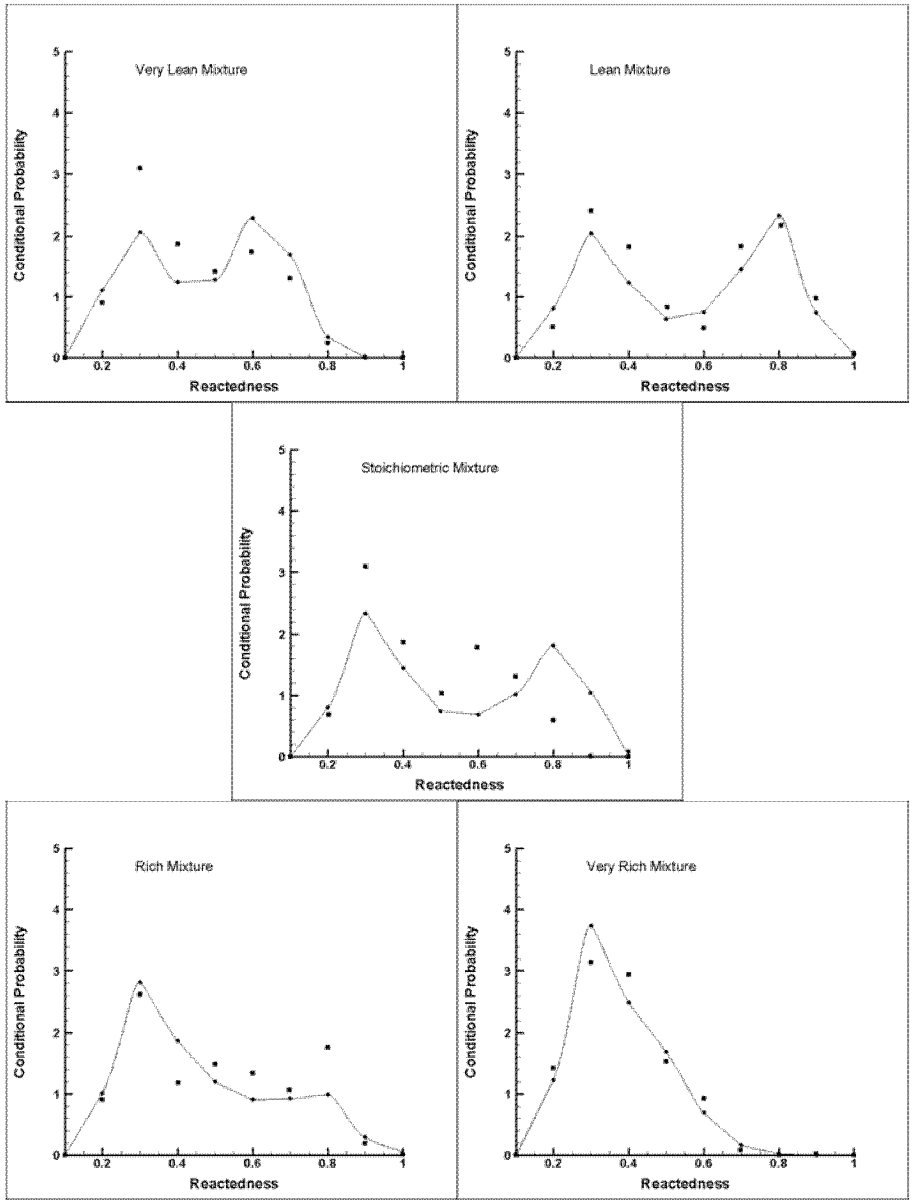

Figure 5.7: Conditional probability density function of the reactedness calculated from CO_2 for the flame F at x/d=15 (lines: simulation; symbols: experiments).

The reactedness of CO_2 mass fraction which is understandable follows almost the same trend with temperature's bimodality at x/d=15 in figure 5.7. It comes out from the theory that the main species mass fractions increase or decrease monotonically with the temperature. When the fluid parcels flow to further downstream regions (x/d=30 & 45) the shape and the intervals of bimodality slightly deviate from those of temperature (Figures 5.8 & 5.9). Except for very lean mixtures one may easily detect the bimodality characteristics for all mixture fraction intervals at x/d=30 in figure 5.8. Partially premixing is evident in all type of mixtures at this downstream radial profile. The reactedness of CO_2 mass fraction loses its bimodality feature

when the fluid parcels reach a position at x/d=45 in figure 5.9 and they start to exhibit less partially premixed behavior.

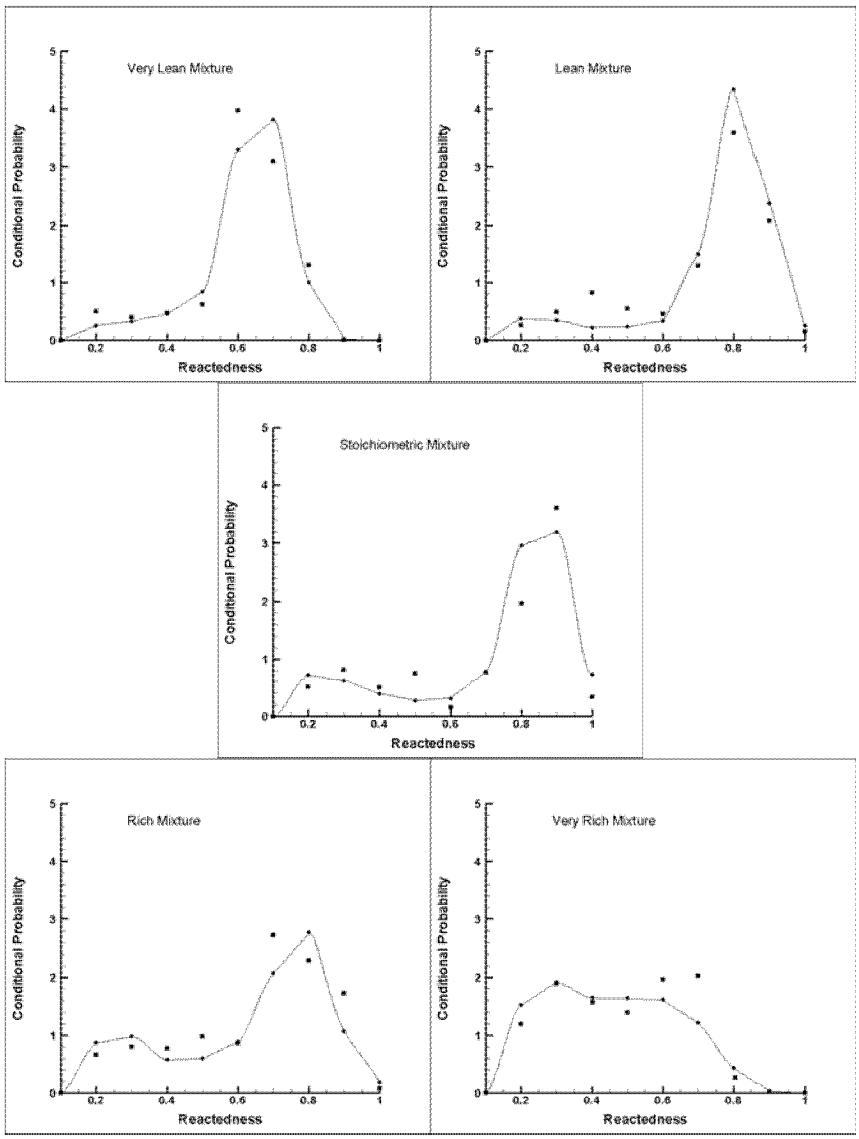

Figure 5.8: Conditional probability density function of the reactedness calculated from CO_2 for the flame F at x/d=30 (lines: simulation; symbols: experiments).

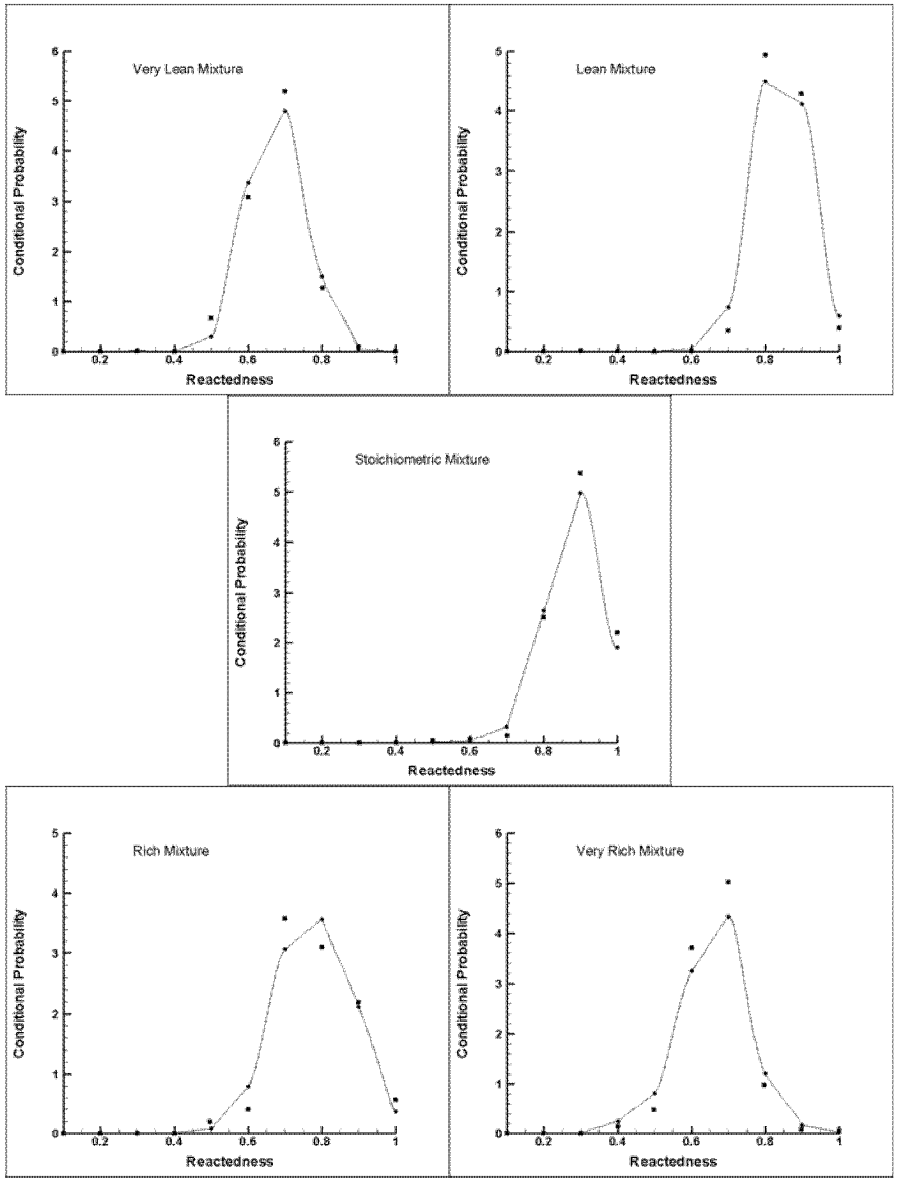

Figure 5.9: Conditional probability density function of the reactedness calculated from CO_2 for the flame F at x/d=45 (lines: simulation; symbols: experiments).

5.3. Reactedness Parameter

Although a mixture is composed of different species in different proportions, it has a unique mixing fraction value at each node in the turbulent flow field. The given reactedness definition in Eqn. (1) produces different bimodality shapes for different scalars. The reactedness of different scalars implies different levels of reaction at each node (Figures 5(3-9)). In order to create a single characteristic bimodality shape for a given mixture fraction

value, we introduce a new reactedness parameter for the bimodality analysis. The idea is to use a single global reactednesss definition, which includes all species in its formulation. It would be a better method for the bimodality analysis to represent partially premixing, local extinction and re-ignition processes. Here, we propose a reactedness definition in Eqn. (4) as it is in chapter 4 (Eqn. 6).

$$\mathbf{R} = \mathbf{1} - \left\{ \frac{\mathbf{min}\left(\frac{Y_{O_2}}{s}, Y_{CH_4} \right)}{Y_{CO_2} + Y_{H_2O} + Y_{CO} + Y_{H_2} + \mathbf{min}\left(\frac{Y_{O_2}}{s}, Y_{CH_4} \right)} \right\} \tag{4}$$

The reactedness $\mathbf{R}$ takes a value between zero and one for frozen and fully burnt mixtures respectively. It reflects the progress of the reaction in the turbulent flow field. In order to be consistent with the previous bimodality analysis, the intervals are selected as they are given in table 5.1. The probability of $\mathbf{R}$ being in the interval bounded by x and y is calculated as follows:

$$p(x \le R \le y) = \frac{n_{R,x,y}}{N} \tag{5}$$

where $n_{R,x,y}$ is the number of data points falling in $x \le R \le y$ and N is the total number of data points sampled in the mixture fraction range which is considered. The area under each cpdf curve bounded by the horizontal axis is equal to one.

The calculated data of the flame F at different radial positions (x/d=15, 30, and 45) are used in the analysis of the new reactedness. The radial profile at x/d=15 is also selected for the analysis of the flame E. This radial profile has more suppressed temperatures in the experimental data field compared to the other radial positions for all flames (see figure 5.2 for the distribution of experimental scattering data field).

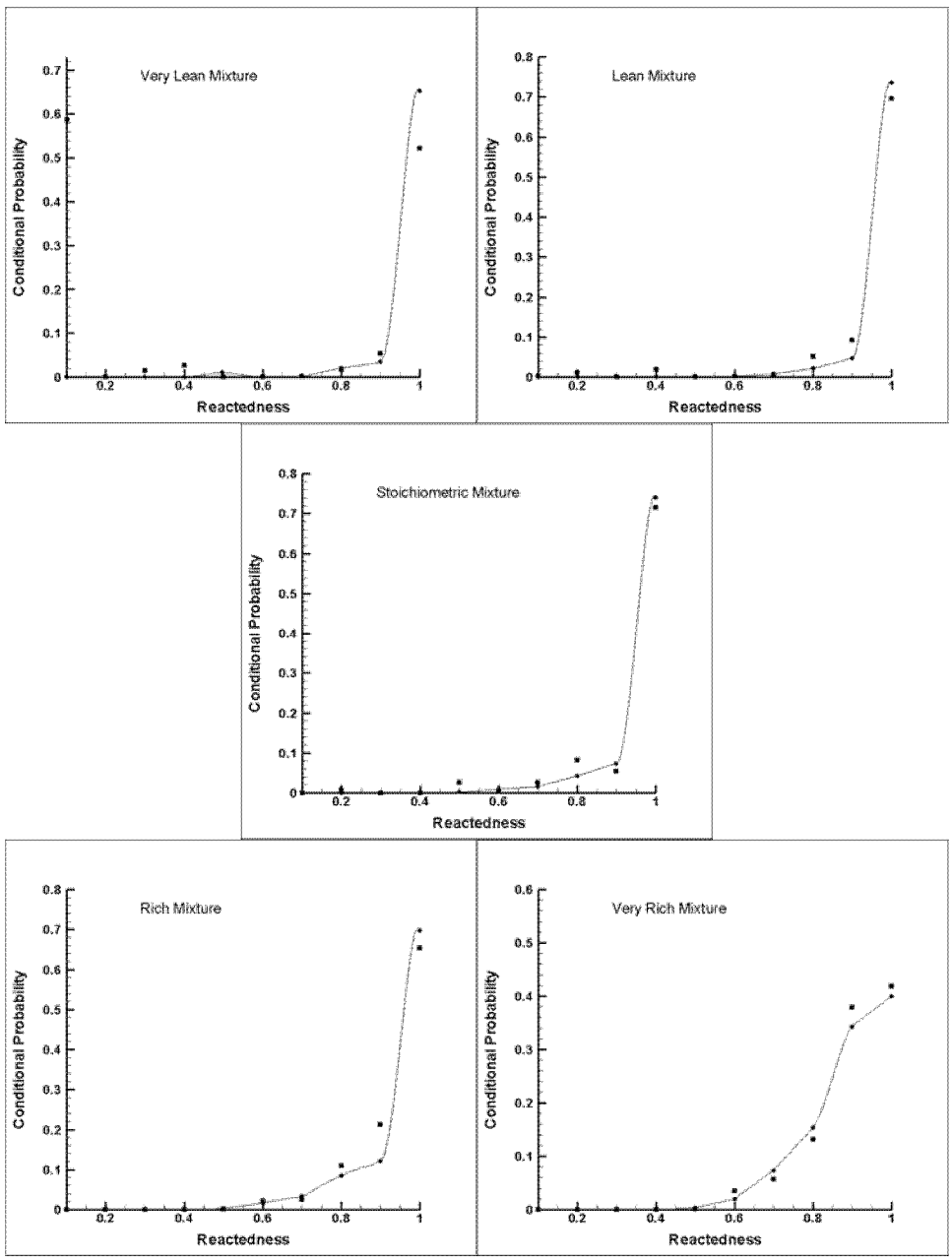

Figure 5.10: Conditional probability density function of the reactedness calculated from Eqn. (4) for the flame E at x/d=15 (lines: simulation; symbols: experiments).

The conditional probability density function (cpdf) of the reactedness for the flame E at x/d=15 does not exhibit strong bimodality (Fig.5.10). This may be due to the contribution of interim species in Eqn. (4). As it was discussed in the previous section, different scalars showed different levels of bimodality at different radial profiles for varying mixture fraction intervals. One of these scalars can mask the others bimodality characteristic if they are used in a combined equation as given in Eqn. (4).

Although there is no observed strong characteristic bimodality in the flame E, there are some indications of partial premixing when the mixture fraction interval varies from very lean to very rich mixture. The reactedness level is equal to one ($\mathbf{R = 1}$) when one of the reactants is depleted. If a reaction takes place and products are formed, the reactedness level starts to increase until one of the reactants is consumed.

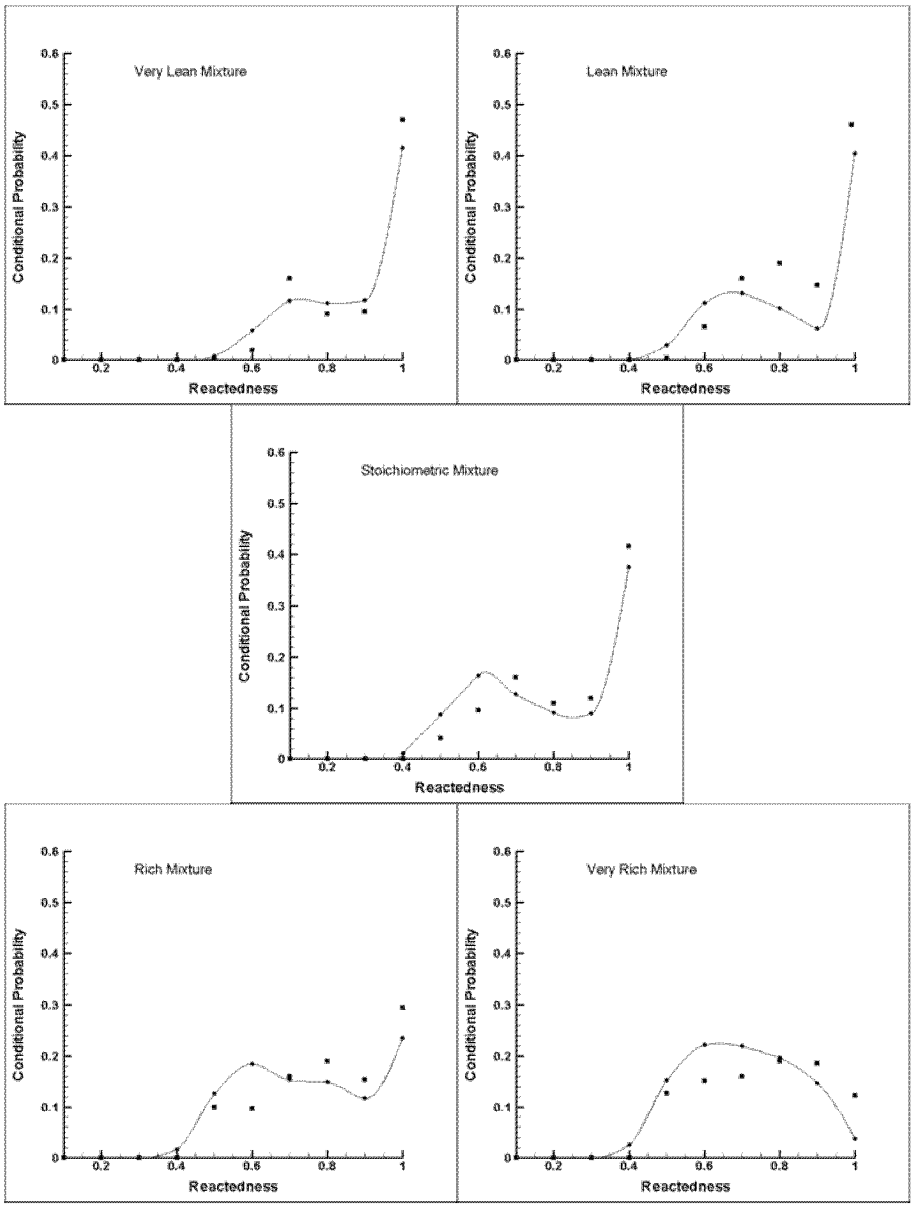

Figure 5.11: Conditional probability density function of the reactedness calculated from Eqn. (4) for the flame F at x/d=15 (lines: simulation; symbols: experiments).

The analysis of cpdf of **R** is extended to the flame F that showed highest bimodality in our previous analysis. This flame is studied for different axial positions from near to far downstream regions (x/d=15, 30, and 45). Except for very rich mixtures, the other mixture fraction intervals show distinct bimodality at near downstream region (x/d=15) in figure 5.11. The partially premixed nature of the mixtures is significant when the mixture interval changes from very lean to very reach mixture.

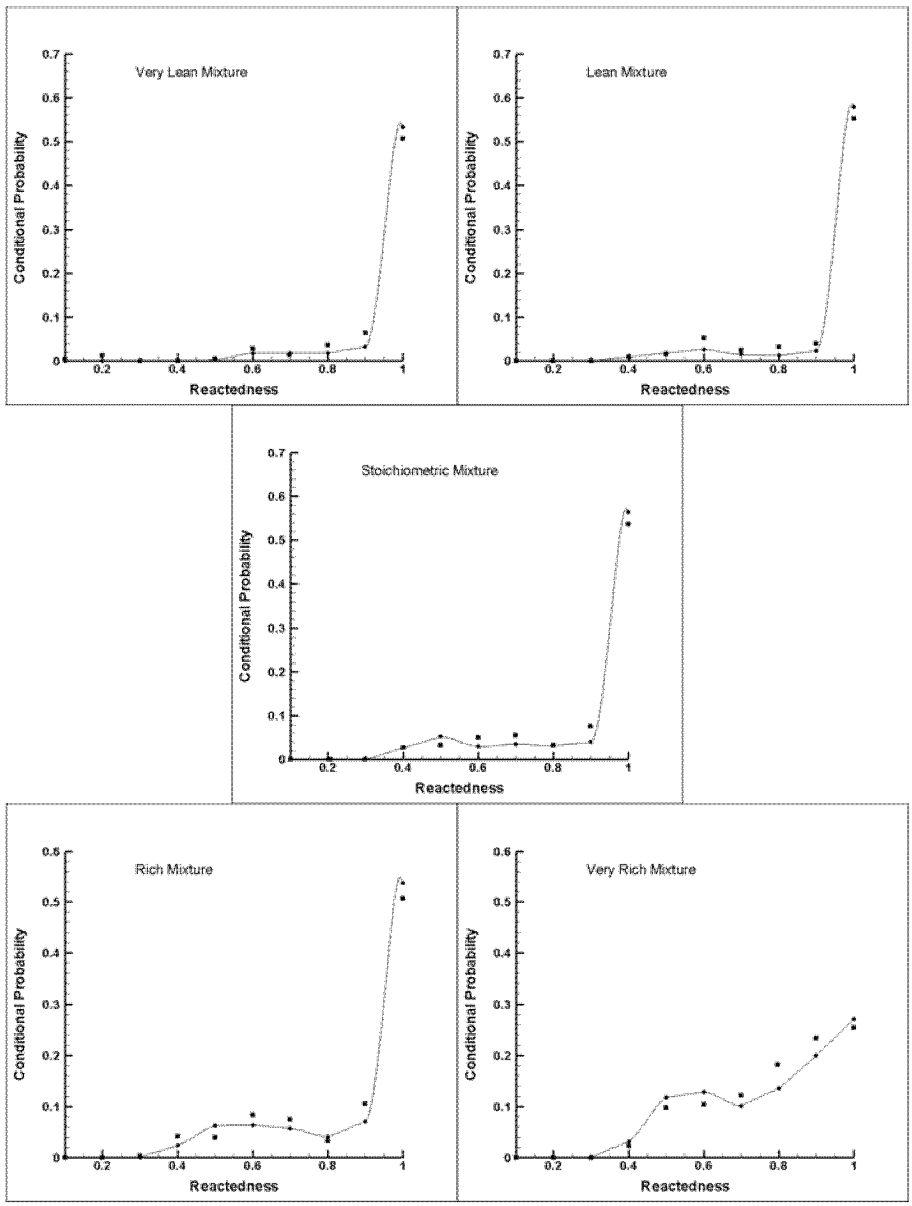

Figure 5.12: Conditional probability density function of the reactedness calculated from Eqn. (4) for the flame F at x/d=30 (lines: simulation; symbols: experiments).

The shape of the bimodality is more distinct for stoichiometric, rich and very rich mixtures at x/d=30 (see Fig. 5.12). The partial premixing still plays a role for all mixture fraction intervals. The very rich mixture fraction interval exhibits the highest partial premixed feature.

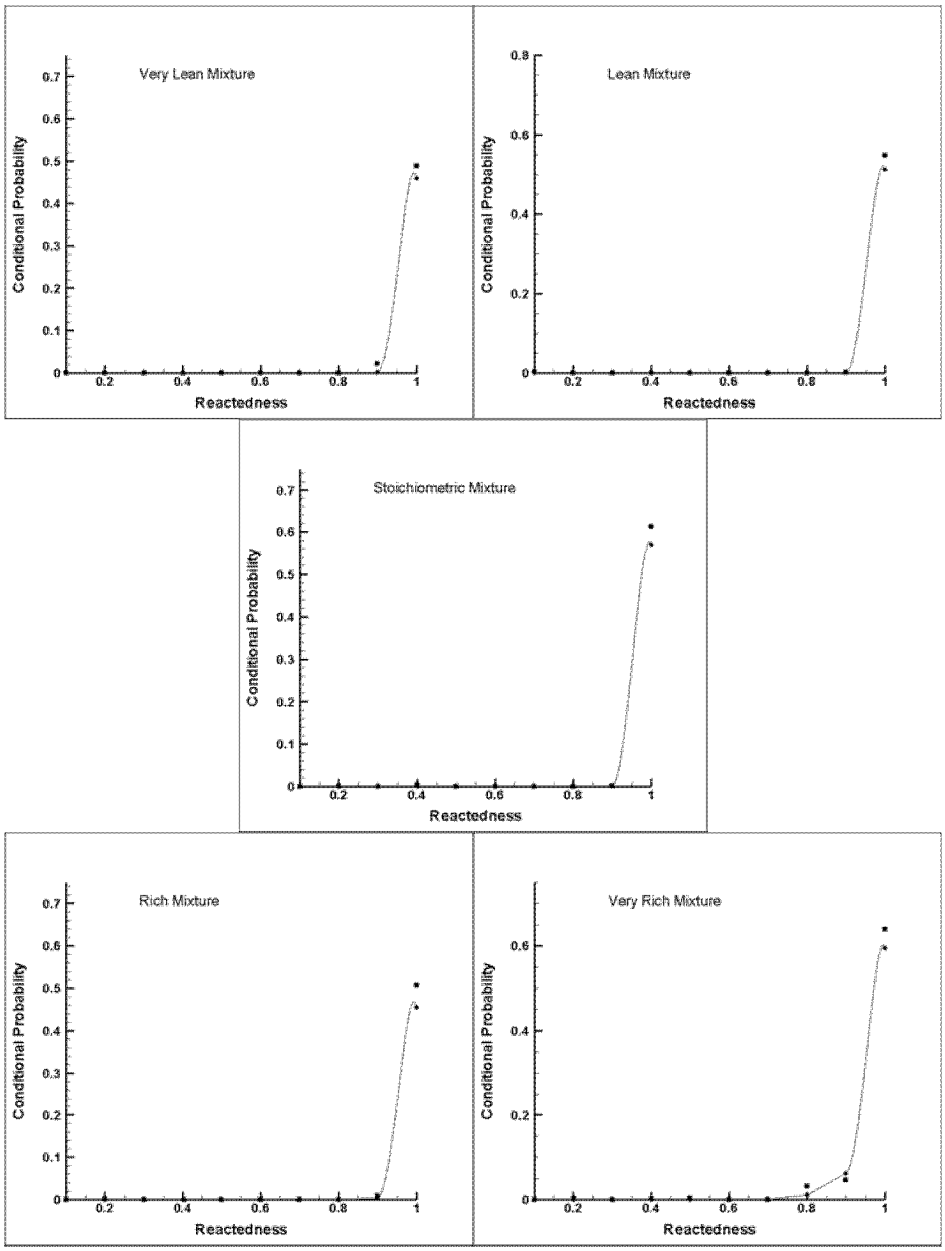

Figure 5.13: Conditional probability density function of the reactedness calculated from Eqn. (4) for the flame F at x/d=45 (lines: simulation; symbols: experiments).

Figure 5.13 presents the cpdf of reactedness parameter at x/d=45. The stoichiometric flame length value for the flame F is equal to 49.25 d [68]. Therefore the calculated reactedness value shown in Eqn. (4) approaches one at x/d=45. The bimodal shapes are disappeared at this

radial position for all mixture fraction intervals. Some partial premixed fluid parcels are still observed in the very rich mixture.

As a result of the reactedness analysis for the flame F, we observed the formation of bimodal shapes at near downstream. When the fluid parcels flow into further downstream the characteristic shape of the bimodality was lost. The amount of the partial premixed fluid parcels in the mixture was increased, when the mixture fraction intervals vary from lean to very rich mixture. The bimodal features generally were observed for lean, stoichiometric and rich mixtures at the same axial position.

In this chapter, the clasical bimodality and the new reactedness analysis were performed on the experimental and the calculated data. The comparisons were made at the different radial profiles for the predefined mixture fraction intervals. The conditional probability density functions of calculated data are consistent with those of experimental data. These results verify the introduced model which is able to capture the dynamic interactions between unsteady turbulent flow and the finite rate chemistry.

Chapter VI

Summary and Conclusions

The objective of the thesis is to introduce a transient laminar flamelet model coupled with Large Eddy Simulation (LES) in order to capture unsteady thermochemical dynamics of highly turbulent flames at low Damköhler numbers.

In this study, we used upgraded version of the transient laminar flamelet model (TLFM) which was developed at LTNT/ETH for non-premixed flames subjected to high strain rates in an unsteady turbulent flow field. The pre-calculated laminar flamelet libraries in TLFM were implemented to the commercial flow solver LES model to simulate a series of turbulent nonpremixed methane piloted-jet flames, Sandia D, E, and F flames.

Statistical turbulence models (RANS) are time independent models. Therefore the resolved scales do not reflect any temporal information. Large Eddy Simulation has advantage of producing time dependent predictions. LES captures average flow field and turbulent mixing (mixture fraction field) much better than RANS approaches. This is an important requirement for any successful combustion modelling. The large scale structures are solved and the small scale structures are modelled in this method. Strong effects of unsteady turbulent fluctuations on chemical reactions may cause local extinction in turbulent diffusion flames when the reactions are slow compared to the turbulence time scale. After local extinction, the flame reignites further downstream where the mixing rates are more relaxed. The accuracy of the modelling of local extinction and reignition phenomena requires a model that captures the non-linear interactions between chemistry and turbulence.

Dynamic analysis of diffusion flames is one of the analysis tools to identify extinction and reignition phenomena in the reacting turbulent flow field. Time dependent feature and better turbulence solution capacity of LES allow this analysis. Although the model presented in this

paper is not very complicated for implementing it to any system, it captures the chemistry and turbulent flow field interactions sufficiently well. The results show that the model can be a candidate for the simulation of diffusion flames, which have regions being governed by partially premixed processes.

Partial premixing of the fluid parcels is widely observed at highly strained reacting turbulent flow fields. After local extinction of the fuel-air mixture, some extinguished fluid parcels may flow further downstream and mix with fuel and air to reignite as a partially premixed mixture. In order to investigate partially premixed features of the flames, the pure diffusion and partially premixed diffusion flamelet libraries were used and discussed. Partially premixed libraries were created due to the mixing ratios of fuel and air at the inlet of the piloted Sandia flames. The differences between those two flamelet libraries were studied in chapter 3. The simulation results of three Sandia flames with those two different flamelet libraries were investigated in chapters 4 and 5.

The major advantage of using partially premixed libraries in these simulations was observed in prediction of the interim species. The underpredicted interim species mass fractions as a result of using pure diffusion libraries were replaced with quite accurate predictions due to the corrected reduced scalar fields in the partially premixed libraries especially in the fuel rich mixtures.

The main difference between the introduced coupling model and the classical flamelet model is the additional progress variable used to follow dynamic interactions between turbulence and finite rate chemistry. The unsteady effects might be included in to the flamelet models by solving the transient Peters equations with an initial guess that represents a partially premixed state. Partial premixing might be considered by an appropriate progress variable as it was modeled in the reactedness definition in chapter 4.

The reaction is triggered by the initial conditions due to the introduced progress variable and developed by the residence time of the fluid parcels in the control volume. This definition makes the simulation more sensitive to instantaneous changes in the turbulent flow field. Our simulation studies showed that the averaged turbulent characteristic time definitions in RANS on the basis of the turbulent kinetic energy and its dissipation rate led runs to select steady state flamelet libraries because of the calculated longer characteristic turbulent time.

The scalar dissipation rate expresses the influence of the turbulent flow field on the flamelet equations. The level of the scalar dissipation rate plays a critical role in the determination of the locally extinguished regions in the reacting turbulent flow field. The introduced scalar dissipation rate describes the contributions of the diffusion in two parts, molecular and turbulent diffusion parts. The model captures the effects of both turbulent fluctuation and molecular diffusion in the flow field. The contribution of the molecular mixing into the scalar dissipation rate at the near downstream is more important as compared to the far downstream and this contribution should be taken into account.

The interface routines and their coupling with the flow solver are some of the critical tasks in the flamelet modelling studies. The new and more efficient coupling strategy was developed and implemented during this study. In contrast to the classical flamelet models coupling method, the presented coupling strategy makes the library interpolations and then calculates the PDF integrals that are stored as a part of the libraries as they were described in chapter 3. This improvement is very crucial in terms of computational costs since it increases the speed of the simulation up to 30 times compared to the classical models. In this method, there is almost no limitation for the number of the simulated species and types of the integrals in PDF calculations. Flexibility is also offered for the number of the nodes in the computational domain due to the drastic decrease in the computational cost.

The time averaged results were compared with the experimental data for velocity, mixture fraction, temperature and mass fractions of the species at the centreline and various radial profiles. The main and minor species profiles are in agreement with the experimental data. It is important that the simulated temperature fields in the fuel rich part of the flames indicated that the local extinction and the reignition phenomena are predicted well with this modeling approach. The hybrid flamelet model overcomes the limitations of the fast chemistry and steady flamelet models by using a dynamic chemical variable, namely progress variable, in addition to the kinematic variable, dissipation rate, in order to parameterize flamelet evolution.

The comprehensive comparisons of the basic dynamic characteristics of the Sandia flames between measurements and calculations were performed by using scalar statistics conditional on the mixture fraction and the bimodality analysis. Those analysis and the results of the time

averaged comparisons certified that the presented model can account for the local extinction and the reignition phenomena in the unsteady reacting turbulent flow fields.

Appendix

Interpolation Scheme

The function f defines the mass fraction of any species as a combination of five variables. x, y, z, β, θ are the variables that are computed in the computational domain. $x_i, y_i, z_i, \beta_i, \theta_i$ are the values of the variables at the vicinity of the computed x, y, z, β, θ.

$x_i, y_i, z_i, \beta_i, \theta_i$ are determined by the user in the definition of the problem. Those values are used in order to create artificial solutions.

$$x_1 \le x \le x_2 \ , \ y_1 \le y \le y_2 \ , \ z_1 \le z \le z_2 \ , \beta_1 \le \beta \le \beta_2 \ , \theta_1 \le \theta \le \theta_2$$

$$F_{33333} = f\left(x, y, z, \beta, \theta\right)$$
$$F_{11111} = f\left(x_1, y_1, z_1, \beta_1, \theta_1\right)$$
$$F_{22222} = f\left(x_2, y_2, z_2, \beta_2, \theta_2\right)$$

$$F_{11113} = \frac{F_{11112} - F_{11111}}{\theta_2 - \theta_1} \times \left(\theta - \theta_1\right) + F_{11111}$$
$$F_{11123} = \frac{F_{11122} - F_{11121}}{\theta_2 - \theta_1} \times \left(\theta - \theta_1\right) + F_{11121}$$
$$F_{11133} = \frac{F_{11123} - F_{11113}}{\beta_2 - \beta_1} \times \left(\beta - \beta_1\right) + F_{11113}$$

$$\boldsymbol{F}_{11213}=\frac{\boldsymbol{F}_{11212}-\boldsymbol{F}_{11211}}{\theta_2-\theta_1}\times\left(\theta-\theta_1\right)+\boldsymbol{F}_{11211}$$

$$\boldsymbol{F}_{11223}=\frac{\boldsymbol{F}_{11222}-\boldsymbol{F}_{11221}}{\theta_2-\theta_1}\times\left(\theta-\theta_1\right)+\boldsymbol{F}_{11221}$$

$$\boldsymbol{F}_{11233}=\frac{\boldsymbol{F}_{11223}-\boldsymbol{F}_{11213}}{\beta_2-\beta_1}\times\left(\beta-\beta_1\right)+\boldsymbol{F}_{11213}$$

$$\boldsymbol{F}_{11333}=\frac{\boldsymbol{F}_{11233}-\boldsymbol{F}_{11133}}{z_2-z_1}\times\left(z-z_1\right)+\boldsymbol{F}_{11133}$$

$$\boldsymbol{F}_{12333}=\frac{\boldsymbol{F}_{12233}-\boldsymbol{F}_{12133}}{z_2-z_1}\times\left(z-z_1\right)+\boldsymbol{F}_{12133}$$

$$\boldsymbol{F}_{12233}=\frac{\boldsymbol{F}_{12223}-\boldsymbol{F}_{12213}}{\beta_2-\beta_1}\times\left(\beta-\beta_1\right)+\boldsymbol{F}_{12213}$$

$$\boldsymbol{F}_{12133}=\frac{\boldsymbol{F}_{12123}-\boldsymbol{F}_{12113}}{\beta_2-\beta_1}\times\left(\beta-\beta_1\right)+\boldsymbol{F}_{12113}$$

$$\boldsymbol{F}_{12223}=\frac{\boldsymbol{F}_{12222}-\boldsymbol{F}_{12221}}{\theta_2-\theta_1}\times\left(\theta-\theta_1\right)+\boldsymbol{F}_{12221}$$

$$\boldsymbol{F}_{12213}=\frac{\boldsymbol{F}_{12212}-\boldsymbol{F}_{12211}}{\theta_2-\theta_1}\times\left(\theta-\theta_1\right)+\boldsymbol{F}_{12211}$$

$$\boldsymbol{F}_{12123}=\frac{\boldsymbol{F}_{12122}-\boldsymbol{F}_{12121}}{\theta_2-\theta_1}\times\left(\theta-\theta_1\right)+\boldsymbol{F}_{12121}$$

$$\boldsymbol{F}_{12113}=\frac{\boldsymbol{F}_{12112}-\boldsymbol{F}_{12111}}{\theta_2-\theta_1}\times\left(\theta-\theta_1\right)+\boldsymbol{F}_{12111}$$

$$\boldsymbol{F}_{13333}=\frac{\boldsymbol{F}_{12333}-\boldsymbol{F}_{11333}}{y_2-y_1}\times\left(y-y_1\right)+\boldsymbol{F}_{11333}$$

$$F_{21113}=\frac{F_{21112}-F_{21111}}{\theta_2-\theta_1}\times\left(\theta-\theta_1\right)+F_{21111}$$

$$F_{21123}=\frac{F_{21122}-F_{21121}}{\theta_2-\theta_1}\times\left(\theta-\theta_1\right)+F_{21121}$$

$$F_{21133}=\frac{F_{21123}-F_{21113}}{\beta_2-\beta_1}\times\left(\beta-\beta_1\right)+F_{21113}$$

$$F_{21213}=\frac{F_{21212}-F_{21211}}{\theta_2-\theta_1}\times\left(\theta-\theta_1\right)+F_{21211}$$

$$F_{21223}=\frac{F_{21222}-F_{21221}}{\theta_2-\theta_1}\times\left(\theta-\theta_1\right)+F_{21221}$$

$$F_{21233}=\frac{F_{21223}-F_{21213}}{\beta_2-\beta_1}\times\left(\beta-\beta_1\right)+F_{21213}$$

$$F_{21333}=\frac{F_{21233}-F_{21133}}{z_2-z_1}\times\left(z-z_1\right)+F_{21133}$$

$$F_{22333}=\frac{F_{22233}-F_{22133}}{z_2-z_1}\times\left(z-z_1\right)+F_{22133}$$

$$F_{22233}=\frac{F_{22223}-F_{22213}}{\beta_2-\beta_1}\times\left(\beta-\beta_1\right)+F_{22213}$$

$$F_{22133}=\frac{F_{22123}-F_{22113}}{\beta_2-\beta_1}\times\left(\beta-\beta_1\right)+F_{22113}$$

$$F_{22223}=\frac{F_{22222}-F_{22221}}{\theta_2-\theta_1}\times\left(\theta-\theta_1\right)+F_{22221}$$

$$F_{22213}=\frac{F_{22212}-F_{22211}}{\theta_2-\theta_1}\times\left(\theta-\theta_1\right)+F_{22211}$$

$$F_{22123}=\frac{F_{22122}-F_{22121}}{\theta_2-\theta_1}\times\left(\theta-\theta_1\right)+F_{22121}$$

$$F_{22113}=\frac{F_{22112}-F_{22111}}{\theta_2-\theta_1}\times\left(\theta-\theta_1\right)+F_{22111}$$

$$F_{23333} = \frac{F_{22333} - F_{21333}}{y_2 - y_1} \times \left(y - y_1 \right) + F_{21333}$$

$$F_{33333} = \frac{F_{23333} - F_{13333}}{x_2 - x_1} \times \left(x - x_1 \right) + F_{13333}$$

Bibliography

[1] Energy policies of IEA countries, Switzerland 2003 Review, http://www.iea.org/Textbase/publications.

[2] http://www.acunu.org/millennium.

[3] http://www.newsviews.info/editorialjune03.html.

[4] Pope, S.B., in *Turbulent Flows*, Cambridge University Press, (2000).

[5] Smagorinsky, J., "General Circulation Experiments with the Primitive Equations". *Month. Weath. Rev.*, 93:99-165, (1963).

[6] K. Akselvoll and P. Moin, "Large eddy simulation of turbulent confined coannular jets and flow over a backward facing step". *Report TF-63*, Thermosciences Division, Dept. of Mech. Eng., Stanford University, Stanford, California, (1995).

[7] Menon S., Yeung P. K., and Kim W. W., "Effect of Subgrid Models on the Computed Interscale Energy Transfer in Isotropic Turbulence". *Computers and Fluids*, Vol. 25, No. 2, pp. 165-180., (1996).

[8] S. Ghosal, T. S. Lund, P. Moin and K. Akselvoll, "A dynamic localization model for large-eddy simulation of turbulent flows". *J. Fluid Mech.* 286, 229 (1995).

[9] M. Germano, U. Piomelli, P. Moin and W. H. Cabot, "A dynamic sub-grid-scale eddy viscosity model". *Phys. Fluids* A 3, 1760 (1991).

[10] Meneveau C., "Statistics of turbulence subgrid-scale stresses: Necessary conditions and experimental tests". *Phys. Fluids* 6, 815 (1994).

[11] P. Moin, K. Squires, W. Cabot, S. Lee, "A dynamic subgrid-scale model for compressible turbulence and scalar transport". *Phys. Fluids* A 3, pp. 2746-2757 (1991).

[12] K. Akselvoll and P. Moin, "Large eddy simulation of turbulent confined coannular jets and flow over a backward facing step". *Report TF-63*, Thermosciences Division, Dept. of Mech. Eng., Stanford University, Stanford, California, (1995).

[13] S. Chester, F. Charlette, and C. Meneveau, "Dynamic Model for LES Without Test Filtering:Quantifying the Accuracy of Taylor Series Approximations". *Theoret. Comput. Fluid Dynamics* 15: 165–181, (2001).

[14] Pitsch, H and Steiner, H., "Large-eddy simulation of a turbulent piloted methane air diffusion flame (Sandia Flame D) ". *Phys. Fluids*, vol. 12, no. 10, pp. 2541-2554. (2000).

[15] Chapman, D. R., "Computational aerodynamics development and outlook". *AIAA J.* 17, 1293-1313, (1979).

[16] Peters, N., in *Turbulent Combustion*, Cambridge University Press, (2000).

[17] Poinsot T., Veynante D., *in Theoretical and Numerical Combustion*, R.T. Edwards Inc., (2001).

[18] Vervisch, L. and Poinsot T., "Direct Numerical Simulation of non-premixed turbulent combustion". *Annual Review of Fluid Mechanics* 30, 655-692, (1998).

[19] Williams, F.A. 1985, in *Combustion Theory*, Benjamin Cummings, (1985).

[20] Magnussen, B.F. and Mjertager, G. H. "On mathematical modeling of turbulent combustion". 16th Symp. (Int.) on combustion, The Combustion Institute, Pittsburgh, 719-727, (1976).

[21] Klimenko A. Y. "Multicomponent diffusion of various scalars in turbulent flow". Fluid Dyn. 25 327–34,(1990).

[22] Bilger R. W., "Conditional moment closure for turbulent reacting flow". *Phys. Fluids* A 5 436, (1993).

[23] Kronenburg, A., Bilger, R. W. and Kent, J. H., "Second Order Conditional Moment Closure for Turbulent Jet Diffusion Flames". *Proc. Combust. Inst.* 29:1097-1104, (1998).

[24] Klimenko A. Y., " Multicomponent diffusion of various scalars in turbulent flow". *Fluid Dyn.* 25 327–34, (1990).

[25] Klimenko A Y, "On the relation between the conditional moment closure and unsteady flamelets". *Combust. Theory Modelling* 5 , 275–294, (2001).

[26] Dopazo C. and E. E. O'Brien, ''Functional formulation of nonisothermal turbulent reactive flows''. *Phys. Fluids* 17, 1968, (1975).

[27] Pope, S.B., ''PDF methods for turbulent reacting flows''. *Prog. Energy Combust. Sci.* 11, 119 ,(1985).

[28] Van Slooten P.R., Jayesh, and S. B. Pope, ''Advances in PDF modeling for inhomogeneous turbulent flows''. *Phys. Fluids* 10, 246, (1998).

[29] Delarue B.J. and S. B. Pope, ''Application of PDF methods to compressible flows''. *Phys. Fluids* 9, 2704, (1997).

[30] Zhu M., K. N. Bray, O. Rumberg, and B. Rogg, ''PDF transport equations for two-phase reactive flows and sprays''. *Combust. Flame* 122, 327, (2000).

[31] Demiraydin, L., Gass J., and Poulikakos D. "On the behavior of a coupled transient flamlet/Pdf transport equation model for nonpremixed turbulent flames". *Combust. Sci. and Tech.*, 175, 1729-1760. (2003).

[32] Peters N., "Local quenching of diffusion flamelets and non-premixed turbulent combustion". *Western States Section of Combustion Institute*, paper WSS 80-4, Spring Meeting, Irvine, CA. (1980).

[33] Kuznetsov, V.R. "Effect of turbulence on the formation of large superequilibrium concentration of atoms and free radicals in diffusion flames". *Meha. Zhidkosti Gasa*,6 , 3-9, (1982).

[34] Peters, N. "Laminar flamelet concepts in turbulent combustion". *21st Symposium (International) on Combustion,* The Combustion Institute, 1231-1250. (1986).

[35] Bray, K. N.,C. and Peters, N. "Laminar flamlets in turbulent flames". In P.A. Libby and F.A. Williams, editors, *Turbulent Reacting Flows*, pages 63-113, academic Press, London. (1994).

[36] Peters N. "Laminar diffusion flamelet models in non-premixed turbulent combustion". *Progress in Energy and Combustion Science* 10, 319-339, (1984).

[37] Effelsberg, E. and Peters, N. "Scalar dissipation rates in turbulent jets and jet di_usion flames". *In Proc. Twenty-Second Symp. (Int'l) on Combustion*, 693-700. (1988).

[38] Fox R. O., "Computational Models for Turbulent Reacting Flows". *Cambridge University Press*, (2003).

[39] Jimenez, J., Linan, A., Rogers, M. & Higuera, F. "A priori testing of sub grid models for chemically reacting nonpremixed turbulent shear flows". *J. Fluid Mech.* 349, 149-171, (1997).

[40] Ferreria, J.C. "Flamelet modelling of stabilization in turbulent non-premixed combustion". *Dissertation*, (1996).

[41] Demiraydin, L., "Numerical investigation of turbulent nonpremixed methane-air flames". *Dissertation*, (2002).

[42] Byrne, G. D., Hindmarsh, A. C., and Brown, P. N. (1997). http://www.netlib.org/.

[43] Mell, W.E., Nilsen, V., Kosaly, G. And Riley, J.J., "Investigation of closure models for nonpremixed turbulent reacting flows". *Phys. Fluids*, vol. 6, No.3, pp.1331-1356, (1994).

[44] Bilger, R. W., " The structure of diffusion flames". *Combust. Sci. and Tech.* 13, 150-170, (1976).

[45] Kothnur, P. S. and Clemens N. T., "Experimental investigation of the relationship between strain and dissipation layers in a gas-phase turbulent jet". *AIAA-2001-1023, AIAA 39th Aerospace Sciences Meeting*, (2001).

[46] Kothnur, P. S. and Clemens N. T., "Effects of unsteady strain rate on scalar dissipation structures in turbulent planar jets". *Phys. Fluids*, submitted in (2004).

[47] Batchelor, G.K., "The effect of homogeneous turbulence on material lines and surfaces". *Proc. Roy. Sci. London* A. 213, 349-366, (1952).

[48] Dowling, D. R., "The estimated scalar dissipation rate in gas-phase turbulent jets". *Phys. Fluids* A 3, 2229-2246, (1991).

[49] Darabiha, N., "Transient behavior of laminar counterflow hydrogen-air diffusion flames with complex chemistry". Combustion Science and Technology, 86, 163-181 (1992).

[50] Barlow, R.S., and Chen, J-Y., "On transient flames and their relationship to turbulent methane-air jet flames". Twenty-Fourth Symposium (International) on Combustion, 24,pp 231-237 (1992).

[51] Im, H.G., Law, C.K., Kim, J.S., and Williams, F.A., "Response of counterflow diffusion flames to oscillating strain rates". Combustion and Flame, 100, 21-30 (1995).

[52] Im, H.G., and Chen, J.H., "Chemical response of Methane/Air diffusion flames to unsteady strain rate". Combustion and Flame, 118, 204-212 (1999).

[53] Cuenot, B., Egolfopoulos, F.N., and Poinsot, T., "An unsteady laminar flamelet model for non-premixed combustion". Combustion, Theory and Modeling, 4, 77-97 (2000).

[54] Omerbegovic, K. "Development of a transient flamelet libraries with realistic boundary conditions". *Diplomthesis*, (2003).

[55] Bray, K.N.C., Libby, P.A., in *Turbulent Reacting Flows* (P. A. Libby and F. A. Williams, Eds.). Academic Press, London, (1994).

[56] CFX 5.7., Theory Documentation.

[57] Jones, W. P., "Turbulence modeling and numerical solution methods for variable density and combustion flows", in *Turbulent Reacting Flows* (P. A. Libby and F. A. Williams, Eds.). Academic Press, London, (1994).

[58] Janicka, J., and Peters, N., " Prediction of turbulent jet diffusion flame lift-off using a pdf transport equation". *19th Symposium on combustion*, 367-374, The Combustion Institute, Pittsburgh. (1982).

[59] Cussler, E. L. Diffusion Mass Transfer in Fluid Systems, *Cambridge University Press*. (1997).

[60] Ferreira, J. C. "Steady and Transient Flamelet Modeling of Turbulent Nonpremixed". Combustion. Prog. in Comp. Fluid Dynamics, 1, 29-42, (2001).

[61] Masri, A. R., Bilger, R. W. and Sterner, S. H., "Dynamics of flames and reactive systems". *AIAA Progress in Astronautics and Aeronautics*, J. R. Brown, N. Manson, A. K. Oppenheim and R. I. Soloukhin (Eds.), Vol. 95,pp.293-304 (1984).

[62] Takahashi, F. and Goss, L. P., *Twenty-Third Symposium (International) on Combustion*, pp.677-683, The Combustion Institute, Pittsburgh (1990).

[63] Takahashi, F. and Goss, L. P., *Twenty-Fourth Symposium (International) on Combustion*, pp.351-359, The Combustion Institute, Pittsburgh (1992).

[64] Smith, L. L., Dibble, R. W., Talbot, L., Barlow, R. S. and Carter, C. D., *Combust. Flame* 100, 153 (1995).

[65] Vanquickenborne, L. and Van Tiggelen, A., *Combust.Flame* 10, 59 (1966).

[66] Barlow, R. S., and Frank, J. H., "Twenty-Seventh Symposium (International) on Combustion, The Combustion Institute, Pittsburgh", p. 1087, (1998).

[67] Ch. Schneider, Dreizler A., Janicka J. and Hassel E.P. "Flow field measurements of stable and locally exstinguishing hydrocarbon-fuelled jet flames". Combustion and Flame 135, 185–190, (2003).

[68] Barlow R., Eds.,TNF Workshop, http://www.ca.sandia.gov/TNF, Sandia National Laboratories.

[69] Baykal, S.A., Gass, J. and Poulikakos, D., " Investigation of lift-off phenomenon by transient laminar flamelets coupled with LES" (in preparation).

[70] Masri, A.R., Dibble, R.W. and Barlow, R. S., "The structure of turbulent nonpremixed flames revealed by raman-rayleigh-lif measurements". *Prog. Energy. Combust. Sci.* 22, 307-362, (1996).

[71] Starner, S.H., Bilger, R.W., Dibble, R.W., Barlow, R.S., "Piloted Diffusion Flames of CO/CH4/N2 and CO/H2/N2 Near Extinction". *Combust.Flame* 83:63-74 (1991).

[72] Xu, J. and Pope, S. "PDF calculations of turbulent nonpremixed flames with local extinction". Combust. Flame, 123, 281-307, (2000).

[73] Pitsch H., Cha C. M., and Fedotov S., "Flamelet modelling of non-premixed turbulent combustion with local extinction and re-ignition". Combust. Theory Modelling, 7 , 317–332, (2003).

[74] Sripakagorn P., Kosaly G., and Pitsch H., "Local extinction–reignition in turbulent nonpremixed combustion". CTR Ann. Res. Briefs 117–28, (2000).

[75] Cha C. M., and Pitsch H., "Higher-order conditional moment closure modelling of local extinction and reignition in turbulent combustion". Combust. Theory Modelling, 6, 425–37, (2002).

[76] Sripakagorn P, Mitarai S., Kos´aly G., and Pitsch H., "Extinction and reignition in a diffusion flame (a direct numerical study)". Journal of Fluid Mechanics, Vol. 518, pp. 231-259, (2004).

[77] Mitarai, S., Kosaly G. and Riley J. J., "A new Lagrangian flamelet model for local extinction and re-ignition". Combustion and Flame, Vol. 137, pp.306-319, (2004).

[78] Sripakagorn, P., Kosaly G., and Riley J. J., "Investigation of the influence of Reynolds number on extinction and reignition". Combustion and Flame, Vol. 136;351-363, (2004).

[79] Akselvoll K. and Moin P., "Large eddy simulation of turbulent confined coannular jets and turbulent flow over a backward facing step". *Technical Report TF-63,* Department of Mechanical Engineering, Stanford University, (1995).

[80] Cabot W. and Moin P., "Approximate Wall Boundary Conditions in the Large-Eddy Simulation of High Reynolds Number Flow". Flow, Turbulence and Combustion, Vol. 63, 269 – 291, (2000).

[81] Scotti A., Meneveaue C., Lilly D. K., "Generalized Smagorinsky model for anisotropic grids". Phys. Fluids A, Vol. 5, No. 9, 2306-2308, (1993).

[82] Piomelli U., "Large-eddy simulation: achievements and challenges". Progress in Aerospace Sciences, 35, 335-362, (1999).

[83] Lilly, D.K. "A proposed modification of the Germano subgrid-scale closure method". J. Physics Fluids A, 4, 633, (1992).

[84] Bardina J., Ferziger J. H., and Reynolds W. C., "Improved Subgrid Scale Models for Large-Eddy Simulation". AIAA Paper 80-1357, (1980).

[85] Meneveau C., and Katz J., "Scale-Invariance and Turbulence Models for Large-Eddy Simulation". Annu. Rev. Fluid Mech., (2000).

[86] Liu S., Meneveau C., and Katz J., "On the Properties of Similarity Subgrid-Scale Models as Deduced from Measurements in a Turbulent Jet". J. Fluid Mech. 275, 83 (1994).

[87] Anderson, R. and Meneveau C., "Effects of the similarity model in finite-difference LES of isotropic turbulence using a Lagrangian dynamic mixed model ". Flow, Turb. & Comb 62 ,201-225, (1999).

[88] Zang, Y., Street, R. L. & Koseff, J. R., " A dynamic mixed subgrid-scale model and its application to turbulent recirculating flows". Phys. Fluids. 5, 3186-3196, (1993).

[89] Horiuti, K., "A new dynamic two-parameter mixed model for large-eddy simulation". Phys. Fluids A. 9, 3443-3464, (1997).

[90] Yoshizawa A., "A statistically derived subgrid model for the large eddy simulation of turbulence". Phys. Fluids 25, 1532 (1982).

[91] Carati, D., Ghosal, S., Moin, P., "On the representation of backscatter in dynamic localization models". Phys.Fluids 7, 606–616, (1995).

[92] Maas U., Pope S. B., "Simplifying Chemical Kinetics: Intrinsic Low-Dimensional Manifolds in Composition Space". Comb Flame 88, 239, (1992).

[93] Maas U., Pope S. B., "Implementation of Simplified Chemical Kinetics Based on Intrinsic Low-Dimensional Manifolds". 24th Symposium (International) on Combustion, The Combustion Institute, Pittsburgh, S 103, (1993).

[94] Nieuwstadt F.T.M., Hunt J.C.R. and Brethouwer G., "Micro structure and lagrangian statistics of the scalar field with a mean gradient in isotropic turbulence". Fluid Mechanics and its applications. IUTAM Symposium on Turbulent Mixing and Combustion, Kluwer Academic Publishers., p. 33 –43., (2002).

[95] Nieuwstadt F.T.M., Hunt J.C.R. and Brethouwer G., "Micro structure and lagrangian statistics of the scalar field with a mean gradient in isotropic turbulence". J. Fluid Mech. (2003), vol. 474, pp. 193-225, (2002).

[96] Frederiksen R.D., Dahm W.J.A., and Dowling D.R., "Experimental assessment of fractal scale similarity in turbulent flows. Part 1. One-dimensional intersections". Journal of Fluid Mechanics, Vol. 327, p. 35-72, (1996).

[97] Frederiksen R.D., Dahm W.J.A., and Dowling D.R., "Experimental assessment of fractal scale similarity in turbulent flows. Part 4. Effects of Reynolds and Schmidt numbers". Journal of Fluid Mechanics, Vol. 377, p. 169-187, (1998).

[98] Pierce C. D., "Progress-variable approach for large-eddy simulation of turbulent combustion". *Dissertation*, (2001).

[99] Brethouwer, G., Hunt, J.C.R., Nieuwstadt, F.T.M.,"Micro-structure and Lagrangian statistics of the scalar field with a mean gradient in isotropic turbulence". J. Fluid Mech., Vol. 474, p.193-225, (2003).

[100] http://www-berkeley.ansys.com/hexa/hexap2.htm.

[101] http://www.unige.ch/sciences/chifi/cpb/windig.html.

[102] Su, L.K., and Dahm, W.J.A., "Scalar Imaging velocimetry measurements of the velocity gradient tensor field in turbulent flows. II. Experimental results". Physics of Fluids, 8,1883-1906 (1996).

[103] Su, L.K., and Clemens, N.T., "Planar measurements of the full three-dimensional scalar dissipation rate in gas-phase turbulent flows". Experiments in Fluids, 27, 507-521 (1999).

[104] Libby, P.A., and Williams, F.A. Fundamental aspects and a review, in P.A. Libby and F.A. Williams, editors, Turbulent Reacting Flows, 1-61, Academic Press, London. (1994).

Curriculum Vitae

Personal Information

Name	**:** Şevket A. Baykal
Date of Birth	**:** 07th October 1972
Place of Birth	: Giresun/Turkey
Nationality	**:** Turkish
Sex/Marital Status	**:** Male/Single

Education & Professional Experience

2005 – Present	Postdoctoral Researcher
	Laboratory of Thermodynamics in Emerging Technologies
	Eidgenössische Technische Hochschule (ETH) in Zürich, Switzerland
2001 – 2005	Research Assistant
	Laboratory of Thermodynamics in Emerging Technologies
	Eidgenössische Technische Hochschule (ETH) in Zürich, Switzerland
1999 – 2000	System Programmer
	Turkish Land Forces in Istanbul, Turkey
1997 – 1999	Process Engineer
	DUSA/KORDSA in Kocaeli, Turkey
1997 – 1997	Deputy Adviser
	Turkish Grand National Assembly (TBMM) in Ankara, Turkey
1995 – 1998	Master of Science in Aeronautical Engineering,
	Research Assistant
	METU in Ankara, Turkey
1989 – 1995	Bachelor of Science in Aeronautical Engineering
	Middle East Technical University (METU) in Ankara, Turkey
1985 – 1988	**Giresun High School** in Giresun, Turkey